Spring 2020

Longitudinal Brain Tumor Tracking, Tumor Grading, and Patient Survival Prediction Using MRI

Linmin Pei
Old Dominion University, lxpei001@odu.edu

LONGITUDINAL BRAIN TUMOR TRACKING, TUMOR GRADING, AND PATIENT SURVIVAL PREDICTION USING MRI

by

Linmin Pei
M.S. December 2011, Norfolk State University

A Dissertation Submitted to the Faculty of
Old Dominion University in Partial Fulfillment of the
Requirements for the Degree of

DOCTOR OF PHILOSOPHY

ELECTRICAL AND COMPUTER ENGINEERING

OLD DOMINION UNIVERSITY
May 2020

Approved by:

Khan M. Iftekharuddin (Director)

Jiang Li (Member)

Christian Zemlin (Member)

Michel Audette (Member)

ABSTRACT

LONGITUDINAL BRAIN TUMOR TRACKING, TUMOR GRADING, AND PATIENT SURVIVAL PREDICTION USING MRI

Linmin Pei
Old Dominion University, 2020
Director: Dr. Khan M. Iftekharuddin

This work aims to develop novel methods for brain tumor classification, longitudinal brain tumor tracking, and patient survival prediction. Consequently, this dissertation proposes three tasks. First, we develop a framework for brain tumor segmentation prediction in longitudinal multimodal magnetic resonance imaging (mMRI) scans, comprising two methods: feature fusion and joint label fusion (JLF). The first method fuses stochastic multi-resolution texture features with tumor cell density features, in order to obtain tumor segmentation predictions in follow-up scans from a baseline pre-operative timepoint. The second method utilizes JLF to combine segmentation labels obtained from (i) the stochastic texture feature-based and Random Forest (RF)-based tumor segmentation method; and (ii) another state-of-the-art tumor growth and segmentation method known as boosted Glioma Image Segmentation and Registration (GLISTRboost, or GB). With the advantages of feature fusion and label fusion, we achieve state-of-the-art brain tumor segmentation prediction.

Second, we propose a deep neural network (DNN) learning-based method for brain tumor type and subtype grading using phenotypic and genotypic data, following the World Health Organization (WHO) criteria. In addition, the classification method integrates a cellularity feature which is derived from the morphology of a pathology

image to improve classification performance. The proposed method achieves state-of-the-art performance for tumor grading following the new CNS tumor grading criteria.

Finally, we investigate brain tumor volume segmentation, tumor subtype classification, and overall patient survival prediction, and then we propose a new context-aware deep learning method, known as the Context Aware Convolutional Neural Network (CANet). Using the proposed method, we participated in the Multimodal Brain Tumor Segmentation Challenge 2019 (BraTS 2019) for brain tumor volume segmentation and overall survival prediction tasks. In addition, we also participated in the Radiology-Pathology Challenge 2019 (CPM-RadPath 2019) for Brain Tumor Subtype Classification, organized by the Medical Image Computing & Computer Assisted Intervention (MICCAI) Society. The online evaluation results show that the proposed methods offer competitive performance from their use of state-of-the-art methods in tumor volume segmentation, promising performance on overall survival prediction, and state-of-the-art performance on tumor subtype classification. Moreover, our result was ranked second place in the testing phase of the CPM-RadPath 2019.

This dissertation is dedicated to my parents, Xineng Pei and Jiaoe Gao.

ACKNOWLEDGMENTS

I would like to express my deepest gratitude to my adviser, Dr. Khan M. Iftekharuddin for giving me the opportunity to work in his research group and for his continuous guidance and advice throughout my Ph.D. program. His mentoring helped me to expand my knowledge and to develop the skills that will help my career as a researcher. I am honored to have worked for such a renowned and visionary professor.

I would also like to thank members of my advisory committee: Dr. Jiang Li, Dr. Christian Zemlin, and Dr. Michel Audette for their time, as well as for their valuable guidance and suggestions.

I am most grateful to my parents, Xineng Pei, and Jiaoe Gao, for the support and guidance, and for encouraging me to fulfill my ambitions in higher education.

Finally, I wish to acknowledge Lasitha S. Vidyaratne, Megan Anita Witherow, and Alex Glandon for being supportive friends with valuable input and advice throughout my Ph.D. I also thank all of my colleagues at the ODU Vision Lab for their support and encouragement.

TABLE OF CONTENTS

Page

LIST OF TABLES

Table Page

LIST OF FIGURES

Figure Page

CHAPTER 1

INTRODUCTION

Gliomas in central nervous system (CNS), the most common primary brain malignancies, originate from glial cells in the brain [1]. In the US, 23 out of 100,000 in the population have been reported as patients with brain tumors annually, from 2011-2015 [2]. According to the report, 392,982 cases consisted of 30.9% patients with

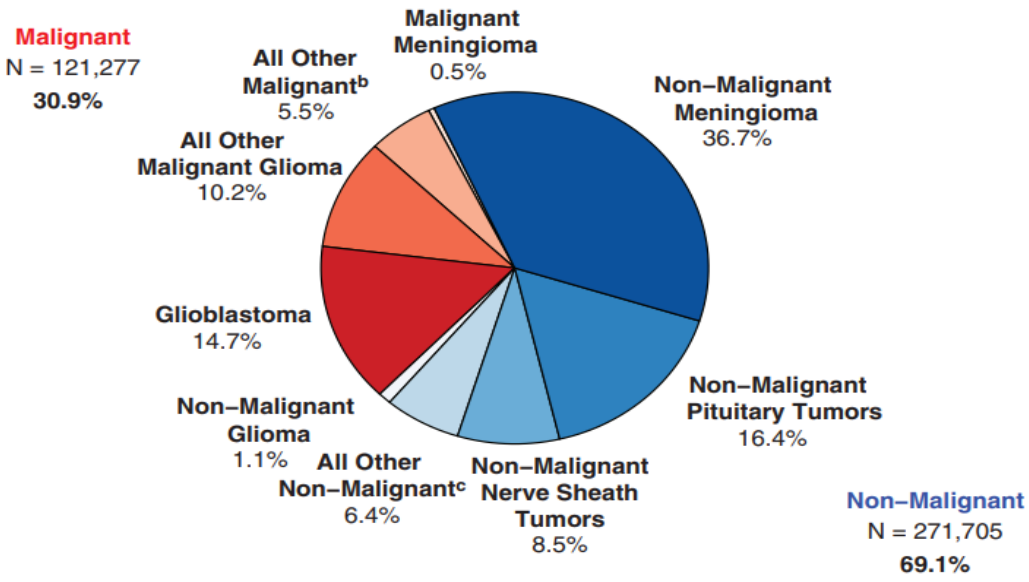

Figure 1. Distribution of primary brain and other CNS tumors reported during 2011-2015 [1].

malignant tumors and 69.1% patients with non-malignant tumors [2], as shown in Figure 1.

Prior to 2016, a brain tumor may have been graded as I, II, III, and IV respectively, based on the growth rate, the presence of definitive tumor margins, and the vascularity, according to the World Health Organization (WHO)'s 2007 diagnostic schema [3]. In 2016, WHO adapted to a new tumor classification criterion based on both phenotype and genotype [4]. In general, a patient's survival period is associated with the tumor grade. The survival period of a patient with a low-grade tumor is much longer than that of a

patient with a high-grade tumor. According to the report, from 2011-2015, for patients with malignant tumors, the estimated five- and ten- year relative survival rates were 35.0% and 29.3%, respectively [2]. Glioblastoma multiforme (GBM), originating from glial cells and growing by infiltrating surround tissues, is the most common and a highly aggressive type of glioma. The median of the survival period for a patient with GBM still remains at 12-16 months, even though there have been many treatment advancements [5]. Less than 4% of treated patients with GBM are alive after five years [5-7]. The short survival period of patients with GBM is not only because of the rapid tumor growth, but is also due to the tumor's invasion to surrounding brain tissues [8]. Early and proper detection of the tumor grade may result in a good prognosis [9].

To achieve a proper prognosis, treatment planning, and follow-up to the patients, accurate detection, and segmentation of brain tumor are critical. Manual tumor segmentation by radiologists is very tedious, time consuming, and prone to human error [10]. Consequently, computer-aided brain tumor analysis is desired. In a clinic, several image modalities are used for tumor diagnosis, such as computerized tomography (CT), magnetic resonance imaging (MRI), digital pathology image (DPI), etc. CT is used for brain tumor detection in its early stages [11]. In its later stages, a structural MRI is widely used for brain tumor analysis, especially for tumor detection and segmentation [1, 12-17]. In the literature, many methods have been proposed to detect and segment brain tumors, such as the active contours-based and atlas-based methods. However, performances of tumor segmentation using atlas-based methods are suffering from the quality of their image registration. To overcome this issue, brain tumor segmentation is treated as a classification problem. Traditional machine learning classifiers, such as K-nearest

neighbor (KNN), support vector machine (SVM), and random forest (RF), are generally used. As we know, effective and robust feature extraction is the prerequisite for traditional machine learning based brain tumor segmentation methods. In recent years, with the success of deep learning in many fields, such as computer vision, speech recognition, etc., deep learning-based methods have also been applied to medical imaging processing, including brain tumor detection, segmentation, grading, etc.

Diffuse low-grade gliomas (LGG) and intermediate-grade gliomas are infiltrative brain neoplasms which include the histological classes Astrocytoma, Oligodendrogliomas, Oligoastrocytomas, and World Health Organization (WHO) grade II and III neoplasms. High-grade gliomas are mainly Glioblastoma (WHO grade IV). Although LGG patients have a longer survival period than those with HGG, the LGGs have been found to typically progress to secondary GBMs with time, and they cause eventual death [9]. Tracking longitudinal brain tumor changes over time is critical for treatment management. Tracking is not only related to accurate tumor volume segmentation, but it also reveals information about tumor development over time. Moreover, similar to brain tumor classification, tumor tracking may be useful for patient survival prediction. Finally, even though there are a few studies on longitudinal brain tumor tracking in the literature, there is still a lack of robust methods.

This dissertation proposes a novel framework for longitudinal brain tracking, a new tumor grading following the new WHO tumor classification criterion, and a robust deep learning architecture for brain tumor segmentation, tumor subtype classification, and overall patient survival prediction.

1.1 Problem Statement

The topics mentioned above require efficient commuter-aided brain tumor analysis and abnormal tumor tissue segmentation methods. Even though there has been a plethora of techniques on brain tumor analysis and segmentation proposed in the literature, computer-aided brain tumor analysis is still a challenging task due to multiple factors. First, brain tumors can have an unpredictable appearance, infiltration to surrounding tissue, intensity heterogeneity, size, shape, and location variation [18]. Second, tumors have different degrees of aggressiveness, variable prognosis, and various heterogeneous histology [1]. Third, intensity gradients between adjacent structures can be obscured due to tumor penetration or bias field artifacts [12]. Lastly, MR images may be acquired following different protocols in clinical trials [19].

Among the brain tumor analysis tasks, accurate tumor detection and volume segmentation are very important for tumor assessment and prognosis. The brain tumor analysis methods are generally categorized in two groups: traditional feature-based machine learning methods (such as K-nearest neighbors [20], support vector machine [21], random forest [22], etc.) and more recent deep neural network-based methods. For traditional machine learning-based methods, feature extraction is a challenging task.

In general, LGGs are found to typically progress to HGGs, and to eventual death [9]. Longitudinal brain tumor tracking may be accomplished in at least two ways: a) via image-based tumor volume segmentation, and b) via computational modeling for tumor growth. As mentioned before, image-based tumor volume segmentation remains challenging because of imaging artifacts, the variety of image acquisition protocol, and tumor complex characteristics. Computational tumor growth modeling may be categorized as a microscopic model or a macroscopic model, according to the observation

scale. The macroscopic model, which refers to the reaction-diffusion formalism, is widely used in studies in the literature, because this model considers both microscopic proliferation and macroscopic diffusion. Tumor growth modeling is difficult because of two reasons: a) mass effect happens when the tumors invade and push the surrounding tumor [23, 24], and b) tumors grow at different rates in different types of brain tissues. For example, tumors have a faster growth rate in white matter (WM) than in gray matter (GM) [25].

As mentioned in the previous section, the WHO CNS tumor classification guideline changed in 2016. Prior to 2016, tumor classification was mainly based on histologic appearance in pathologic slides [3]. Specifically, tumors were classified according to microscopic similarities with different putative cells of origin and differentiation level [4]. The histological features of mitotic activity, microvascular proliferation, and necrosis are used when grading diffuse glioma. However, since using only histopathology data for tumor grading is no longer accurate and efficient, a new CNS brain tumor grade classification standard was released by the WHO in 2016 [4]. The new tumor classification standard requires both phenotype and proteomics information. The most common proteomics information has isocitrate dehydrogenase (*IDH*), *X1p/19q codeletion*, Alpha thalassemia/mental retardation syndrome X-linked *(ATRX)*, and O^6-methylguanine-DNA methyl-transferase *(MGMT)*. Since the new tumor classification criteria were released, there have been few studies in the literature that follow the revised tumor grading guidelines.

Recently, deep learning methods have attracted huge attention because of the success in computer vision, pattern recognition, speech recognition, and medical imaging

processing. Although deep learning-based methods for brain tumor analysis have been an active area of research in recent years, relevant tasks, such as tumor segmentation, classification, and overall survival prediction, have mostly been studied individually, ignoring the underlying relationship among these critical analysis tasks. There is a need for developing deep learning methods that consider tumor segmentation, tumor subtype classification, and patient survival prediction as interdependent tasks. Consequently, the overall aim of this dissertation is to develop a longitudinal brain tumor tracking model that will help brain tumor diagnosis and classification, as well as patient survivability prediction.

1.2 Proposed Work and Contributions

This dissertation proposes novel methods for longitudinal brain tumor volume segmentation and tracking using multimodal MRI, a tumor subtype grading that uses a deep learning-based method, and tumor classification and survival prediction that uses a deep learning Context Aware-based Convolutional Neural Network (CANet). It follows the new WHO tumor classification guideline using structural MRI, and patient survival prediction is completed by using both structural MRI and clinical data. Consequently, our first dissertation goal is to improve longitudinal brain tumor tracking by integrating tumor segmentation and tumor growth modeling using multimodal magnetic resonance imaging (mMRI) scans. This comprises two methods: feature fusion and joint label fusion (JLF). The first method fuses stochastic multi-resolution texture features with tumor cell density features to obtain tumor segmentation predictions in follow-up timepoints, using data from a baseline pre-operative timepoint. The second method utilizes JLF to combine segmentation labels obtained from (i) the stochastic texture feature-based and the

Random Forest (RF)-based tumor segmentation method and (ii) another state-of-the-art tumor growth and segmentation method, known as boosted Glioma Image Segmentation and Registration (GLISTRboost, or GB).

The overall novelty of this work is two-fold: a) tumor cell density is used as a novel feature to obtain tumor growth segmentation prediction for a prior successful stochastic multiresolution RF-based segmentation method, and b) it obtains improved tumor segmentation performance of another successful tumor segmentation tool, GB, by fusing labels obtained from the tumor segmentation using a RF-based method.

The second goal of the dissertation is to perform brain tumor grading by analyzing phenotype and proteomics information, using deep learning. This dissertation proposes a joint analysis of histopathology and proteomics patient data using DNN for brain tumor grade type and subtype classification, following the new WHO tumor grade criteria. The work utilizes digital pathology images and four pieces of proteomics information (*IDH*, *X1p/19q*, *ATRX*, and *MGMT*) to obtain improved tumor classification accuracy. The contribution has two parts: 1) development of a deep learning-based method for tumor grading by utilizing phenotype and proteomics information, and 2) integration of cellularity obtained from digital pathology image (DPI) to improve tumor grading accuracy.

Our final goal in this study is to build a robust deep learning architecture suitable for multiple tumor analysis tasks, including brain tumor segmentation, tumor subtype classification, and overall survival prediction. This dissertation proposes a context-aware deep learning method known as the Context Aware Neural Network (CANet). We offer three contributions, as follows: First, we propose a context-aware deep learning-based

method for brain tumor segmentation. Second, we utilize a hybrid method for overall survival prediction, which integrates the deep learning and traditional machine learning methods. Finally, although the new WHO tumor classification criteria indicate the use of both pathology images and proteomics information along with MRI, the proposed method is effective in tumor classification using structural MRI data only. A summary of the dissertation goals and contributions is listed in Table 1.

We have several peer reviewed publications resulting from the dissertation contributions, as follow: The research finding related to Dissertation Goal 1 is published in the 2015 IEEE International Conference on Bioinformatics and Biomedicine (BIBM) [15], Conference of Medical Imaging 2017: Computer-Aided Diagnosis [14], and Journal of Biomedical Signal Processing and Control (BSPC) [13]. The research findings related to Dissertation Goal 2 are under review by the Journal of Medical Image Analysis (MIA). Finally, the overall contributions of the Dissertation Goal 3 result were accepted as a conference paper in the Society of Photo-Optical Instrumentation Engineers (SPIE) Medical Imaging, and an expanded version of this Goal 3 is currently under review by the journal Scientific Reports – Nature. Moreover, we participated the Computational Precision Medicine: Radiology-Pathology Challenge on Brain Tumor Classification 2019 (CPM-RadPath) [26], also known as National Institute Health (NIH) Computational Precision Medicine 2019 Challenge, for the proposed methods of our Dissertation Goal 3. Our result is ranked in second place in the testing phase [27].

Table 1. Summary of proposed contribution in the dissertation.

Research Goal	Topic	Contributions
1	Improve longitudinal brain tumor tracking by integrating tumor segmentation and tumor growth modeling	Introduction of tumor cell density obtained from tumor growth model as novel feature to tumor segmentation prediction, and use joint label fusion to improve tumor segmentation
2	Obtain brain tumor grading by analyzing phenotypic and proteomic information	Development of tumor grading by following new WHO tumor criteria using a deep learning-based method
3	Build a robust model for multiple brain tumor analysis tasks using deep neural network	Development of context-aware deep learning for tumor segmentation, tumor subtype classification, and overall survival prediction.

1.3 Organization of the Dissertation

The rest of the dissertation is organized as follows. Chapter 2 describes the background information of the overall dissertation, mainly including brain tumor in CNS, brain tumor segmentation, longitudinal brain tumor tracking, brain tumor growth modeling, tumor grading, and basis of deep neural network (DNN). Chapter 3 proposes the two methods: the feature fusion method and the joint label fusion method, for the first dissertation goal. Chapter 4 investigates the new WHO tumor classification criteria and also briefly introduces digital pathology image and proteomics information. State-of-the-art comparison to other works is provided as well. Chapter 5 discusses the proposed context-aware deep learning architecture for multiple tumor analysis tasks. The chapter also briefly introduces the experimental data. Finally, the dissertation concludes in Chapter 6, with a summary and suggestions for future work.

CHAPTER 2

BACKGROUND REVIEW

This chapter reviews the relevant information on tumor segmentation, tumor growth modeling, longitudinal tumor tracking, tumor grading, the artificial neural network, and overall patient survival prediction.

2.1 Brain Tumor Segmentation

In the U.S., out of all deaths, 2.5% are caused by brain tumor. A brain tumor is a heterogeneous mass of tissue that is formed by an accumulation of abnormal cells. Compared to normal tissues, it has highly irregular properties, including multiple cell phenotype, heterogeneous density, high intra-tumoral pressure, and tortuous vasculature [28]. For diagnosis, prognosis, and treatment planning, detection and quantization of a brain tumor is an important step. Tumors may have an unpredictable appearance, with a huge variation in size, shape, and location, as shown in Figure 2. As such, the process of distinguishing different abnormal tumor tissues such as necrosis (NC), peritumorally

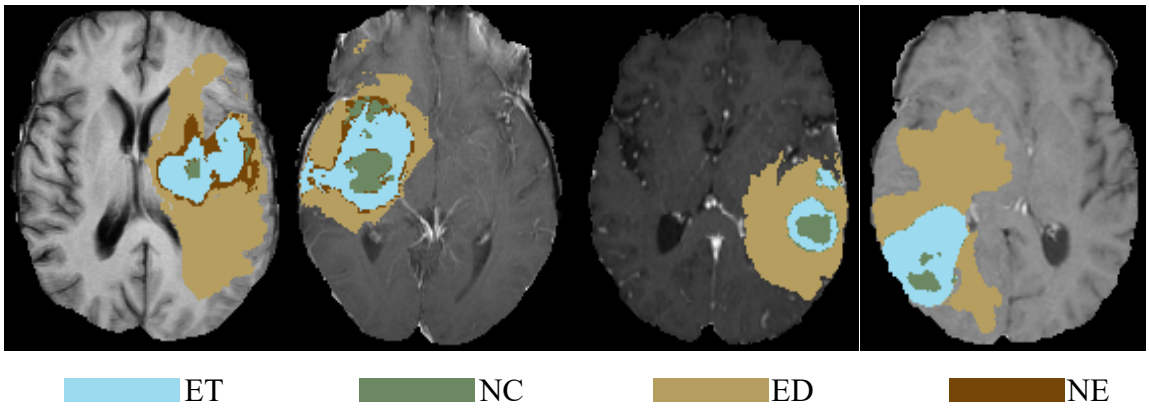

Figure 2. Four cases of tumor on MRI. Note that these pre-processed images are overlaid with ground truth. All data obtained from BraTS Challenge. ET-enhancing tumor, NC-necrosis, ED-peritumorally edema, NE-non-enhancing tumor.

edema (ED), non-enhancing tumor (NE), enhancing tumor (ET), also known as brain tumor segmentation, is very challenging.

The segmentation of the various brain tumor sub-regions (i.e., ET, NE, and ED) has commonly been addressed as a classification problem in the existing literature [29, 30]. This involves robust feature extraction as critical for such methods, followed by SVM and Random Forest (RF) being widely used as classifiers [13, 16, 31, 32]. The general idea of feature-based methods is to extract features and provide them to a classifier, in order to learn the most representative of the class(es) in question, and hence to obtain segmentation labels in new unseen cases. In recent years, deep learning has been successfully applied across many domains, including computer vision, speech recognition, and medical imaging processing (brain tumor detection and segmentation), among others. [29, 33, 34].

There are many studies proposed for image-based brain tumor segmentation in the literature. Among conventional machine learning-based methods, K-nearest neighbors, support vector machine (SVM), and AdaBoost are widely used [20, 21, 32]. In recent years, deep learning-based methods have been shown to outperform conventional machine learning-based methods for tumor segmentation. However, longitudinal brain tumor tracking using deep learning methods may not be feasible, as these deep learning methods need large amount of data and, in general, there is a lack of that large volume of longitudinal tumor tracking data available.

2.2 Tumor Growth Modeling

With tumor growth modeling, we can simulate brain tumor development over time. The interest of tumor growth simulation has many aspects. First, it provides a better

understanding of the physiology of the tumor growth. Second, a tumor growth model may be used to quantify a tumor's aggressiveness for a given patient. Finally, using the growth model can improve therapy planning (in surgery or radiotherapy) by better defining the tumor invasion region based on the local estimation of the tumor cell density [24]. It can help in predicting the tumor over time from a limited number of patient observations.

Tumor growth models can be categorized into two groups based on the observation scales [24]:

- Cellular and microscopic models. These models take the action behavior of individual cell into account for the subject; more complex models consider the interaction between the cells and the environment.
- Macroscopic models. These models are based on local tumor cell density. Most of the models rely upon a reaction-diffusion equation to account for tumor propagation.

Cellular and microscopic models are widely used in the literature [35-37]; however, these models do not consider the interactions between cells and tissues. Macroscopic models mainly use a reaction-diffusion formalism. These models take both the microscopic proliferation and the macroscopic diffusion into account for tumor growth. In this study, we aim to build a tumor growth model by solving the reaction-diffusion equation.

2.3 Longitudinal Brain Tumor Tracking

Longitudinal brain tumor segmentation prediction is not only related to the accurate

segmentation of the various tumor sub-regions, it also reveals information about tumor development over time. Monitoring longitudinal brain tumor changes is useful for the follow-up of treatment-related changes, the assessment of treatment response, and the guiding of dynamically changing treatments, including surgery, radiation therapy, and chemotherapy. To model and predict the growth of a tumor, a reaction-diffusion equation is generally employed [23, 24, 38-41]. Hu *et al*. simulated one-dimensional tumor growth based on logistic models [42]. Sallemi *et al.* simulated brain tumor growth based on cellular automata and the fast marching method [43]. Similar works for tumor growth prediction are proposed in [23, 24, 28, 39, 41, 44]. However, none of these methods explicitly obtains tumor segmentation using growth patterns as features. Clatz *et al.* proposed a GBM tumor growth simulation by solving a reaction-diffusion equation using the finite element method [45]. Xu *et al.* used phase fields to model cellular growth and reaction-diffusion equations for the dynamics of angiogenic factors and nutrients [46]. We recently proposed a novel tumor cell density feature obtained from a tumor growth model which assesses temporal changes of tumor cell density based on biophysical tumor growth modeling, for segmentation prediction [14].

Tumor growth modeling, combined with segmentation, is useful in understanding the extent of a tumor as the tumor growth. Bauer *et al*. proposed tumor growth-based segmentation [47]. Boosted Glioma Image Segmentation and Registration (GLISTRboost), a state-of-the-art method, is used for segmentation by incorporating a glioma growth model [48]. GLISTRboot utilizes a gradient boosting multi-class classification. Brain Tumor Image Analysis (BraTumIA) is a tool for longitudinal brain

tumor segmentation [49]; however, both state-of-the-art tools ignore the internal relationship between different timepoint scans.

As noted above, current works that discuss longitudinal brain tumor tracking in the literature highly focus on tumor segmentation, mostly ignoring the importance of tumor growth. Another challenge to the work is the lack of longitudinal tracking data. In this study, we propose novel methods for longitudinal tumor tracking by integrating tumor segmentation and tumor growth modeling with a limited amount of longitudinal MRI data.

2.4 Brain Tumor Grading

Based on the similarity of tumor cells to normal cells, the growth rate, the presence of definitive tumor margins, and the vascularity, they are classified as Grade I, II, III, and IV by the World Health Organization (WHO) [3]. Grade I tumors are the most discrete, with a slow growth rate. Grade II tumors have a slow growth rate, but are able to invade surrounding tissue. Grade III tumors have actively reproducing abnormal cells that infiltrate adjacent cells, and Grade IV tumors are the most malignant, with rapid proliferation and infiltration to surrounding tissue [50-52]. Grades III and IV are categorized as high grade, and the rest are low grade.

A new CNS brain tumor grade classification standard was released by the WHO in 2016 [4]. Due to the drawbacks of tumor grading based only on histology, proteomics information has recently been used for tumor classification [53-56]. With the new standard for tumor grading, isocitrate dehydrogenase (*IDH*) mutation in proteomics information is identified as one of the major criteria [57]. In addition, other molecular

mutations, such as *ATRX*, *X1p/19q codeletion*, and *MGMT* have also been studied for glioma proteomics classification [58].

2.5 Artificial Neural Networks

Artificial neural networks (ANNs) are computing methods inspired by the biological neural networks of human/animal brains. An ANN is composed of neurons, which are simple and interconnected processors. The neurons are interconnected for signal processing. The process consists of data collection, analysis and processing, network structure design, the number of hidden layers, the number of hidden units, initializing, training the network, network simulation, weights/bias adjustments, and testing the network [59]. ANNs are considered as a universal approximators that have the ability to approximate a given function distribution. A neuron is the main component of a neural network, and the perceptron is the most used model. Figure 3 shows a graphical representation of a perceptron.

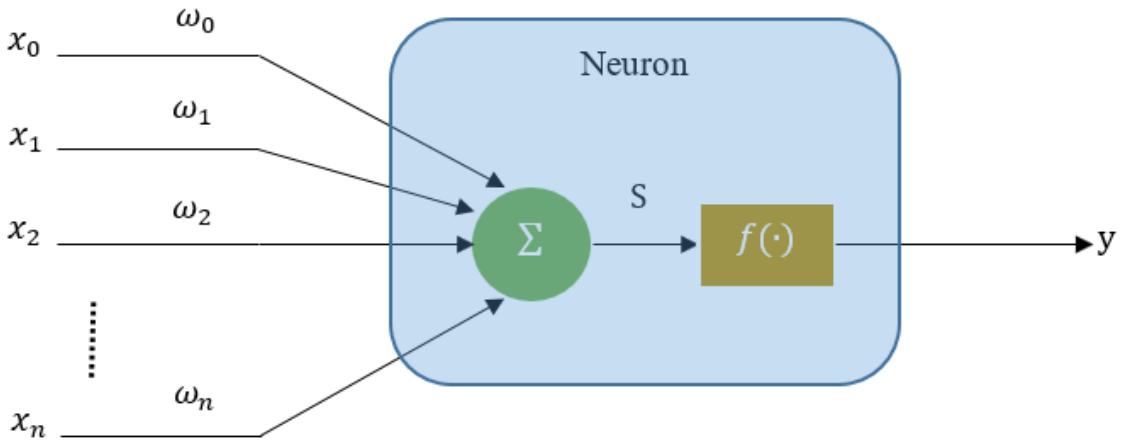

Figure 3. A graphical representation of a perceptron. x_i and ω_i are inputs to the neuron and the corresponding weight, respectively. $f(\cdot)$ is an active function. y is the final output.

Label $x_0, x_1 \ldots, x_n$ are the inputs to the neuron. Note that the input x_0 in the model is a fixed input that is typically set to 1 and provides a weighted external bias to the neuron. Each input to the neuron is multiplied with the corresponding weights, and then summed together. The final output is obtained by transforming the summation via an activation function, $f(\cdot)$. The model can be mathematically written as follows:

$$y = f(s) = f(\sum_{i=0}^{n} x_i \cdot \omega_i) \quad (1)$$

The popular activation functions include sigmoid, tanh function, sin/cos function, polynomial function, rectified linear, etc.

2.5.1 Multilayer Perceptron

A multilayer perceptron (MLP) is a class of feedforward ANN that contains one or more hidden layers and can learn non-linear functions. A typical MLP with a single hidden layer is shown in Figure 4. The leftmost layer is called the input layer. The rightmost layer is the output layer. The middle layer is called the hidden layer [60]. The

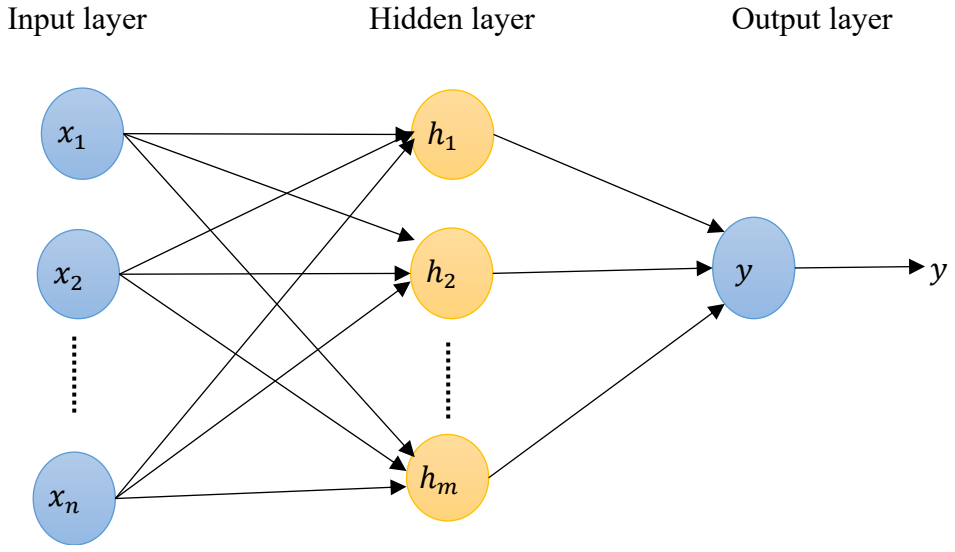

Figure 4. A graphical representation of a multilayer perceptron with a single hidden layer.

MLP shows the capability to approximate any sufficiently smooth function, and it is regarded as a universal approximator.

In a supervised MLP model, the ultimate goal is to minimize the error or the cost function between the target and the prediction obtained from the model. To adjust the training weights and biases using a gradient descent algorithm, the backpropagation algorithm is well-known for computing such gradients [61]. MLP is a popular machine learning solution, and it has been successfully used in diverse fields, such as speech recognition, image recognition, and others.

2.5.2 Convolutional Neural Network

Convolutional neural network (CNN) is a class of deep neural networks most commonly used for visual imagery analysis. The idea of CNN is not new, but its application has been limited due to memory and hardware constraints [62]. Since the mid-2000s, deep neural network training has been feasible because of the increased availability of large datasets and hardware improvements. Figure 5 shows MNIST [63] handwritten digits recognition, using CNN.

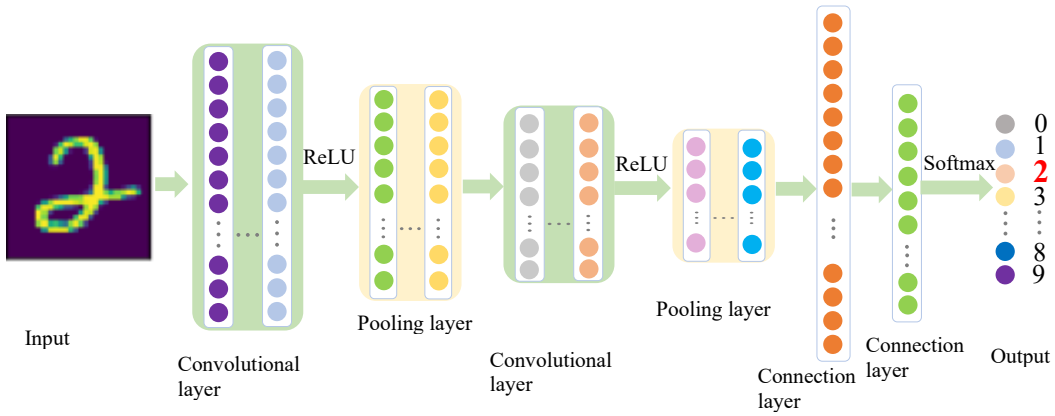

Figure 5. A CNN application for handwritten digits recognition.

A typical CNN contains convolutional layer, a pooling layer, an activation function, and a fully connected layer. The convolutional layer determines the output of the neurons that are connected to the local regions of the input through convolutional operation. The pooling layer performs downsampling along the spatial dimensionality of the given input, and further reduces the number of parameters within that activation [64]. Max pooling is the most commonly used for reducing the spatial size of feature maps. The activation function usually follows the convolutional layer. Nonlinearity between layers ensures that the model is more expressive than a linear model [62]. The activation functions include sigmoid, tanh, rectified linear unit (ReLU), and leaky-ReLU, among others. The fully connected layer contains neurons that are directly connected to the neurons in the two adjacent layers, without being connected to any layers within them [64]. It usually produces class scores from the activations in a classification application.

2.6 CNN-based brain tumor segmentation

In recent years, CNN-based methods have been successfully applied in medical imaging analysis, such as in brain tumor segmentation [33, 34], nuclei segmentation [65], and liver segmentation [66]. There are different methods for preparing input data for CNN-based tumor segmentation methods, such as patch-based [34], 2D slice-based [67], and 3D volume-based [33]. Each method has advantages and disadvantages. The patch-based method has the fastest training process, yet it may produce lots of misclassification in testing phase. The 2D slice-based method has a moderate training time and generates a more accurate result than that of patch-based method in the testing phase. The 3D volume-based method requires large graphic processing unit (GPU) memory. The 3D

volume-based method takes the longest training time, but provides the best performance in the testing phase, compared to the other two methods. All of the CNN architectures used for brain tumor segmentation have both encoding and decoding modules. The encoding module is used to extract the convolutional dense features, and the decoding module is used to reconstruct the dense features to the corresponding segmentation. The trainable network attempts to minimize the loss between segmentation and ground truth.

The CNN-based method offers the best state-of-the-art performance in tumor segmentation. Comparing the patch-based to the 3D volume-based method, the improvement for the 3D method mainly depends on the computational capability of the GPU. Most brain tumor cases have much more peritumorally edema than necrosis; this causes a data imbalance problem that may not help much for the 3D volume-based method in distinguishing the majority and the minority sub-tumors. We, however, propose a context-aware deep learning-based method that captures a global context information for relieving the data imbalance issue and helps to achieve better tumor segmentation performance.

2.7 Patient Survival Prediction

In general, patients with LGG have a longer survival period than those with HGG. Patient survival prediction is important for prognosis. Recently, the focus has been shifted to predicting the clinical outcome with non-invasive methods, instead of using invasive methods [68, 69]. There are many studies about predicting the survivability of patients with brain tumors in the literature [70, 71]. All of these methods extract a large number of radiomic image features, including shape and texture, in computed tomography images of the patient with brain tumors, and then apply regression methods

for survival prediction. Zeina *et al.* propose a feature-guide deep radiomics for glioblastoma patient survival prediction [69]. The authors first use a hybrid method for tumor segmentation, which utilizes RF and UNet, and then they extract volumetric features and texture features, including piecewise triangular prism surface area (PTPSA) and multi-fractional Brownian motion (mBm). Finally, XGBoost is applied on these features for the survival prediction.

Since hand-crafted feature extraction is very challenging, CNN may be used as a dense feature extraction tool. Few CNN-based methods are also proposed for survival prediction [72, 73]. However, many of these methods study survival prediction and segmentation independently, without exploring the inter-connection between survival prediction and tumor segmentation steps. In this work, we propose a feature-based method for survival prediction by integrating a tumor segmentation step using a CNN.

CHAPTER 3

IMPROVED LONGITUDINAL BRAIN TUMOR TRACKING

3.1 Chapter Overview

This chapter proposes a novel longitudinal brain tumor segmentation prediction using two different fusion approaches. The first one is called as “feature-fusion” approach, where unique tumor growth-based cell density and texture features are used. The second approach refers to label-fusion, where segmentation labels obtained from two state-of-the-art tumor growth and stochastic texture models are utilized. In the feature-fusion-based segmentation prediction method, we build upon a stochastic multiresolution texture model to obtain cell density information from tumor growth patterns as novel features and then fuse them with texture features. The tumor growth model is based on a reaction-diffusion equation that is solved in 3D using a Lattice-Boltzmann method (LBM), a class of computational fluid dynamics method for fluid simulation. On the other hand, the proposed joint label-fusion method fuses segmentation labels obtained from a hybrid generative-discriminative brain tumor segmentation method that incorporates a biophysical tumor growth model and the stochastic tumor segmentation models, to achieve tumor segmentation predictions. For traditional multi-atlas label fusion, multiple target images are registered and weighted by comparing target image to multiple atlas images. Further, the reference labels are obtained by considering tissue labels from registering the target image to the atlas images. In this study, due to the presence of multiple tumors in the provided mMRI volumes, we did not use healthy atlases as reference images, but instead created consensus average images across all patients for

each MRI modality. The reference labels are obtained by the RF and the GB segmentation models. The fusion weight is obtained proportional to inverse of intensity difference by target images to reference images.

3.2 Literature Review

This section provides a brief literature review on brain tumor segmentation, tumor segmentation prediction.

3.2.1 Brain Tumor Segmentation

Brain tumors may be classified as benign or malignant based on grade, and primary or metastatic based on origin. According to the World Health Organization (WHO), tumors of the central nervous system (CNS) may be graded as I, II, III and IV, based on multiple factors including similarity of tumor cells to normal cells, growth rate, presence of definitive tumor margins, and vascularity. Among these classes, grade III tumors contain actively reproducing abnormal cells that infiltrate between adjacent cells, and grade IV tumors are the most malignant with rapid tumor cell proliferation and infiltration to surrounding tissues [51, 52]. Recently, WHO suggested a new CNS tumor classification, based on both phenotype and genotype expressions in addition to growth pattern and behaviors [4]. Glioblastoma (formerly glioblastoma multiforme, GBM) is the most common and deadly among all human primary CNS tumors [5], with extensive heterogeneity radiographically reflected by various sub-regions, comprising enhancing (ET) and non-enhancing tumor (NET), as well as peritumorally edematous/invaded tissue (ED). Glioblastoma originates from glial cells and grows by infiltrating surrounding tissues. Even though there have been many treatment advancements, the median overall survival period of patients diagnosed with GBM still remains 12-16 months [5].

The segmentation of the various brain tumor sub-regions (i.e., ET, NET, and ED) has commonly been addressed as a classification problem in existing literature [29, 30], with robust feature extraction being critical for such methods, and SVM and convolutional neural networks (CNN) being widely used as classifiers. The general idea of feature-based methods is to extract features and provide them to a classifier, to learn the most representative of the class(es) in question, and hence obtain segmentation labels in new unseen cases. However, to the best of our knowledge, tumor cell density pattern has not been used as a feature in tumor segmentation prediction by others. The cell density feature can be obtained from solving the biophysical tumor growth modeling such that to predict potential tumor development in the future.

Brain tumor detection, segmentation, and tracking its changes over time (henceforth, tumor segmentation prediction) is of particular importance for diagnosis, treatment planning, and monitoring. In practice, manual tumor segmentation by radiologists is tedious, time consuming and prone to human error. Brain tumor segmentation over time is a critically challenging task due to its unpredictable appearance, infiltration to surrounding tissue, intensity heterogeneity, size, shape, and location variation [18]. There are many brain tumor segmentation techniques published in the literature. Gooya *et al*. introduced a generative approach for registering a probabilistic atlas of a healthy population to brain MRI scans with glioma and simultaneously segmenting these scans into tumor and healthy tissue labels [40, 74]. Cuadra *et al*. proposed an atlas-based segmentation of pathological brain MRI scans using a lesion growth model [75]. Bauer *et al*. also introduced an atlas-based segmentation of brain tumor images using a Markov random field-based tumor growth model and non-rigid registration [47]. However, these

atlas-registration based techniques may be tedious and error prone since they require accurate deformable image registration of tumor bearing slices with the atlas. To avoid the issues with image registration, other studies consider the brain tumor segmentation as a feature-based classification problem. Islam *et al*. extracted sophisticated texture features among others and applied the AdaBoost algorithm to segment tumors [76]. Reza *et al*. proposed an improved texture features based multiple abnormal brain tissue classification method using Random Forest (RF) [17, 77]. Support vector machine (SVM) has also been used as a classifier for brain tumor segmentation [21]. In addition, others have utilized super-pixels to classify tumor tissue. Wang *et al*. used a graph-based segmentation technique to over-segment images into homogeneous regions [78, 79]. Pei *et al*. applied simple linear iterative clustering (SLIC) to obtain super-pixel [22]. Kadkhodaei *et al*. applied a semi-supervised "tumor-cut" method to over-segment images. The super-pixel-based segmentation relies on the quality of the approach used for the over-segmentation. Finally, over recent years, various approaches based on CNN have been used for brain tumor segmentation [29, 80].

3.2.2 Longitudinal Brain Tumor Tracking

Longitudinal brain tumor segmentation prediction is not only related to the accurate segmentation of the various tumor sub-regions, but also reveals information about the tumor development over time. Monitoring longitudinal brain tumor changes is useful for follow-up of treatment-related changes, assessment of treatment response and guiding dynamically changing treatments, including surgery, radiation therapy, and chemotherapy. Figure 6 shows a longitudinal brain tumor example for a patient from

BraTS 2015 patient dataset [18]. This figure shows that enhancing, necrosis and other surrounding tissues of the tumor for an example patient in timepoint 2 are evolving (increasing) during the elapsed time by comparing that of timepoint 1.

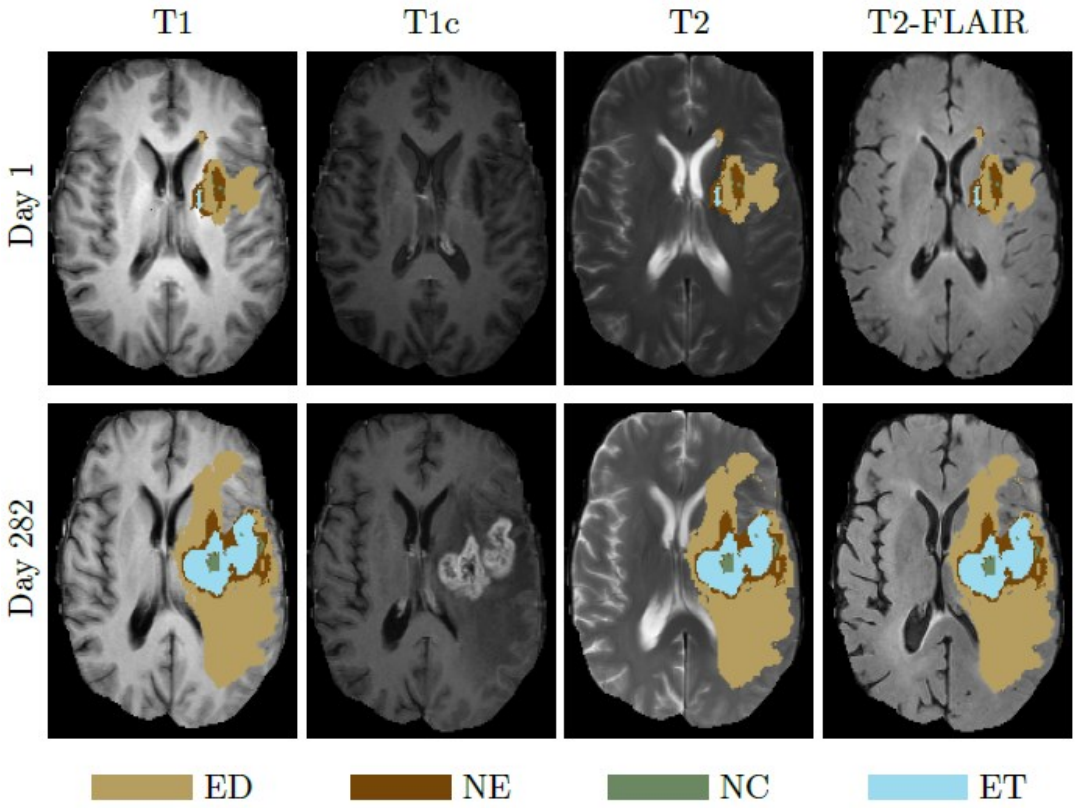

Figure 6. A longitudinal brain tumor example. Top row from left to right: T1, T1c, T2, T2-FLAIR, and ground truth (GT) at timepoint 1. Bottom row shows the corresponding images at timepoint 2 (282 days after timepoint 1).

To model and predict the growth of a tumor, a reaction-diffusion equation is generally employed [23, 24, 38-41]. Hu *et al*. simulated one-dimensional tumor growth based on logistic models [42]. Sallemi *et al.* simulated brain tumor growth based on cellular automata and fast marching method. However, none of these methods explicitly obtains tumor segmentation using growth patterns as features. Clatz *et al.* proposed a GBM tumor growth simulation by solving the reaction-diffusion equation using finite element method [45]. Xu *et al.* used phase fields to model cellular growth, and reaction-diffusion

equations for the dynamics of angiogenic factors and nutrients [46]. We recently proposed a novel feature, which assesses temporal changes of tumor cell density, based on biophysical tumor growth modeling, for segmentation prediction [21]. Meier *et al.* used a fully automatic segmentation method for longitudinal brain tumor volumetry [49]. However, Meier's work only focuses on analyzing each timepoint independently, and does not include a setting to integrate knowledge from prior timepoints for longitudinal tumor study.

3.3 Background

In this section, we discuss texture features, random forest (RF) classification, tumor growth modeling, and joint label fusion.

3.3.1 Multi-fractal Brownian Motion (mBm) Texture Feature Extraction

The mBm is a nonstationary zero-mean Gaussian random process that corresponds to the generalization of fractional Brownian motion (fBm) [17]. The fBm considers a rough heterogeneous appearance of tumor texture in brain MRI. In the fBm process, the local degree of Hurst index (H) is a constant. The value of H determines the randomness of the fBm process. However, tumor texture in MRI may appear as a multifractal structure that is a time (t) and/or space varying process and is represented by mBm. The mBm process is defined as $x(at) = a^{H(t)}H(t)$, where $x(t)$ is the mBm process with a scaling factor, a, and the time varying Hurst index $H(t)$. The mBm features effectively model spatially varying heterogeneous tumor texture. Its derivation combines the multi-resolution analysis enabling one to capture spatially varying random inhomogeneous tumor texture

at different scales [76]. More details for these multiscale texture features and their efficacy in brain tumor segmentation can be found in [17, 76, 77].

3.3.2 Random Forest Classification

Random forest (RF) is an ensemble learning method for classification, regression, and other tasks [81]. The RF classifier is heavily used for medical image analysis due to its very fast, and efficient multi-class handling capability. Assume there are n samples and $(\vec{v}_i)c\vec{v}_{i=1}^{n}$ feature vectors with outcomes y_i. Data is represented as: $D = [(\vec{v}_1, y_1), \cdots, (\vec{v}_n, y_n)]$. The feature vector ($d$ dimension) of a sample $\vec{v}_i$ is represented by $\vec{v}_i = (v_{i1}, \cdots, v_{id})$. A classification tree is a decision tree, in which each node has a binary decision based on whether $\vec{v}_i$ is less than a threshold α. At each node, feature v_{id} and threshold α are chosen to minimize resulting 'diversity' in the children nodes that are measured by Gini criterion. Ensemble of classifiers $h = [h_1(\vec{v}), \cdots, h_K(\vec{v})]$ and we define parameters of the decision tree for each classifier $h_k(x)$ to be $\theta_k = (\theta_{k1}, \theta_{k2}, \cdots, \theta_{kp})$. We can write: $h_k(\vec{v}) = h(\vec{v}|\theta_k)$. A RF classification is based on a family of classifiers $[\{h(\vec{v}|\theta_k), k = 1, \cdots, K\}]$ with parameters θ_k, which are randomly chosen from a model vector θ.

In RF classification, given a fixed ensemble $h = [h_1(\vec{v}), \cdots, h_K(\vec{v})]$, where $\vec{v}$ is a random vector and K is the number of trees in the forest, the estimated probability for predicting class c for a sample set, is defined as:

$$p(c|\vec{v}) = \frac{1}{K}\sum_{t=1}^{K} p_t(c|\vec{v}), \tag{2}$$

where $\mathrm{p_t}(c|\vec{v})$ is the estimated density of class labels at the t^{th} tree. The final multi-class decision function of the forest is defined as:

$$C(\vec{v}) = arg\ \max_{c \epsilon l}\ p(c|\vec{v}), \tag{3}$$

There generalization error (GE) has an upper bound in form of

$$GE \leq \bar{\rho}\frac{1-s^2}{s^2}, \tag{4}$$

where $\bar{\rho}$ is the mean correlation between pairs of trees in the forest, and s is the strength of the set of classifiers.

3.3.3 Biophysical Tumor Growth Model

Tumor growth describes an abnormal growth of tissue, which usually involves cell proliferation, invasion, and mass effect to the tumor surrounding tissues. During cell invasion, tumor cells migrate as a cohesive and multicellular group with retained cell-cell junctions and penetrate to surrounding healthy tissues. Tissues in the brain may deform due to mass effect. Biophysical tumor growth modeling simulates the interactive process occurring between the abnormal tissue (i.e., tumor) and the surrounding brain tissues, and parameterizes the collective changes in the brain, including death, infiltration to surrounding tissues, and proliferation. The reaction-diffusion equation has been widely used to model brain tumor growth [23, 39, 41, 42], using a diffusion and a logistic proliferation term given as:

$$\frac{\partial n_s}{\partial t} = D\nabla^2 n_s + \rho n_s(1 - n_s), \tag{5}$$

$$D\nabla n_s . \vec{n}_{\partial\Omega} = 0, \tag{6}$$

where n_s is the tumor cell density, D is the diffusion coefficient while infiltrating, and ρ is the proliferation rate. Equation (5) enforces Neumann boundary conditions on the brain domain Ω, and $\vec{n}$ is unit normal vector on the $\partial\Omega$ pointing inward to the domain.

3.3.4 Joint Label Fusion

Joint label fusion has been developed in recent years and used for analysis of medical images [22, 78]. Comparing to the single-atlas based method, multi-atlas-based label fusion reduces errors associated with any single atlas propagation in the process of combination, and the weight for each atlas is computed independently. However, different atlases may produce similar label errors. To solve this issue, Wang *et al*. proposed an advanced multi-atlas label fusion, known as joint label fusion [82]. Multi-atlas label fusion enforces co-registration with sample images to target image and minimizes independent errors to improve the segmentation result [83]. In general, the label map $\hat{L}$ is computed by using the following equation:

$$\hat{L} = arg\,\max_{L} p\left(L\middle|I; \hat{I}_n, \emptyset_n\right), \tag{7}$$

where $\hat{I}_n$ is the n-th training image, and $\emptyset_n$ is the transfer function during image registration. L is the candidate label map of the testing image I. Joint label fusion achieves consensus segmentation given as,

$$\bar{L} = \sum_{i=1}^{n} \omega_i(x) p(l|x, \hat{I}_n), \tag{8}$$

where $\omega_i(x)$ is individual voting weight, and $p(l|x, \hat{I}_n)$ is the probability that x votes for label l. The weight is determined by:

$$\omega_x = \frac{M_x^{-1} 1_n}{1_n^t M_x^{-1} 1_n}, \tag{9}$$

where $1_n = [1; 1; \cdots; 1]$ is a vector of size n and M_x is the pairwise dependency matrix that estimates the likelihood of two atlases both producing wrong segmentations on a per-voxel basis for the target images.

The dependency matrix is computed as:

$$M_x(j,k) \sim \sum_{m=1}^{L_M} \langle \left| A_F^m\left(\mho(x(j))\right) - T_F^m(\mho(x)) \right|, \left| A_F^m\left(\mho(x(k))\right) - T_F^m(\mho(x)) \right| \rangle, \quad (10)$$

where m indices correspond to all modality channels, and $\left| A_F^m\left(\mho(x(j))\right) - T_F^m(\mho(x)) \right|$ is the vector of absolute intensity difference between a selected atlas image and the target image over local patches $\mho$ centered at voxel $x(j)$ and x, respectively. $\langle \cdot,\cdot \rangle$ is the dot product. L_M is the total number of modalities [82].

3.4 Methods

This study proposes two distinct methods for longitudinal brain tumor segmentation prediction: a feature-based and joint-label fusion-based. Application of the proposed methods, assumes appropriate pre-processing of the provided multimodal MRI brain scans, consisting of noise reduction, bias field correction, scale standardization, and histogram matching.

3.4.1 Feature Fusion Based Method

The method proposed in this study utilizes tumor growth patterns as novel features to improve texture-based tumor segmentation in longitudinal MRI. The proposed pipeline is shown in Figure 7.

By using the proposed feature-based fusion, the vector $\vec{v}$ is defined as:

$$\vec{v} = [FD, n_s, I_{pre}, I_{post}, \cdots, Hist], \quad (11)$$

And the label of target image is defined as:

$$L = \underset{c \epsilon L}{argmax} \frac{1}{K} \sum_{t=1}^{K} p_t(c|\theta_k, \vec{v}), \quad (12)$$

where c is the candidate label of the target image. K is number of trees applied. $\vec{v}$ is a feature vector. θ_k is the classifier parameter obtained from training process at k^{th} tree.

FD describes the mBm features, n_s is the tumor cell density as derived by the tumor growth model (Eq. 5), I_{pre} and I_{post} are the image intensities before and after intensity normalization (scale standardization [84]), respectively. $Hist$ is the intensity histogram of all modalities (T1, T1c, T2, and T2-FLAIR).

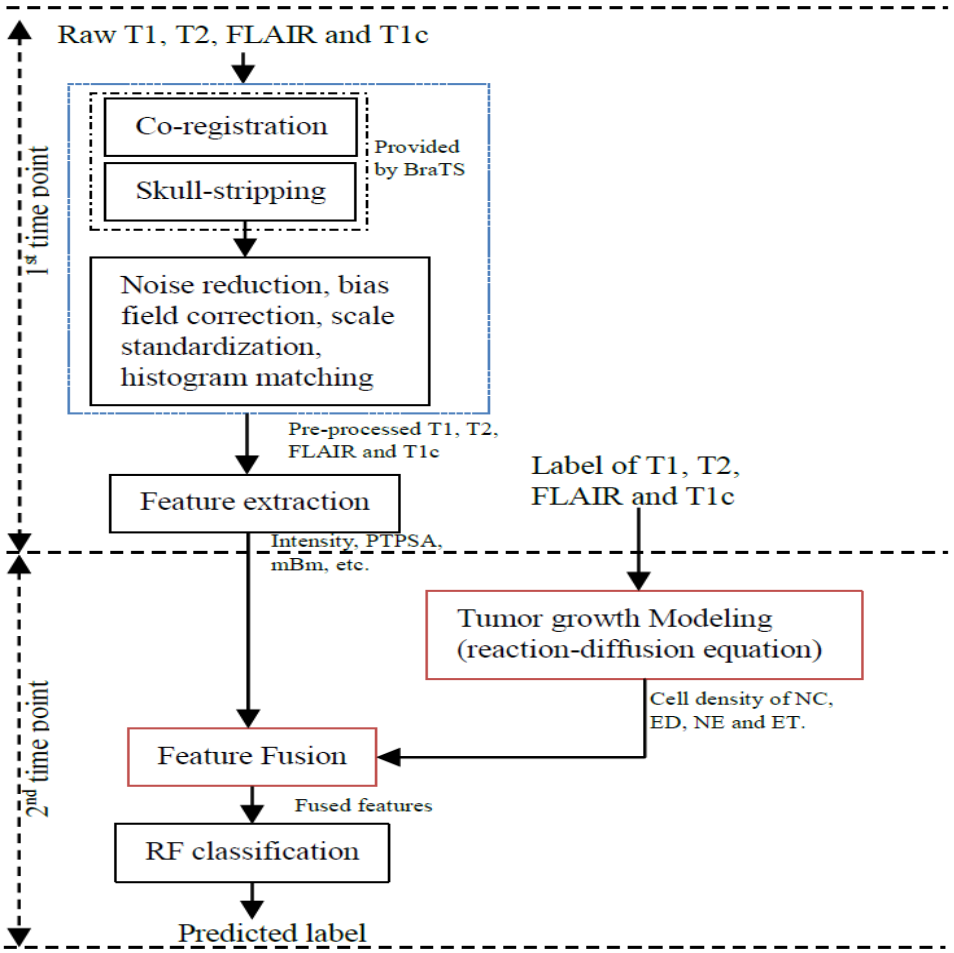

Figure 7. Pipeline of the proposed method. At the 1st scan date, we extract texture (e.g., fractal, and mBm) and intensity features, and obtain the ground truth label map for different brain tissues from baseline pre-operative (i.e., first timepoint) multimodal MRI scans. The ground truth at this first timepoint is used to obtain the tumor growth modeling and enable to predict cell density for the next timepoint. Finally, considering the cell density pattern as a new feature, we fuse it with other features using a RF classifier to generate the label of second timepoint.

Two feature types were used in the proposed method, representing local and spatial descriptors. Local features comprise the intensity of each modality before and after scaling standardization, as well as after histogram matching, their pairwise intensity differences among image modalities, and the cerebrospinal fluid (CSF) mask, obtained by the CSF expected intensity across modalities. Spatial features include a fractal feature extracted from multi-modal MRI, named piecewise-Triangular Prism Surface Area (PTPSA), the mBm features that combine both multiresolution-fractal and wavelet analyses for each modality after scaling standardization, and 6 gabor-like Texton features.

3.4.2 Joint Label Fusion Based Method

Label fusion has been successfully used for tumor segmentation in recent years [82, 83]. The method proposed here employs joint label fusion for improving tumor segmentation prediction by fusing stochastic feature-based tumor labels, with

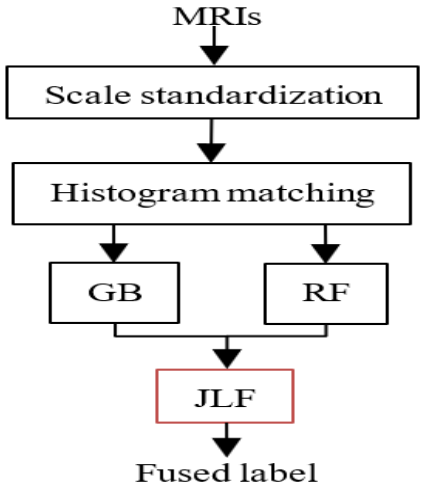

Figure 8. Pipeline for joint label fusion-based tumor segmentation prediction.

segmentation labels obtained from a hybrid generative-discriminative brain tumor segmentation method that incorporates a biophysical tumor growth model, namely GLISTRboost [48, 85, 86] (GB). The proposed pipeline is shown in Figure 8. Initially,

GB is applied on the 2nd timepoint in parallel with independent application of the RF-based approach, and their output segmentation labels are then fused together leading to the consensus result.

All provided MRI scans were affinely co-registered to an atlas template [87] and skull-stripped by BraTS. We then scaled all modality intensities for one reference subject to the range [0-255] and then matched the histograms of each modality across all subjects. The error dependence matrix (Eq. 10) was then computed between the target and the reference image, which describes the consensus average images across all patients. By using the error dependency matrix, we calculate the voting weight (Eq. 9), and finally the agreement label (Eq. 8) is obtained.

In GB, the probabilities of ET and NE are defined as:

$$f(Y|\Phi, h, q) = \prod_{x\in\Omega} \sum_{k=1}^{K} \pi_k(h(x)|q) f_k(y(x)|\Phi), \qquad (13)$$

where Y is the observation set, Φ is the intensity distribution, h the reference domain, q the tumor growth model parameters, π_k the k abnormal tissue, and $f_k(\cdot)$ is a multivariate Gaussian distribution.

Application of the joint label fusion method requires all four provided MRI volumes, the label map L_{GB} obtained by GB (Eq. 14), and the segmentation result L_{RF} obtained by Eq. 3 and 4. The voting weights are obtained by computing the error dependency matrix from all the available modalities to the reference images (Eq. 10). For calculating the dependency matrix (Eq. 10), $\mho(x)$ is a $5 \times 5 \times 5$ patch centered at location x. A^m ($m \in [1, 2, 3, 4]$ describes the volumes T1, T1c, T2, and T2-FLAIR of the training images, respectively. T^m is the target image. A is the reference image including the GB

segmentation (A_{GB}) and RF classification (A_{RF}). The candidate labels at location x for either the GB or the RF segmentations are defined as:

$$p(l|x) = \sum_{i=1}^{2} \omega_{x(i)} p(l|x(i), A(i)) = \omega_{x(1)} p(l|x(1), A_{GB}) + \omega_{x(2)} p(l|x(2), A_{RF}) =$$

$$\frac{M_{x(1)}^{-1} 1_N}{1_N^t M_{x(1)}^{-1} 1_N} p(l|x(1), A_{GB}) + \frac{M_{x(2)}^{-1} 1_N}{1_N^t M_{x(2)}^{-1} 1_N} p(l|x(2), A_{RF}) , \quad (14)$$

Let's define Dirac delta function $\delta(l|x)$ as 1, if the predicted label is the same as the reference label, otherwise 0, then, Eq. (13) becomes:

$$p(l|x) = \frac{M_{x(1)}^{-1} 1_N}{1_N^t M_{x(1)}^{-1} 1_N} \delta_{GB}(l|x) + \frac{M_{x(2)}^{-1} 1_N}{1_N^t M_{x(2)}^{-1} 1_N} \delta_{RF}(l|x) , \quad (15)$$

where the dependency matrix of M is computed by using Eq. 10. In the special case of the images among atlases being the same, $\frac{M_{x(1)}^{-1} 1_N}{1_N^t M_{x(1)}^{-1} 1_N} = \frac{M_{x(2)}^{-1} 1_N}{1_N^t M_{x(2)}^{-1} 1_N} = 0.5$, then the Eq. 15 will be simplified as a majority voting method, and $p(l|x) = 0.5(\delta_{GB}(l|x) + \delta_{RF}(l|x))$. Therefore, it is recommended to choose an odd number of templates.

3.4.3 Lattice-Boltzmann Method for Tumor Growth Modeling

To solve the reaction-diffusion equation (Eq. 5), different methods such as finite element method (FEM) [24] and Lattice-Boltzmann method (LBM) [41] may be used. We use the LBM method, due to its computational efficiency and easy parallelization. The LBM is defined as [88]:

$$f_s(\vec{x} + \vec{e}_i, i, t+1) - f_s(\vec{x}, i, t) = \Omega_S^{NR} + \Omega_S^R, \quad (16)$$

where $f_s(\vec{x}, i, t)$ is the one particle distribution function of specifies s with velocity $\vec{e}_i$ at time t and dimensionless position $\vec{x}$. $\Omega_S^{NR}$is non-reactive term. Ω_S^R is active term.

$$\Omega_S^{NR} = -\frac{[f_s(\vec{x}, i, t) - f_s^{eq}(\vec{x}, i, t)]}{\tau}, \quad (17)$$

where τ is the relaxation time. $f_s^{eq}(\vec{x}, i\,, t)$ is the equilibrium distribution function, which depends on $\vec{x}$ and t corresponding to a system with zero mean flow given as:

$$f_s^{eq} = \omega_{s,i} n_s \tag{18}$$

Two-dimensional nine-velocity (D2Q9) model is commonly used in 2D cases. The nine discrete velocities are shown in Figure 9.

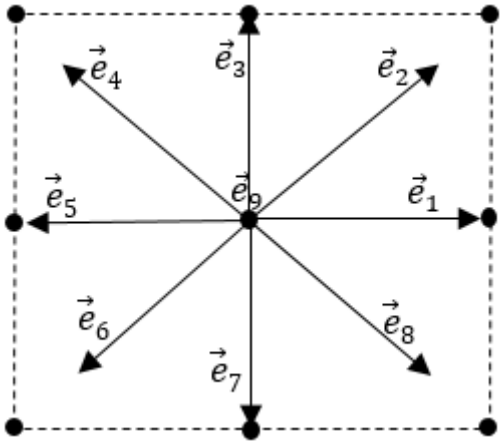

Figure 9. Illustration of the nine discrete velocities in a D2Q9 model.

Let's define:

$$n_s(\vec{x}, t) = \sum_i f_s(\vec{x}, i\,, t) = \sum_i f_s^{eq}(\vec{x}, i\,, t), \tag{19}$$

Here, n_s is the cell density (Eq. 5), and $w_{s,i}$ is dependent on the lattice system:

$$\omega_{s,i} = \begin{cases} \frac{4}{9}, & i = 9 \\ \frac{1}{9}, & i = 1, 3, 5, 7 \\ \frac{1}{36}, & i = 2, 4, 6, 8 \end{cases} \tag{20}$$

By using LBM, the reaction-diffusion equation (Eq. 5) can be recovered as:

$$\frac{\partial n_s}{\partial t} = \frac{1}{3}\left(\tau_s - \frac{1}{2}\right)\frac{\partial^2 n_s}{\partial x^2} + \rho n_s(1 - n_s), \tag{21}$$

$$\Omega_S^R = \rho n_s(1 - n_s), \tag{22}$$

Setting $D = \frac{1}{3}\left(\tau_s - \frac{1}{2}\right)$ offers solution for Eq. 5.

The algorithm of the proposed method is listed in Figure 10.

Algorithm

/ Initialization*/*
Initialize the diffusion coefficient D & proliferation rate ρ for a specific tissue.
Initialize weights (Eq. 20).
Set boundary for LBM working space.
Initialize n_s as a matrix with tumor density at starting position.
Repeat until set time limit is reached.
*/*Assignment*/*
For $i = 1{:}\,9$
  Streaming step: move $f_s \rightarrow f_s^*$ in direction of $\vec{e}_i$.
  If the cell hits the boundary
    Tumor cell moves in opposite direction with same speed.
  Else
  Compute f_s^{eq} (Eq. 18).
  Collision step: calculate the updated distribution function f_s (Eq. 16).
 End
End
Compute cell density n_s (Eq. 19).

Figure 10. Algorithm for solving the biophysical tumor growth model using LBM.

3.4.4 Longitudinal Tumor Segmentation Prediction

By longitudinal tumor segmentation prediction, we refer to the accurate delineation of the tumor boundaries in any follow up timepoint, given the segmentation of the tumor in the first scan. This does not only allow for the segmentation of the tumor but it also reveals information about its longitudinal growth and aggressiveness/behavior.

For feature fusion-based method, we build a tumor growth model by solving the reaction-diffusion equation using LBM. Diffusion coefficient D and proliferation rate ρ are important parameters to simulate tumor growth using the model. To predict tissues growth using the model, the parameters of the model are suggested within $[0.02, 1.5]mm^2/day$, and $[0.002, 0.2]/day$ [41]. We empirically set D_{NC}, ρ_{NC} as 0.052,

0.01, D_{ED}, ρ_{ED} as 0.06, 0.009, D_{NE}, ρ_{NE} as 0.03, 0.014, D_{ET}, ρ_{ET} as 0.05, 0.01 for NC, ED, NE, and ET, respectively. For the JLF method, we integrate a stochastic texture feature-based segmentation with another state-of-the-art, named GLISTRboost (GB) to achieve a better segmentation.

3.5 Experiment

3.5.1 Data

The brain tumor scans used to quantitatively evaluate the proposed methods in this study belong to retrospective longitudinal multi-institutional cohorts of patients diagnosed with glioblastoma, from the publicly available Multimodal BRAin Tumor Segmentation (BraTS 2015) challenge dataset [18]. Nine patients with longitudinal multimodal MRI (mMRI) scans with growing tumors along time were chosen from the BraTS 2015 dataset. The brain scans for each patient consist of four MRI modalities, namely native T1-weighted (T1), contrast-enhanced T1-weighted (T1c), T2-weighted (T2) and T2 Fluid-attenuated inversion recovery (T2-FLAIR).

Note that we use the BraTS 2015 dataset instead of the latest BraTS 2018 dataset [18, 86], as the latter provides only pre-operative mMRI scans, whereas the BraTS 2015 data describes paired combinations of pre- and post-surgical mMRI brain scans for each patient, with isotropic resolution images of size 240*240*155. The manually evaluated ground truth labels of these brain scans were also available, allowing for the quantitative validation of the proposed methods. These ground truth labels delineate the tumor sub-regions of necrotic/fluid-filled core (NC), non-enhancing/solid tumor (NE), ET, ED, and everything else grouped together, with labels of 1, 3, 4, 2, and 0, respectively.

3.5.2 Performance Evaluation

In the BraTS dataset, the ground truth is manually annotated by qualified raters, following a hierarchical majority voting rule [18]. To quantitatively evaluate the proposed brain tumor segmentation prediction method, a criteria policy is required. Specifically, there are three different tumor regions, as defined by the BraTS challenge [18]:

1) Region 1 – Whole tumor (WT)

This region defines the whole tumor (WT). Consistent with the BraTS challenge [18], the WT consists of the union of all tumor labels. Although the ED is a peripheral tissue to the tumor core, it is still considered as part of the WT since it is not pure edema but also includes invaded tumor cells.

2) Region 2 – Tumor core (TC)

This region defines the tumor core (TC), which comprises the combination of NC, NE and ET. Note that the TC describes what is typically resected during surgery.

3) Region 3 – Enhancing tumor (ET)

The ET region biologically represents regions of contrast leakage through disrupted blood-brain barrier.

We evaluate the 3D volume overlap by computing the Dice similarity coefficient ($\mathrm{DSC} = \frac{2\cdot|A\cap B|}{|A|+|B|}$) [89], where A and B represent the segmentation labels of a given method and the manually annotated (i.e., ground truth) labels. The DSC value ranges in $[0,1]$, where 0 represents that the two comparing regions do not have any overlap and 1 means that the regions are identical.

3.6 Results

3.6.1 Experiment with Feature Fusion-Based Method

To solve the biophysical brain tumor growth model using LBM, three parameters need to be considered: diffusion coefficient D, proliferation rate ρ and simulated days t. The diffusion coefficient and proliferation rate are variable to the model. Choosing a value for these variables is challenging. The values we used for D is within [0.02, 1.5] mm^2/day, and $\rho\epsilon[0.002, 0.2]day^{-1}$, after considering the available literature [41]. Figure 11 shows an example of longitudinal tumor growth using the proposed method and as depicted by ground truth labels in a single slice for a patient in the BraTS 2015 dataset.

We then apply the tumor growth model to real patient data from the BraTS dataset, where each patient's scan includes information of all sub-regions, i.e., NC, ED, NE, and ET. We simulate all these abnormal tissues separately, and then fuse them all into the final label map of the patient. Parameters vary among the various tissues [41]. By using the LBM model, we obtain the cell density patterns for the NE, ET, and the WT tissues, respectively. Note that the WT comprises all sub-regions including ED and NC. Following previous work [17], we use a total of 30 features including fractal, mBm, intensity and intensity difference among MRI modalities.

For specification of Eq. 12, label $c \in (0, 1, 2, 3, 4)$ which represents background, NC, ED, NE, and ET, respectively. K is empirically chosen as 20, and number of random features is 4, which is approximately equal to the square root of total number of features. Addition of cell density as a feature, results in 30 features (density of NC, ED, NE, and ET) extracted from each MRI slice. Figure 12 gives an illustrative example of comparing two cases between tissue segmentation obtained before and after adding cell density as a

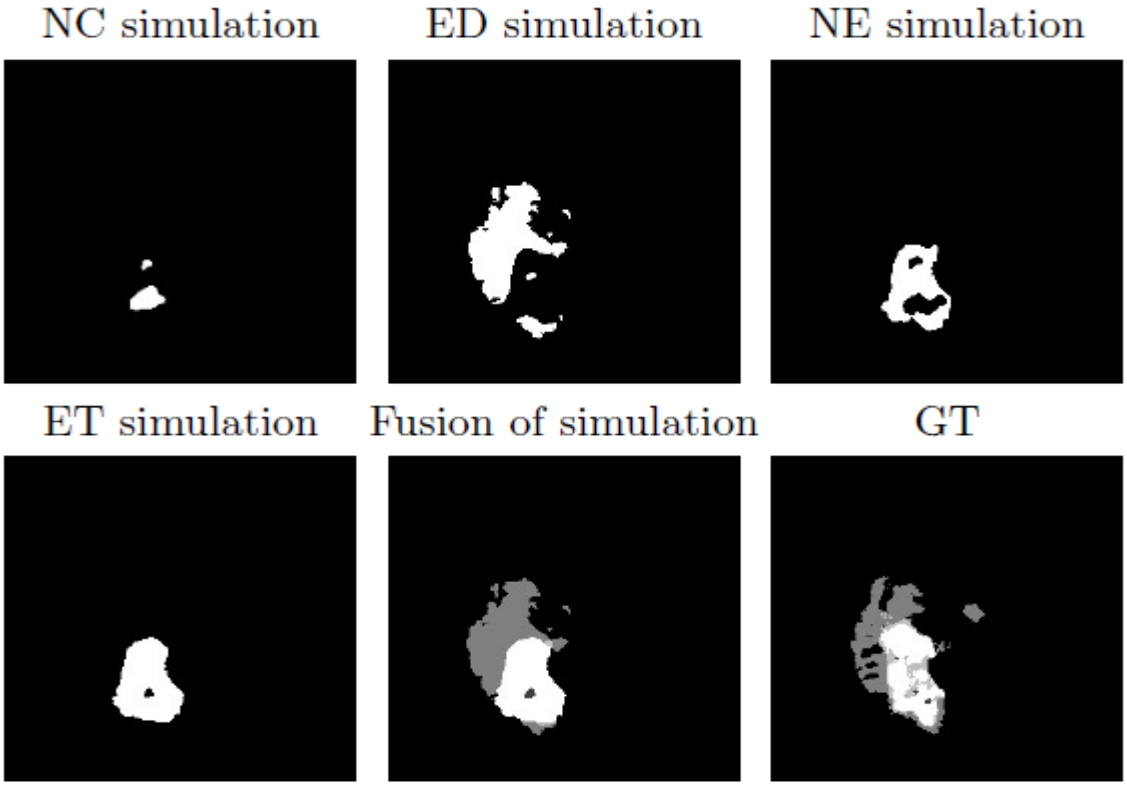

Figure 11. An example of longitudinal tumor growth by using proposed method for one slice of patient 439. (top left) Simulated NC with $D = 0.052$, $\rho = 0.01$. (top middle). ED with $D = 0.06$, $\rho = 0.009$. (top right) NE with $D = 0.03$, $\rho = 0.014$. (bottom left) ET with $D = 0.05$, $\rho = 0.01$. (bottom middle) Fused label and (bottom right) ground truth of the second scan data.

feature type for a patient.

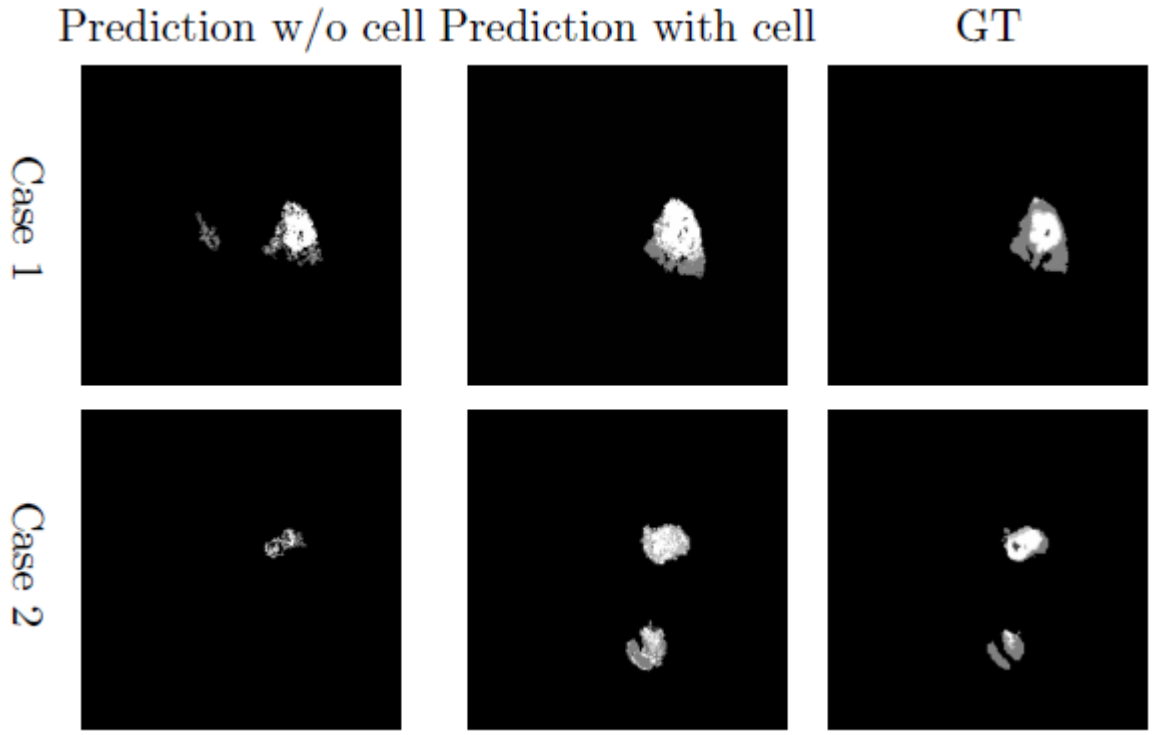

Figure 12. Examples of tumor segmentation prediction by using the proposed method. (Left column) Without cell density feature, (middle column) With cell density feature, and (right column) the ground truth of second time scan.

We evaluate the performance of the proposed method and compare the DSC to the segmentation prediction without cell densities features (Figure 13). We further evaluate the statistical significance of the obtained results using paired t-test for all patients. The p-values for segmentation prediction obtained with and without inclusion of the cell density feature show statistical significance for WT, TC, and ET tissues (Table 2). The paired t-test analysis shows that fusion of tumor growth pattern with texture and intensity features offers a significant improvement in the segmentation prediction of TC and ET tissue regions. However, the statistical analysis does not suggest significant improvement

for the WT tissue. We hypothesize that the reason for this is that the WT label, which

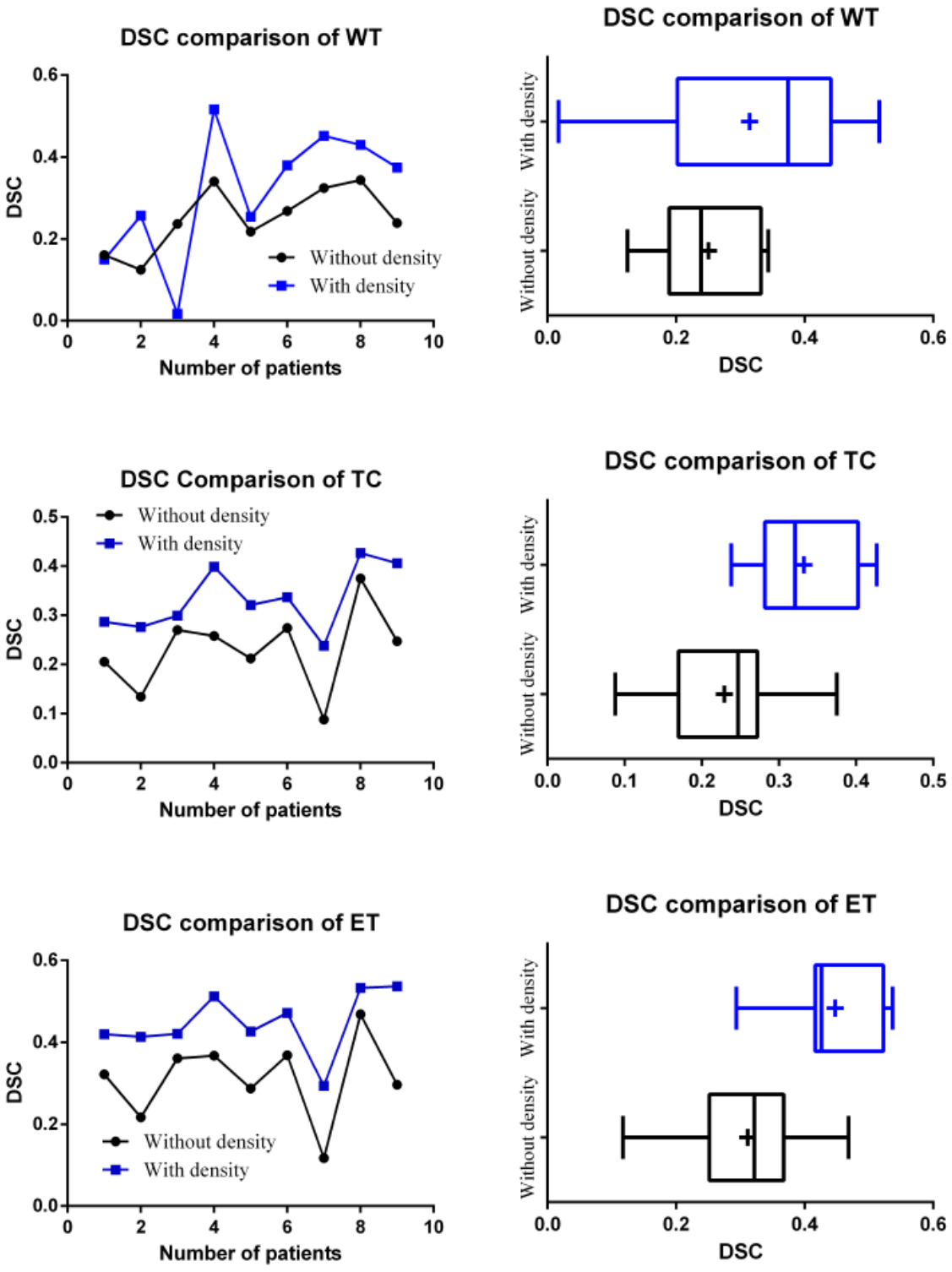

Figure 13. Comparison of tumor growth prediction segmentation using proposed method. Vertical line and "+" indicates the median and the mean, respectively.

represents the abnormal T2-FLAIR signal, is well-segmented by the originally applied method (GB, or RF) and hence there is not substantial significant improvement offered by the proposed method.

Table 2. Paired t-test for comparison of the volume between without and with cell density by using RF only to predict the tumor segmentation labels in timepoint 2, using data from timepoint 1.

	DSC_{WT}	DSC_{TC}	DSC_{ET}
Result w/o cell density	0.251 ± 0.08	0.229 ± 0.08	0.311 ± 0.101
Result with cell density	0.314 ± 0.16	0.332 ± 0.065	0.448 ± 0.076
p-value	0.150	0.0002	0.0002

3.6.2 Experiment with Joint Label Fusion-Based Method

We apply the joint label fusion-based brain tumor segmentation prediction to process data from all nine patients at timepoint 2 (post-op scans). To evaluate the performance, we use a Leave-One-Out cross-validation schema to compute the DSC of segmentations at timepoint 2 from the proposed method and compare to the ground truth and to segmentations generated by GB [48, 86] (Figure 14). An example segmentation prediction result is shown in Figure 15. From the collective summary of comparisons, we note that the proposed method offers better results than GB alone. The result DSC for the proposed method is 0.850 ± 0.055 for WT, 0.836 ± 0.041 for TC, and 0.837 ± 0.0074 for ET.

We also statistically evaluate the segmentation prediction results using ANOVA and the resulting p-values are shown in Table 3. The joint label fusion-based (JLF) method offers statistically significant improvements on tumor segmentation performance for the WT and ET regions, when compared to the results of the GB method. The overall performance is better than GB and RF across all patients, as shown in Figure 14.

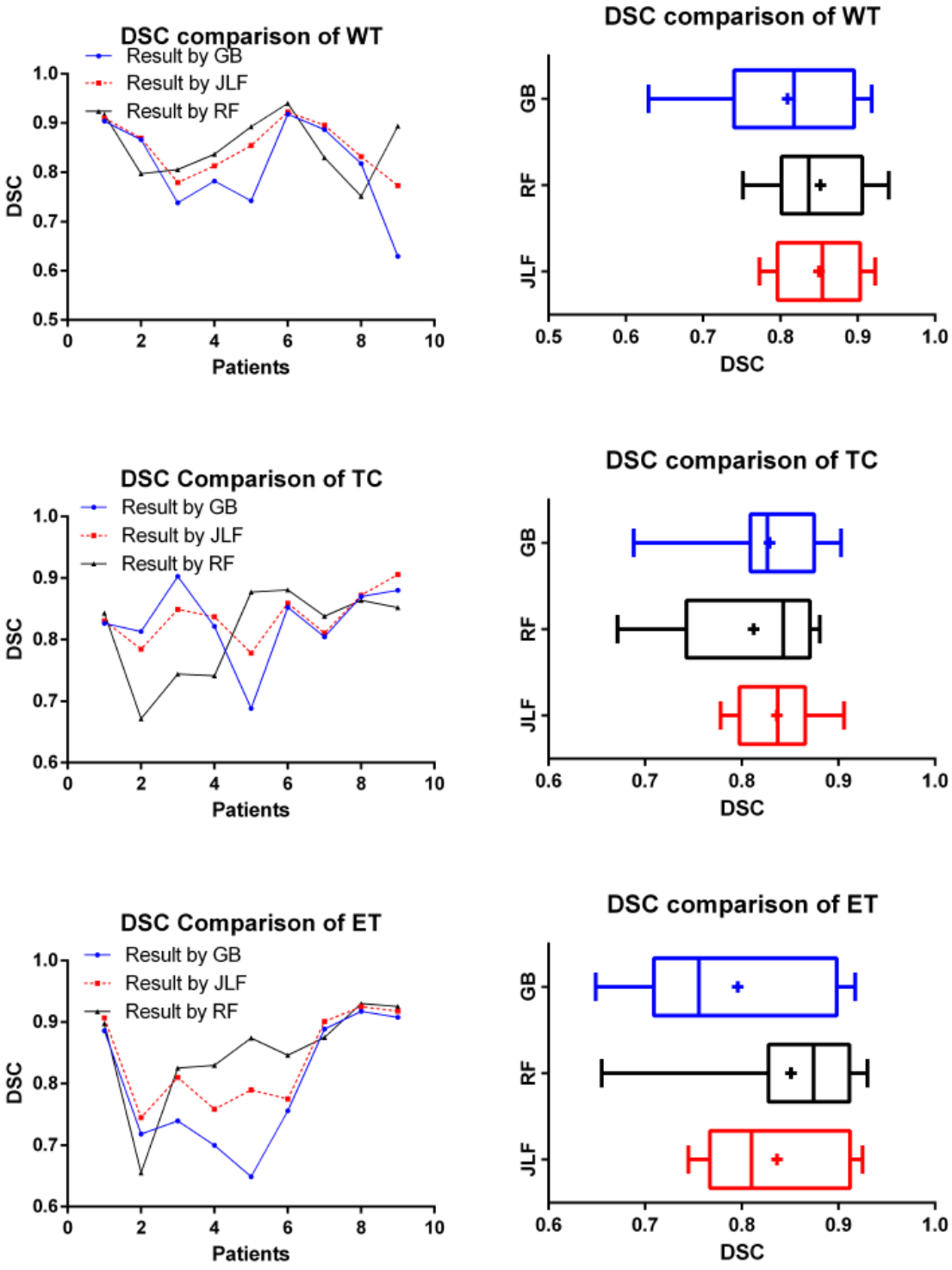

Figure 14. DSC comparison results among GB, RF, and proposed method (JLF) at time 2. Vertical line and "+" indicates the median and the mean, respectively.

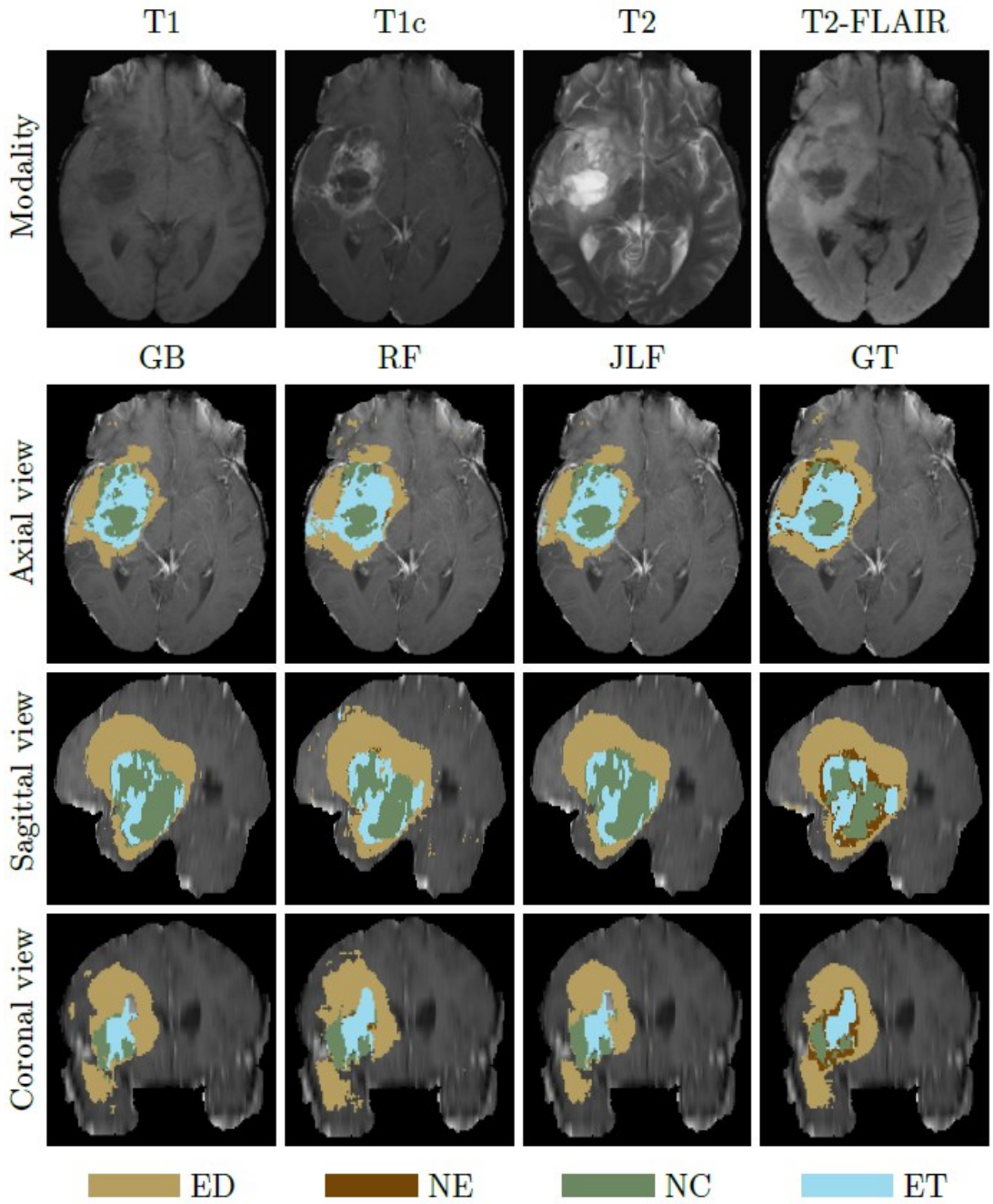

Figure 15. An example of label fusion-based application. The first (top) row denotes the input brain scans. Rows 2-4 illustrate shows the axial, sagittal, and coronal views, respectively, of the T1c input can overlaid with GB, RF, JLF and GT labels.

Table 3. Performance of 3D brain tumor growth prediction segmentation.

	WT	TC	ET
Average DSC by GB	0.810±0.095	0.829±0.062	0.796±0.104
Average DSC by RF	0.852±0.063	0.812±0.074	0.851±0.083
Average DSC by JLF	0.850±0.055	0.836±0.041	0.837±0.0074
Median DSC by GB	0.8177	0.8266	0.7557
Median DSC by RF	0.8369	0.843	0.8743
Median DSC by JLF	0.8544	0.8372	0.81
p-value (GB and JLF)	0.047	0.579	0.023

In addition, we also compare the proposed work with BraTumIA (BTIA) [49], a state-of-art tool that has been previously used for brain tumor segmentation in longitudinal scans. We applied BraTumIA to the patient data used in our experiments and the obtained results shown the superiority of our proposed approach (Table 4). Results for all experiments are also given in false positive and false negative rates (Appendix B).

Table 4. Longitudinal tumor segmentation comparison of average DSC between BraTumIA [49] and JLF.

	DSC_{WT}	DSC_{TC}	DSC_{ET}
BraTumIA [49]	0.761±0.104	0.703±0.186	0.732±0.140
JLF	0.850±0.055	0.836±0.041	0.837±0.075

3.7 Discussion

In this Chapter, we propose two methods for longitudinal brain tumor segmentation prediction, in longitudinal mMRI. Feature fusion using RF and tumor cell density offers improved performance for predicting longitudinal tumor growth. Specifically, this method shows significant prediction improvement of TC and ET abnormal tissues, while there is no significant improvement for WT tissue. On the other hand, the joint label fusion using RF and GB labels shows improvement on WT and ET abnormal tissues over that of the GB labels alone. Note due to availability of limited number of longitudinal tumor growth patient cases used in this study, the segmentation prediction performance is not optimal for all possible types of abnormal tissue.

CHAPTER 4

BRAIN TUMOR GRADING USING PHENOTYPE AND PROTEOMICS INFORMATION

4.1 Chapter Overview

This chapter proposes a joint analysis of histopathology and proteomics patient data using DNN for improving brain tumor grade type and subtype classification following new WHO tumor grade criteria. The work utilizes digital pathology images and four pieces of proteomics information (*IDH*, *X1p/19q codeletion*, *ATRX*, and *MGMT*) to obtain improved tumor classification accuracy. In addition, a specific shape-based measure for abnormal cell nuclei known as cellularity [90] is investigated for its efficacy in tumor subtype classification. Cellularity is used to indicate the probability of cancerous cells of the whole slide image (WSI). Specifically, our work discovers the potential role of cellularity in histopathology image and *IDH* type in proteomics data for subtype classification within Grade III brain tumor.

4.2 Introduction

Gliomas are primary brain tumors that originate from glial cells. Survival period of the glioma patients is highly related to the tumor type and grade. According to a recent report, five-year (2011- 2016) survival rate is 94.1% for pilocytic astrocytoma yet it is only 5.6% for glioblastoma [2]. Overall, 94.1% of patients with pilocytic astrocytoma (LGG grade II), 57.6% of patients with anaplastic oligodendroglioma (LGG grade III), 30% of patients with anaplastic astrocytoma (LGG grade III) survived five years after

diagnosis [2]. Therefore, accurate tumor classification and grading may help in making proper treatment planning and assessing overall prognosis in clinical practice.

Prior to 2016, the World Health Organization (WHO) standard for brain tumor classification has been based on only the histologic appearance in pathologic slides. Tumor grade is classified according to the microscopic similarities with different putative cells of origin and differentiation level [4]. The histological features of mitotic activity, microvascular proliferation and necrosis are used when grading the diffuse glioma. There are many studies in the literature for tumor grading using histopathology images [91-93]. As only histopathology data for tumor grading is no longer accurate and efficient, a new CNS brain tumor grade classification standard has been released by WHO in 2016 [4]. Due to the drawbacks of tumor grading based only histology, proteomics information has recently been used for tumor classification [53-56]. With the new standard for tumor grading, isocitrate dehydrogenase (*IDH*) mutation in proteomics information is identified as one of the major criteria [53].

Computational methods provide an additional method in analyzing proteomics and histopathology data. There are only few works that focus on tumor grade classification using both histopathology and proteomics information in the literature. Most of the tumor classification and grading manuscripts still focus on non-invasive structural MRI and proteomics information [94-96]. These works have specific limitations. First, for the structural MRI-based methods, the authors need to extract manually identified features before further analysis. Secondly, they may classify gliomas by using MRI and proteomics information separately. There has been intense work in literature using Deep Neural Network (DNN) for brain tumor classification [92, 97-99]. DNN is capable of

automatically learning features from raw data for classification of tumor types. A typical convolutional neural network consists of an input layer, multiple hidden layers, and an output layer. The hidden layers typically include convolution layers, activation function layers, pooling layers, and fully connected layers.

4.3 Background

CNS tumor grade classifications has been an intense research area. Based on the different types of patient data, tumor classification and grading methods are generally categorized in two groups: digital pathology-based, and proteomics-based methods. There have been a few works in non-invasive MRI-based tumor grading. Zacharaki *et al.* use a support vector machine (SVM) based machine learning method to classify brain tumor on combining conventional anatomic MRI and perfusion MRI. Their method achieves 96% accuracy for distinguishing LGG and HGG using leave-one-out cross validation [100]. Fusun *et al.* use a SVM to grade gliomas based on multi-parametric MRI [95]. In [96], authors use a machine learning based method for molecular subtyping of gliomas by analyzing the radiomics data. However, these methods may not be suitable for clinical use [100-103].

4.3.1 Digital Pathology-Based Method

Digital pathology images have been the primary source for tumor grade classification prior to the most recent WHO grade criteria. There are many works on tumor grading/classification in the literature. Yonekura *et al.* propose an improved disease stage classification using a convolutional neural network for glioma histopathology images [104]. They obtain classification accuracy is 87.15% for differentiating LGG and HGG.

Ertosun *et al.* propose a gliomas grading method using convolutional neural networks (CNN) [98], which achieves good results. Even though histopathology-based tumor grade classification of low-grade gliomas has been used widely, it is not suitable to predict clinical outcomes due to high intra- or inter-observer variability [91, 105]. Because of inaccurate tumor grade classification using only histopathology information, clinicians usually consider genetic classification to guide clinical decision-making for treatment planning and management of patients with brain tumors [53, 56, 106, 107].

4.3.2 Proteomics-Based Method

Proteomics studies of brain tumors have been critical to understand the proteomics underpinnings of neoplasms. For infiltrating gliomas, proteomics classification are more reliably reflected underlying tumor biology than traditional morphology [108]. proteomics underpinning of primary central nervous system has changed the perspective to tumor diagnosis and classification [108]. Few works study tumor grade by introducing proteomics information. *IDH* mutation has shown to be present in about 80% of LGG grade II and grade III and secondary HGG [109]. *IDH* 1/2 encodes the Krebs or citric acid cycle family of metabolic enzymes [54]. Furthermore, patients with *IDH*-mutated gliomas have significantly longer survival than for those with *IDH* wild-type tumor [55]. On the other hand, there are some works on tumor grading using histopathology data in the literature. Kong *et al.* proposed a computer-aided classifying grade of neuroblastic differentiation on whole-slide histology images [110]. Using a method called sequential floating forward selection (SFFS), the authors first segment nuclei, extract hand-crafted features, apply feature selection method and finally use k-nearest neighbor for classification. Barker *et al.* propose an automated brain tumor type classification in

whole-slide digital pathology images using local representative tiles [93]. In another work, nuclei segmentation is obtained by using hysteresis thresholding and watershedding, feature selection, and an Elastic Net Classification for brain tumor grading. In [92], Mousavi *et al.* proposed an automated brain tumor grade discrimination based on spatial domain analysis. The authors developed a method for cell segmentation and a customized operation of spatial and morphological filters to identify microvascular proliferation, then apply a hierarchical decision for LGG and HGG classification. Molecular mutation, such as *IDH 1/2, ATRX, 1p/19q codeletion, TERT,* and *MGMT* have also been studied for glioma proteomics classification [58].

Following the relationship between *IDH* mutation status and glioma classification, Chang *et al.* utilized a residual convolutional neural network to determine *IDH* status in low- and high- grade glioma from MR imaging [111]. By analyzing Japanese glioma patients with *IDH* mutations, Mukasa *et al.* found that *IDH* mutation with intact 1p/19q is useful when assessing prognosis of LGG grade III patients [57]. A strong association has been found between *IDH* canonical mutations and the alpha thalassemia/mental retardation syndrome X-linked (*ATRX)* mutation, whereas *X1p/19q codeletion* and *ATRX* loss barely exists simultaneously [112]. Leeper *et al.* proposed a better proteomics classification method using *X1p/19q codeletion*, *IDH mutation*, and *ATRX* for grade II diffuse glioma [113]. In addition ,the O6-methylguanine-DNA methyltransferase *(MGMT)* is believed to have been associated with longer survival in patient with glioblastoma (HGG) [114]. In Reference [107] the authors study glioma groups based on *X1p/19q*, *IDH* and telomerase reverse transcriptase *(TERT)* promoter mutation in tumors. They found that proteomics groups are interpedently associated with overall survival

among LGG grade II and grade III patients, but not among patients with glioblastoma. All these studies suggest that there is a lack of methods using both histopathology and proteomics data for tumor type and subtype classification as suggested by the latest WHO guidelines. Consequently, the proposed method in this work analyzes pathology images and proteomics data using DNN for achieving an improved tumor type and subtype grading.

4.4 Methodology

In the section, we discuss image pre-processing (color normalization), cellularity and the proposed method using DNN for glioma type and subtype grading.

4.4.1 Pre-processing of Histopathology Data

In histopathology, tissue sample images are commonly stained by a combination of hematoxylin and eosin (H&E). Hematoxylin binds to nuclei with a bluish-purple, and eosin stains acidophilic proteins with a red-pink. The stained tissue biopsies and microarrays are easy sharing and analyzing with computer algorithm [115]. However, due to the color corresponding to difference in slide scanners, there is an undesirable variation in color, which results in image interpretation difficulty. Color normalization can help both pathologists and software in comparing different tissue sample by standardizing image appearance. In this work, we utilize a structure-preserving color normalization and sparse stain separation proposed in [116] to normalize H&E stained tissue images. A given RGB image is converted to an optical density (X) based on Beer-Lambert law, then the stain separation is decomposed by non-negative constraints on the stain density (L) and color appearance matrix (W), which yields,

$$\min_{W,L} \frac{1}{2}\|X - WL\|_F^2 + \lambda \sum_{j=1}^{r} \|L(j,:)\|_1, \quad (23)$$

subjects to,

$$W, L \geq 0, \|W(:,j)\|_2^2 = 1, \quad (24)$$

where λ is sparsity and regularization parameter. r is the number of stains.

Then, the stain separation of source (X_s) and target X_t images are needed to factorize into color appearance and stain density map ($W_s L_s$ and $W_t L_t$). To preserve structure color normalization, we normalize the color appearance of a source image s to a target image t. Finally, we combine a scaled version of the density map with color appearance of the target image to create the normalized source image. It can be expressed as:

$$L_s^{norm}(j,:) = \frac{L_s(j,:)}{L_s^{RM}(j,:)} L_t^{RM}(j,:), \; j = 1, \cdots, r, \quad (25)$$

$$X_s^{norm} = W_t L_s^{norm}, \quad (26)$$

where $L_i^{RM} = RM(L_i) \in R^{r \times 1}, i \in s, t$ and RM computes the pseudo maximum of each row vector at 99%. The registered normalized source image is recovered by:

$$I_s^{norm} = I_0 \, exp(-X_s^{norm}), \quad (27)$$

where I_0 is the illuminating light intensity on the sample [116].

Figure 16 shows three examples of color normalization for different types of H&E tiles. Case A is a LGG grade II that shows oligodendroglioma with mutant *IDH*, wild-type (WT) *ATRX*, *X1p/19q codeletion* and Methylated *MGMT*. Case B is a LGG grade III which has astrocytoma with mutant *IDH*, mutant *ATRX*, non-codeletion of 1p/19q, and

unmethylated *MGMT*. Case C is a HGG that contains glioblastoma with WT *IDH*, WT *ATRX*, non-codeletion of *X1p/19q*, and unmethylated *MGMT*.

4.4.2 Cellularity in Histopathology Data

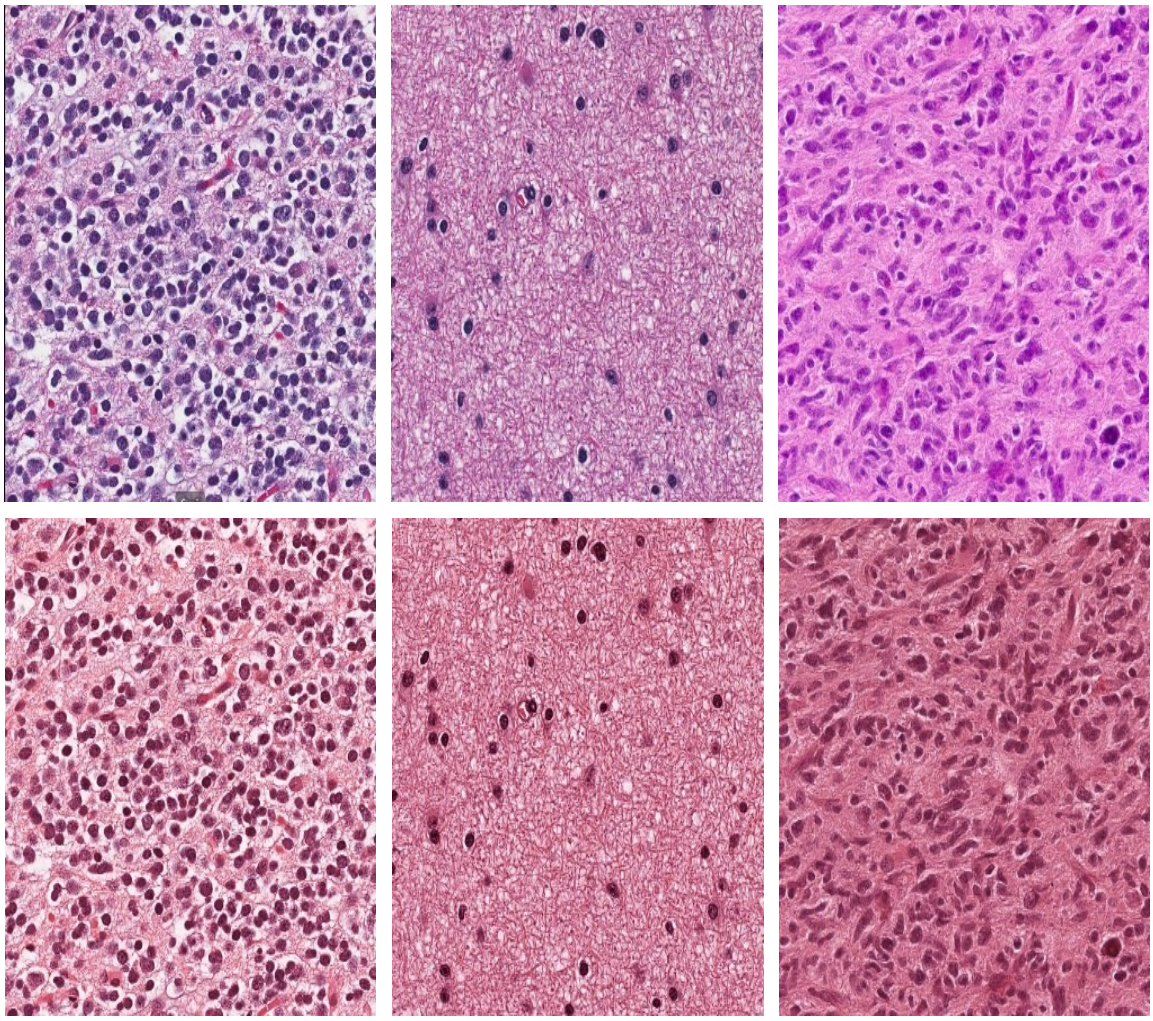

Figure 16. Three color normalization instances representing LGG grades II, III, and HGG. Top row showing original H&E, and bottom row showing the normalized H&E using proposed method. Column from left to right: case A (LGG grade II), case B (LGG grade III), and c (HGG).

Assessment of cellularity is an important component of tumor burden assessment. Cellularity is usually estimated by pathologists in clinical practice and has been used in

breast cancer analysis [90, 117]. The cellularity of any given image is computed as the ratio of the area of a cancerous cell over the whole image area. Nuclei segmentation followed by dilation of the cancerous cell is needed for computing the cellularity, then the cellularity is calculated by area of dilated cancerous cell area over the whole image area. Morphological dilation step is applied on the malignant nuclei to expand the malignant cancerous cells that may account for the presence of cytoplasm around each nucleus [90, 118]. The dilation size is set as 11 as in [90, 118]. Cellularity value ranges within 0 and 1. In our case, the dilation size is empirically set as 12. In general, LGG grade II is defined to have a small cellularity value while HGG has a large value of cellularity. Nuclei segmentation is implemented by using a deep learning based UNet method [119].

4.4.3 Proposed Tumor Grading Method

We use a cascaded convolutional neural network as the underlying model for tumor grading [11]. A multi-class (LGG grade II, LGG grade III, and HGG) classification problem is posed as step-wise binary classification problem. In the first step, we discriminate HGG and LGG using a regular DNN. For LGG, we further apply a residual neural network (ResNet [120]) to distinguish between LGG II and III. The proposed pipeline is shown in Figure 17. Note as our proposed method utilizes both digital pathology images and proteomics information, the resulting pipeline uses two types of DNNs. Finally, cellularity information is introduced to improve tumor type and subtype grading performance.

Accurate classification of LGG grade II from LGG grade III is more challenging as the two tumor types have very similar histopathologic appearance. The DNN model used

for LGG grade II/III is similar to that of LGG/HGG, however, the network contains more layers which may capture a subtle differences between two similar tumor grades. A ResNet architecture is used at the second step. The structure details of these DNNS are listed in Table 5.

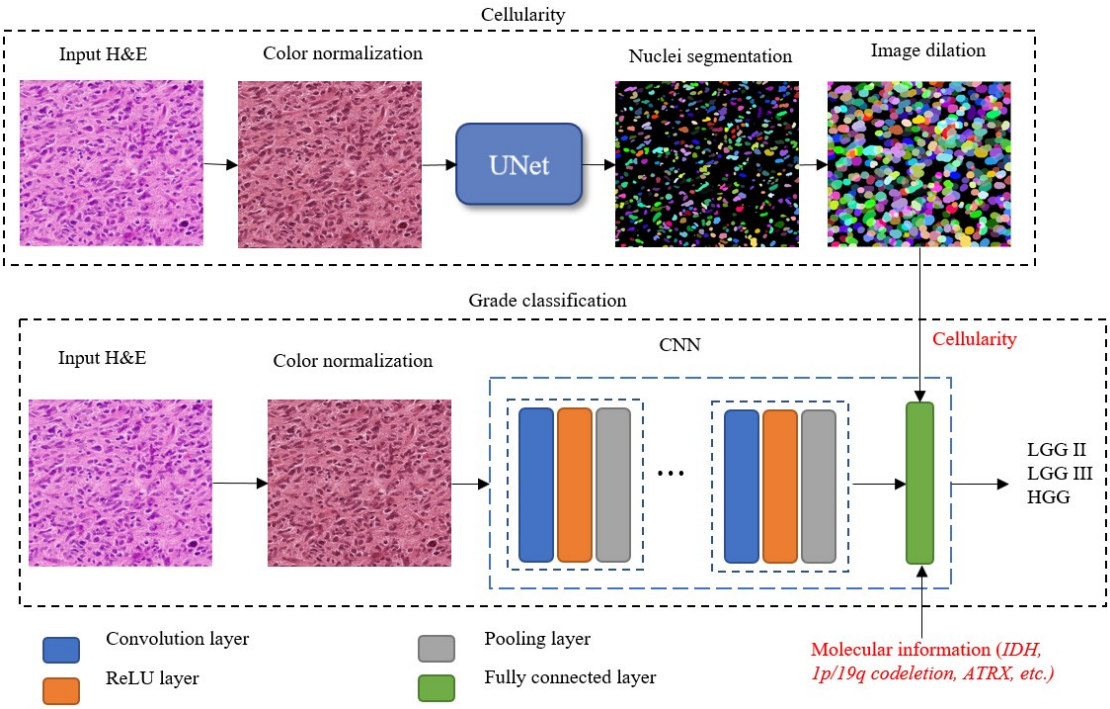

Figure 17. The pipeline has two parts: cellularity and grade classification. In cellularity part, nuclei segmentation of the input H&E is implemented using UNet architecture with Multi-Organ nuclei segmentation data set. Cellularity is computed by using the dilated image. For grade classification part, we use a cascaded DNN for distinguish tumor grade. The first DNN (DNN1) is to classify HGG and LGG, and the second DNN (DNN2) is to distinguish LGG II and III. In DNN module, we attach the proteomics information (*IDH*, *ATRX*, *X1p/19q codeletion* and *MGMT*) to the fully connected layer. For Resnet, there is a skip connection within each block.

Table 5. Deep neural network structures for CNN and ResNet. We show the data size of each layer. In each convolution block, it has 1 convolution layer, 1 ReLU layer, and 1 max pooling layer. We construct a more complex neural network for differentiating LGG II/III by considering the much similarity within them.

Layers	Output size of CNN	Output size of ResNet
Input	512*512*3	512*512*3
Conv. block 1	256*256*8	256*256*8
Conv. block 2	128*128*16	128*128*16
Conv. block 3	64*64*32	64*64*32
Conv. block 4	32*32*64	32*32*64
Conv. block 5	16*16*128	16*16*128
Conv. block 6	8*8*256	8*8*256
Conv. block 7	4*4*512	4*4*512
Conv. block 8	-	2*2*512
Conv. block 9	-	1*1*1024
FC layer 1	8192	1024
FC layer 2	128	128
FC layer 3	2	2

4.5 Experiments and Results

4.5.1 Data

We use 96 public digital diagnostic whole slide hematoxylin and eosin (H&E) stained histopathology images with proteomics and clinical information from The Cancer Genome Atlas (TCGA). The 96 whole slide image (WSI) contains 28 LGG grade II, 36 LGG grade III and 32 HGG. Each WSI can be larger than 1 GB. In order to process this large size image, we divide the WSI into multiple tiles with size 1000×1000. Therefore, we have an overall 96 tiles for the study. We select one tile as a reference, then apply color normalization for the rest of the tiles, so that all tiles have a similar color appearance that preserves original structure. For nuclei segmentation, the training H&E straining data is obtained from Multi-Organ nuclei segmentation challenge, which

contains 30 images and around 22000 nuclear boundary annotations for several organ tissues [65, 121].

To evaluate the proposed method, we use 8-fold cross validation. The dataset is randomly split as training and testing data based on tumor grade of LGG grade II, LGG grade III, and HGG with ratio 8:2. Moreover, in order to increase data sample, we crop sub-regions of patches with size of 512×512. In addition, we also apply data augmentation techniques (random rotation of $90^{\circ}, 180^{\circ}, 270^{\circ}$, random flipping image along axis, and random scaling image by $0.95 \sim 1.1$) to increase the number of training samples.

In our experiments, we consider *IDH1/2, ATRX, X1p/19q*, and *MGMT* as the proteomics information. The proteomics information distribution used in this work is listed in Table 6. There are four histologic glioma subtypes in the experimental data: astrocytoma (AA), oligoastrocytoma (OA), oligodendroglioma (OD), and glioblastoma (GBM). It is worth noting that oligoastrocytoma is strongly discouraged in new WHO classification [4].

Table 6. Proteomics data distribution of patient data used in this work.

Proteomics	Type	LGG grade II	LGG grade III	HGG
IDH	Mutant	25	27	1
	Wild-type	3	9	31
ATRX	Mutant	14	14	0
	Wild-type	13	22	17
	N/A	1	0	12
X1p/19q	Non-codeletion	22	29	32
	Codeletion	6	7	0
MGMT	Unmethylated	4	9	13
	Methylated	24	27	8
	NA	0	0	11

4.5.2 Experiments

First, we compute the cellularity feature as shown in Figure 18. The Figure shows three examples of cellularity. In general, patients with HGG have high value of cellularity, and small cellularity value for low-grade patients.

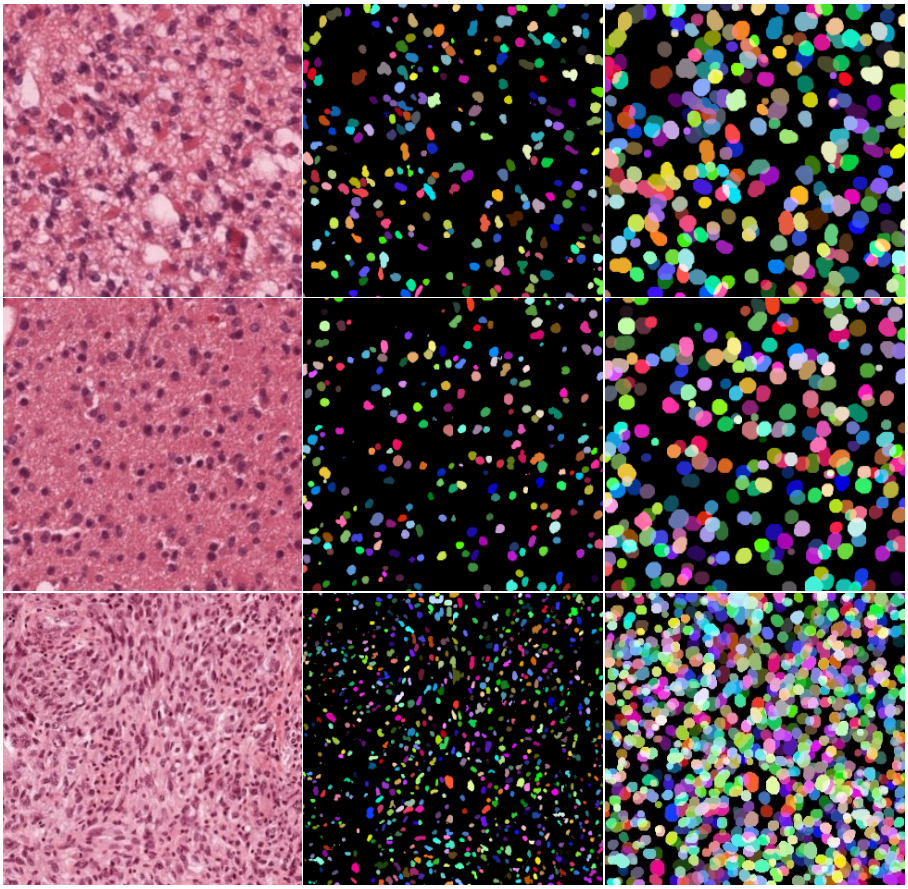

Figure 18. Three examples of tumor cellularity. Column one, two, three are color normalized image, segmentation, dilated segmentation image, respectively. Row1, Row2, and Row 3 are showing LGG grade II, LGG grade III, and HGG, respectively. Cellularity of Row 1, 2, and 3 are 0.4972, 0.4402, and 0.7582, respectively.

As discussed above we use a cascaded convolutional neural network for pairwise tumor grade classification. The proposed DNN is implemented using PyTorch 1.0 on high-performance clustering with Nvidia V-100 GPU. The minibatch size is set as 2 as

the tile size is large and maximum training epoch is set as 80. We use a binary cross-entropy as the objective function. In training phase, we minimize the cross-entropy loss [122] to optimize the model as follows:

$$loss = -\sum_{\forall x} p(x)\, log\big(q(x)\big), \tag{28}$$

where p is the true distribution, and q is the estimated distribution of class. In training phase, we use Adam [123] optimizer with initial learning rate of $lr_0 = 0.001$, and the learning rate (lr_i) is gradually decreased as:

$$lr_i = lr_0 * (1 - \frac{i}{N})^{0.9}, \tag{29}$$

where i is epoch counter, and N is a total number of epochs in training.

4.5.3 Tumor Type Classification

To investigate the impact of networks and cellularity, we compare the classification performance by using different network with and without cellularity. The average of accuracy over 8-fold cross validation is shown in Table 7.

Table 7. Performance of different networks with/without cellularity to tumor classification.

Tumor type	Cellularity information	CNN	ResNet
HGG vs LGG	No cellularity	94.91%	95.18%
	Cellularity	95.34%	94.42%
Grade II vs III	No cellularity	67.71%	69.06%
	Cellularity	66.80%	76.54%

Table 7 shows that the type of network and cellularity does not have noticeable impact on discrimination of HGG versus LGG. In comparison, cellularity shows improvement in the ability of ResNet to capture subtle difference between grade II and

III, and may help to significantly improve the classification accuracy for these two tumor types. The confusion matrix of the proposed method for ResNet with cellularity is shown in Table 8.

Table 8. Confusion matrix of the proposed method using image patches. In the method, we use CNN for discriminating HGG and LGG, and ResNet for distinguishing LGG grade II and III. Both are with cellularity.

		Predicted class		
Actual class		LGG grade II	LGG grade III	HGG
	LGG grade II	601	371	36
	LGG grade III	154	1107	36
	HGG	1	89	1063

This experiment investigates effect of different combinations of patient data using 8-fold cross validation for tumor type classification. The result is shown in Table 9. The regular CNN model offers the best performance when all information (pathology image, proteomics information, and cellularity) is considered with the best performance of 95.34% ± 4.67% for discrimination of LGG vs HGG. ResNet offers the best result with 76.54% ± 7.24% for classification of LGG2 and LGG3.

Table 9. Performance comparison by applying proposed method for different data information.

Tumor Type	Pathology, proteomics and radiology information	Network type	Glioma grading Accuracy
HGG-LGG	Pathology	CNN	92.48% ± 5.30%
	Pathology + proteomics	CNN	94.41% ± 3.69%
	Pathology + cellularity	CNN	93.43% ± 4.95%
	Pathology + proteomics + cellularity	CNN	**95.34% ± 4.67%**
LGG grade II-LGG grade III	Pathology	ResNet	64.84% ± 7.57%
	Pathology + proteomics	ResNet	68.89% ± 8.87%
	Pathology + cellularity	ResNet	66.23% ± 6.11%
	Pathology + proteomics + cellularity	ResNet	**76.54% ± 7.24%**

4.5.4 Tumor Subtype Classification

In this experiment, we study the effect of cellularity feature in discriminating between *IDH* mutation status that may indicate glial aggressiveness within a specific type of brain tumor. The results show potential correlation between cellularity and *IDH* types as shown in Table 10. It shows the average cellularity value and variance among different grade gliomas.

For LGG grade III and HGG, cellularity of glioma patient with Wild-type *IDH* is higher that of Mutant *IDH*. Note that cellularity of Wild-type *IDH* of LGG grade III (0.45) is close to that of Mutant *IDH* of HGG (0.44). Cellularity of glioma patient with Grade III, *IDH* 1/2 wild-type acts aggressively as that of glioblastoma patient with *IDH* 1/2 mutant type. This result suggests that one may predict *IDH* type, and hence, the tumor

subtype (aggressiveness) using the cellularity information. Table 10 also shows that cellularity of patient with *IDH*-mutant type is higher than that of wild type for LGG grade II.

Table 10. Average cellularity and variance for all grade gliomas with IDH type in our data.

Tumor grade	*IDH* mutant-type	*IDH* wild-type
LGG grade II	0.3769±0.0761	0.3908±0.1029
LGG grade III	0.4012±0.0834	0.4500±0.0920
HGG	0.4419	0.5580±0.1014

4.5.5 State-of-the-art Comparison

We compare our result in this work with existing works in the literature as shown in Table 11. Note that the comparison is qualitative rather than quantitative as the patient data, methods, and number of patients are all different for these works. The comparison Table shows that for tumor type classification, our work is comparable in differentiating HGG vs LGG, and offers the best performance on distinguishing LGG grade II vs LGG grade III. With addition of proteomics information, our proposed method offers the highest accuracy for LGG grade II vs. grade III classification.

Table 11. Performance comparison with state-of-art. Accuracy percentage in bold is the best result in the comparison. "-" sign indicates the data is non-available.

Authors	Image type	Number of patients	Method	Accuracy of HGG vs LGG	Cross-validation	Accuracy of LGG II vs LGG III
Mohana Priya K, *et al.[97]*	MRIs	231	SVM	78.26%	-	-
Mehmet G. Ertosun, *et al.* [98]	WSI	7	CNN	96%	-	71%
Ajay Basavanhally *et al.* [124]	WSI	126	Multifield-of-view classifier	93%	-	72%
Mousavi, *et al.* [92]	WSI	138	Decision-tree	84.7%	-	-
Jocelyn Barker, *et al.* [93]	WSI	302	Elastic Net classifier	93.1%	5	-
Aditya Bagari, *et al.*[125]	MRI+Pathology	20	CNN	-	-	90%
Shamim Reza, *et al.* [94]	MRI+ proteomics	66	Random forest	86%	10	-
	WSI+ proteomics	66	SVM	93%	10	-
Our proposed method	WSI+ proteomics	96	CNN	93.11%	8	76.54%

We further compare the preformation of tumor subtype classification using our proposed method to the state-of-the-art. We achieve tumor subtype classification accuracy 71.42%, 62.31%, 68.18%, 96.77% for astrocytoma (AA), oligoastrocytoma (OA), oligodendroglioma (OD), and Glioblastoma (GBM), respectively. In comparison the authors in [126], report accuracy of 65.85%, 46.50%, 60.26%, and 95.54%, for the same tumor subtypes as shown in Table 12. Note unlike [126] our proposed method in this work report both tumor type and subtype classifications following the new WHO criterion.

Table 12. Tumor subtype classification comparison to state-of-the-art.

	AA	OA	OD	GBM	AO
Work in [126]	65.85%	46.50%	60.26%	95.54%	25%
Our method	71.42%	62.31	68.18%	96.77%	-

4.6 Conclusion

In this Chapter, we propose a deep learning-based method for improving brain tumor type and subtype grading using both pathology and proteomics data following the new 2016 WHO classification. The classification method integrates a cellularity feature which is derived from morphology of histologic images to improve classification performance. The experiments show that while type of DNN may not be critical in discrimination of low-grade from high-grade glioma, DNN may have significant impact for discriminating grade II versus grade III. Moreover, we investigate the impact of proteomics and cellularity information on glioma grading. An interesting finding of this work is that the cellularity features show promise in prediction of subtype of LGG grade III with *IDH* mutation. Specifically, for patient with LGG grade III, cellularity of wild-type *IDH* is higher than that of mutant-type, suggesting that cellularity feature obtained from pathology image may be used to classify more aggressive wild-type *IDH* subtype of LGG grade III. These findings may be beneficial to tumor prognosis and treatment planning. In the future, we plan to apply the proposed method for larger patient data to validate the findings in this study.

CHAPTER 5

BRAIN TUMOR SEGMENTATION, TUMOR SUBTYPE CLASSIFICATION, AND SURVIVAL PREDICTION USING DEEP NEURAL NETWORK

5.1 Chapter Overview

This chapter proposes context-aware deep learning for brain tumor segmentation, subtype classification, and overall survival prediction using structural multimodal magnetic resonance images (mMRI). We first propose a 3D context-aware deep learning, that considers uncertainty of tumor location in the radiology mMRI image sub-regions, to obtain tumor segmentation. We then apply a regular 3D convolutional neural network (CNN) on the tumor segments to achieve tumor subtype classification. Finally, we perform survival prediction using a hybrid method of deep learning and machine learning. To evaluate the performance, we apply the proposed methods to the Multimodal Brain Tumor Segmentation Challenge 2019 (BraTS 2019) dataset for tumor segmentation and overall survival prediction, and to the dataset of the Computational Precision Medicine Radiology-Pathology (CPM-RadPath) Challenge on Brain Tumor Classification 2019 for tumor classification. The online evaluation performance suggests that the proposed method offers robust tumor segmentation and survival prediction, respectively. Furthermore, the tumor classification results in this work was ranked second place in the testing phase of the 2019 CPM-RadPath global challenge.

5.2 Background

Gliomas are the most common primary brain malignancies, with varying degrees of aggressiveness, variable prognosis and various heterogeneous regions [1]. In the US, the overall average annual age-adjusted incidence rate for all primary brain and other central nervous system (CNS) tumors has been reported as 23.03 per 100,000 population during 2011-2015 [2]. For patients with malignant tumors, the estimated five- and ten- year relative survival rates are 35.0% and 29.3%, respectively, according to the report from 2011-2015 [2]. The median survival period of patients with glioblastoma (GBM) is about 12-15 months [5]. Diagnosis of tumor subtype and grade is vital for treatment planning and prognosis of the patients. According to a 2016 report of World Health Organization (WHO), classification of tumors in the CNS is based on both phenotype and genotype (i.e., *IDH* mutation and *X1p/19q codeletion* status) [4]. However, structural imaging such as magnetic resonance imaging (MRI) is continued to be used for identifying, locating, and classifying brain tumors [13, 100, 127, 128]. Tumor subtypes include diffuse astrocytoma, *IDH*-wildtype/-mutant, oligodendroglioma, *IDH*-mutant and *1p/19q-codeleted*, glioblastoma, *IDH*-wildtype, etc. [4]. Traditional machine learning-based methods, such as support vector machines (SVM), k-nearest neighbors algorithm (KNN), and random forest (RF) are generally utilized for brain tumor analysis [14, 15, 31, 94, 129-131]. However, these methods have the common limitation of hand-crafted feature extraction in the modeling phase.

Deep learning-based methods overcome the drawback of hand-crafted feature extraction. Deep learning has made it possible to build large-scale trainable models that have the capacity to learn the optimal features required for a given task. Deep learning is powerful and outperforms traditional machine learning in many fields, such as computer

vision [132-134], medical image segmentation [119, 135], and speech recognition [136]. Deep learning is fundamentally composed of a deep neural network structure with several layers. An artificial neural network utilizes a backpropagation algorithm to decrease the error between the prediction and ground truth. However, training artificial neural network models becomes more difficult as the number of layers increase [137]. Deep neural network training has been feasible since the mid-2000s, which brought about increased availability of large datasets and hardware improvements.

As a standard protocol for brain tumor characterization, MRI is able to capture a diverse spectrum of tumor phenotypes [138]. Multimodal MRI (mMRI) provides comprehensive tumor information. For example, post-contrast T1-weighted (T1ce) images are well-known to be correlated with blood brain barrier (BBB) disruption, while T2-weighted (T2) and T2 Fluid Attenuated Inversion Recovery (FLAIR) images are well-known for capturing tumor margins and peritumoral edema [138]. This suggests that the phenotypic differences at the cellular level are also reflected in the imaging phenotype (appearance and shape). While mMRI captures comprehensive brain tumor information, extracting this information through brain tumor analysis, such as tumor segmentation, remains challenging because of the similar phenotypic appearance of abnormal tissues in mMRI images. Figure 19 shows the intensity distribution of three types of abnormal brain tissues in T1, T1ce, T2, and FLAIR images for a representative case. These intensity distributions are highly similar for tumor tissues for all patients in this study. While on T1ce image, enhancing tumor (ET) is easily separable from others, the necrosis (NC) and peritumoral edema (ED) have nearly the same intensity distribution.

Brain tumors have been studied for many years. However, most works study tumor segmentation, classification, and overall survival prediction independently, ignoring the underlying relationship among these critical analysis tasks. In this work, we propose a complete framework for brain tumor study, including tumor segmentation, subtype classification, and overall survival prediction by analyzing mMRI via a deep learning-based neural network architecture.

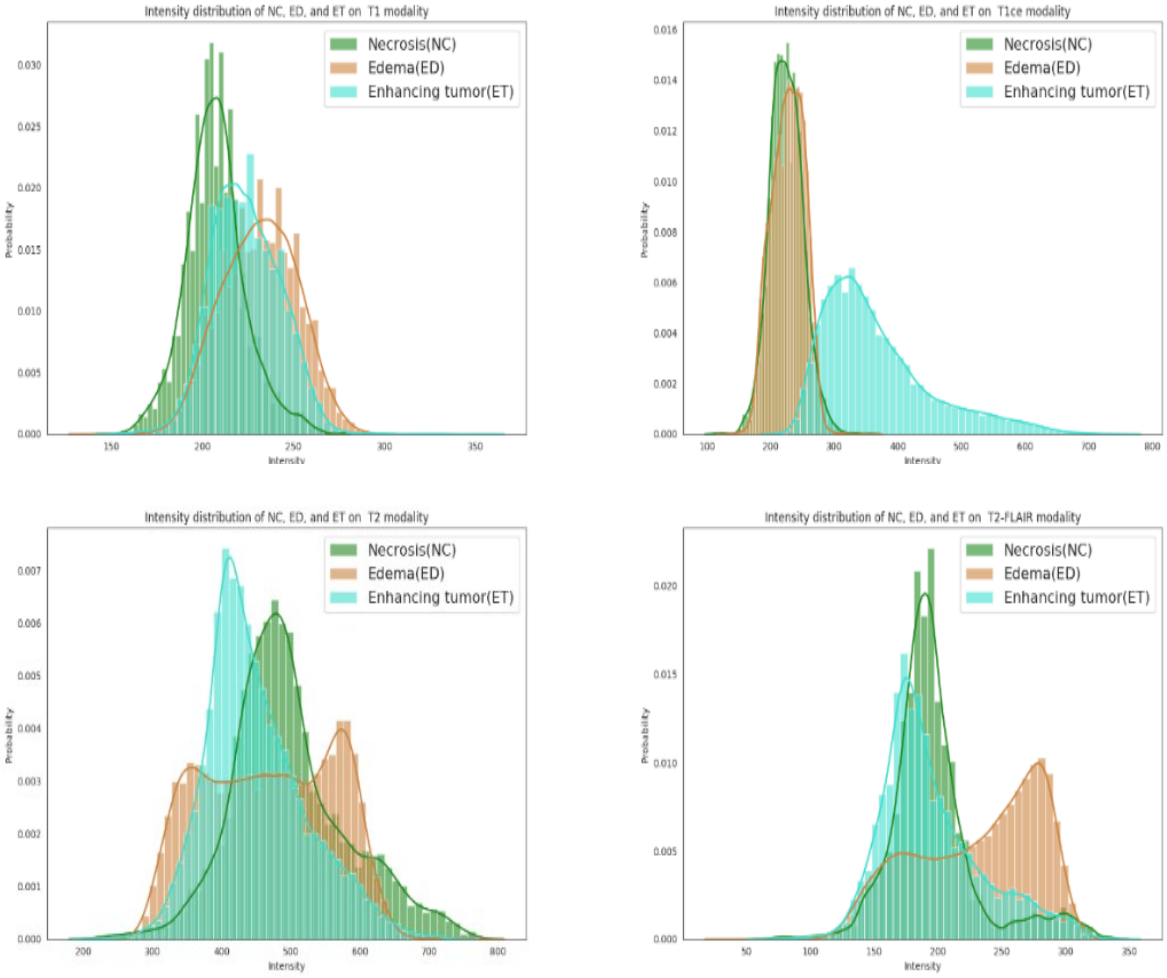

Figure 19. Intensity distribution of necrosis, edema, and enhancing tumor on T1 (top left), T1ce (top right), T2 (bottom left), and FLAIR (bottom right) images of one case.

5.3 Methodology

There are many methods reported in the literature on brain tumor segmentation that include intensity-based, atlas-based, deformable model-base, hybrid-based, and deep learning-based methods [139]. Recently, deep learning-based methods offered better performance for tumor segmentation [29, 33, 34]. For tumor classification, both non-invasive structural MRI and pathology images are utilized to classify brain tumors [126, 140, 141]. Overall survival prediction is to estimate the remaining life span of a patient with brain tumors. Most existing work is based on traditional machine learning and linear regression [1, 142].

Figure 20 illustrates an overview of the proposed framework. In A, there are four raw MRI modalities: T1, T1ce, T2, and FLAIR. The raw images are pre-processed in B, including co-registration, skull-stripping, noise reduction, etc. We then perform a z-score normalization for the brain region only to have zero mean and unit standard deviation. Subsequently, the proposed Context Aware Deep Neural Network (CANet) is applied to segment tumor as shown in C. The segmentation results are shown in D. In E, a 3D CNN is utilized to classify tumor using the segmented abnormal tissues. In F, we extract high-dimensional features using front-end of the CANet, and then apply a linear regression for overall survival prediction.

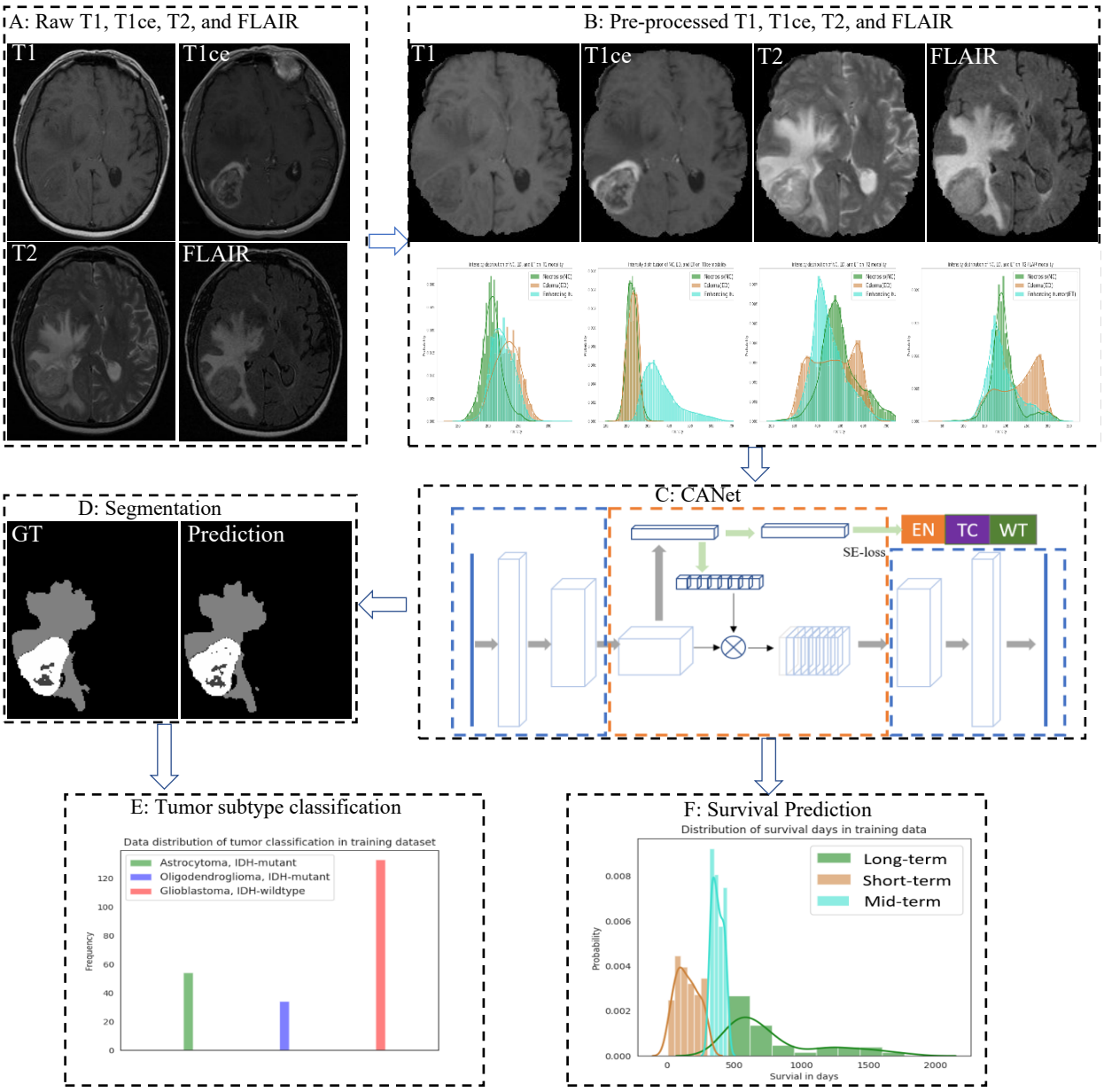

Figure 20. Overview of the methodology and overall work flow.

5.3.1 CNN-Based Tumor Segmentation

An overview of the proposed context-aware deep learning method for tumor segmentation is shown in Figure 21. The proposed CANet captures global texture features and utilizes semantic loss to regularize the training error [143] [119]. The

architecture consists of encoding, context encoding, and decoding modules. The encoding module extracts high-dimensional features of the input. The context encoding module produces updated features and a semantic loss to regularize the model. The decoding module reconstructs the feature maps to an output prediction, so that we compute the difference between the reconstructed output and input images as a regularizer.

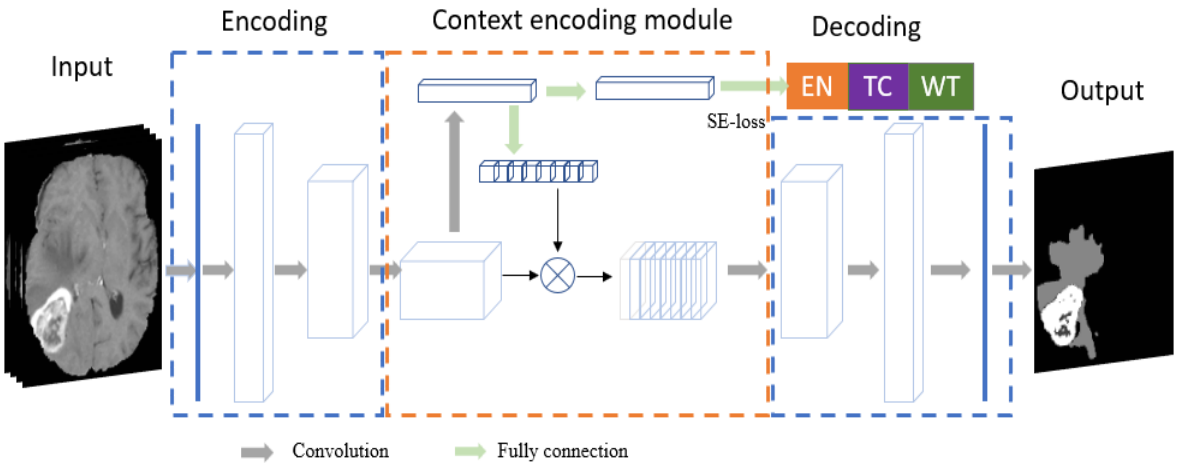

Figure 21. Overview of the proposed CANet architecture for tumor segmentation. It consists of encoding, decoding, and context encoding modules. Encoding and decoding module are UNet-like symmetric. Context encoding module produces semantic loss.

5.3.2 CNN-Based Tumor Classification

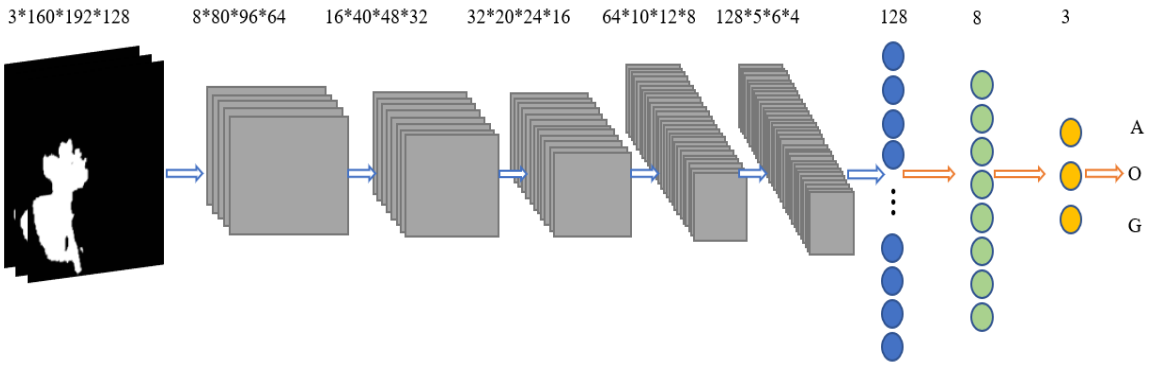

Figure 22. Overview of CNN-based tumor classification. At the last convolutional layer, we apply an average pooling layer to shrink the size.

The pipeline for tumor classification is shown in Figure 22. Overview of CNN-based tumor classification. At the last convolutional layer, we apply an average pooling layer to shrink the size. In this work, the segmented tumor uncertainty in subregions (ET, TC, and WT) from the above section are used as the input of the proposed tumor classification model. We use a regular CNN-based architecture for tumor classification. The probabilities of tumor subregions are convolved and down sampled, then passed through three fully connected layers to achieve classification.

5.3.3 Hybrid Method for Survival Prediction

Instead of extracting features and using a traditional machine learning approach, we utilize the proposed CANet to extract high-dimensional features. We believe that the extracted features from tumor segmentation are associated with overall survival. The features are then selected using the LASSO method [144]. Finally, we apply a linear regression to the selected features for overall survival prediction (as shown in Figure 23).

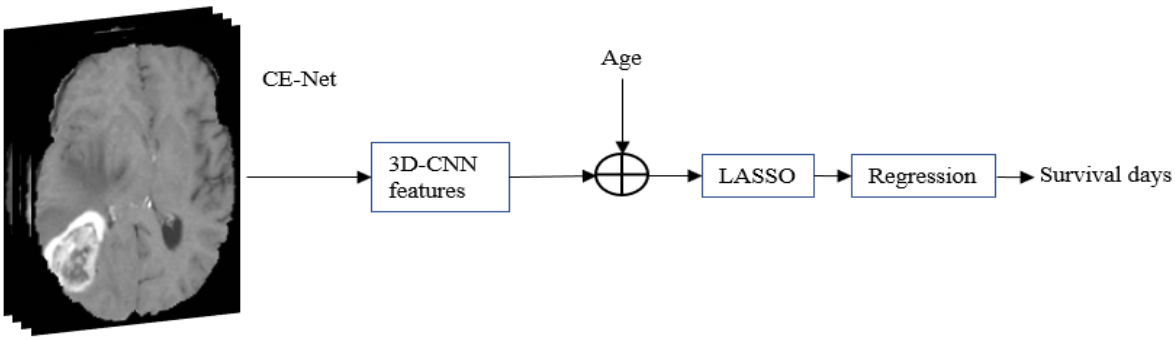

Figure 23. Pipeline of proposed method for overall survival prediction.

5.4 Experiments and Set UP

5.4.1 Data Description

In this work, the experimental data is obtained from Multimodal Brain Tumor Segmentation Challenge 2019 (BraTS 2019) [1, 12, 145-147] for brain tumor segmentation and overall survival prediction and Computational Precision Medicine: Radiology-Pathology Challenge on Brain Tumor Classification 2019 (CPM-RadPath 2019) [148] for tumor classification. The BraTS 2019 dataset includes training, validation, and testing data. The training data has a total of 335 cases consisting of 259 HGG and 76 LGG cases. There are 102 cases obtained from The Cancer Imaging Archive (TCIA) [149], and the rest are from private dataset. Only cases with gross total resection (GTR) are evaluated for overall survival prediction. In addition, there are another independent 125 and 166 cases for the validation and testing phases, respectively. Note that, the grading information, resection status, and ground truth are privately owned by the challenge organizer and not available for public use. For the CPM-RadPath 2019 dataset, training, validation, and testing data are also provided. There are 221, 35, and 73 cases for training data, validation data, and testing data, respectively. Ground truth is available for only the training data. In both datasets, the multimodal MRIs have been pre-processed by the organizers following the protocol in [145]. The summary of gender information for both training datasets is shown in Table 13.

Table 13. Experimental training data summary.

	Gender			Total
	Male	Female	Unknown	
Tumor segmentation	90	76	169	335
Tumor classification	52	46	123	221
Survival prediction	65	41	104	210

For segmentation, the tumor ground truth consists of one/more abnormal tissue(s): necrosis (NC), peritumoral edema (ED), and enhancing tumor (ET). However, performance evaluation is based on tumor sub-regions: enhancing tumor (ET), tumor core (TC), and whole tumor (WT), where TC consists of ET and NC. WT is a combination of TC and ED. For tumor classification, there are three subtypes: lower grade astrocytoma with *IDH*-mutant (Grade II or III), oligodendroglioma with *IDH*-mutant, *X1p/19q* codeleted (Grade II or III), and glioblastoma and diffuse astrocytic glioma with proteomics features of globlastoma, *IDH*-wildtype (Grade IV). For overall survival prediction, there are three categories: short-term (<10 months), mid-term (between 10-15 months), and long-term (>15 months).

5.4.2 Experimental Setup

All experiments in this study are performed in accordance with relevant guidelines and regulations as approved by the institutional IRB committee at Old Dominion University.

Experiment 1: brain tumor segmentation. A total of 335 patients are used for training, and 125 patients are used for validation. Note that the ground truths of the validation dataset are not available to public. At the validation and testing phases, we submit the segmentation results to the challenge portal for BraTS 2019 Online evaluation [150]. For the hyperparameters of the proposed context-aware deep learning, the initial learning rate is set to 0.0001, and decays gradually to 0 at the end of training. Total number of epochs is set to 500. The Adam optimizer is used [123] for gradient descent optimization. In

order to prevent overfitting in the training phase, we apply the Leaky-Relu activation function and drop out with a ratio of 0.2.

Experiment 2: brain tumor classification. There are 221 cases provided in the training phase. We randomly take 80% of the data as training, and use the remaining 20% as our own validation set, while maintaining the same proportion of each tumor subtype in each set. The ground truth of the validation and testing data are privately held by the challenge organizer. In validation phase, we submit the results for CPM-RadPath online evaluation [26]. The hyperparameters are similar to those used in tumor segmentation, but with total number of epochs is set to 2000. Note that for the testing phase, challenge participants are required to submit the wrapped algorithm using Docker [151], a platform to develop, deploy, and run applications inside containers, and tested by the organizer. The ranking is based on the performance evaluated by the organizer. Throughout the process, only the challenge organizer is involved in the testing evaluation.

Experiment 3: overall survival prediction. For the training phase, we randomly split the training data into 80% and 20% sets for training and validation, respectively, while maintaining the same proportion of cases from each risk category in each set. We then apply the trained model to the validation data for online evaluation, and finally apply to the testing data for ranking. The training hyperparameters are similar to that of tumor segmentation, but with total number of epochs is set to 1000.

5.4.2 Evaluation Metrics

For tumor segmentation, dice similarity coefficient (DSC) and Hausdorff distance are used to measure the segmentation quality [89]. DSC quantifies the overlap between two

subsets. It is computed as $DSC = \frac{2|A \cap B|}{|A \cup B|}$ [89], where A and B are two subsets. DSC of 0 means no overlap at all between the subset A and B. DSC of 1 indicates that the subsets are perfectly overlapped. Hausdorff distance measures how far two subsets of a metric space are from each other. It is calculated as $d_H(A, B) = \max\{h(A, B), h(B, A)\}$, where $h(A, B) = \max_{a \epsilon A} \min_{b \in B} \|a - b\|$, $\|\cdot\|$ is the norm operator [152]. Smaller Hausdorff distance means that the two subsets are closer. For evaluation of tumor classification and overall survival prediction, accuracy, and mean square error (MSE) are used.

5.5 Results and Contributions

5.5.1 Results

Experiment 1: brain tumor segmentation. Figure 24 shows a visual comparison of tumor tissue segmentation in axial, coronal, and sagittal views for a representative case for BraTS 2019. The dice similarity coefficient (DSC) and training loss changes are shown in Figure 25. The quantification performance of the validation dataset offered by online evaluation is shown in Table 14. In the Table, row one is the performance without post-processing, while row two is the performance with post-processing steps that includes small object removal and hole filling. We then test the proposed method with BraTS 2019 dataset consisting of 166 cases with unknown tumor grade. The online evaluation offers average DSC of 0.8133, 0.8867, and 0.84031 for ET, WT, and TC, respectively. According to the performance comparison in Table 14, DSC of WT is 1% lower than in the validation phase. However, DSC of ET and TC shows 6% and 4% improvement in the testing phase. Note that the Hausdorff distance in the testing phase is

consistently lower than that of the validation phase. These results suggest that our model offers stable and reliable tumor segmentation results.

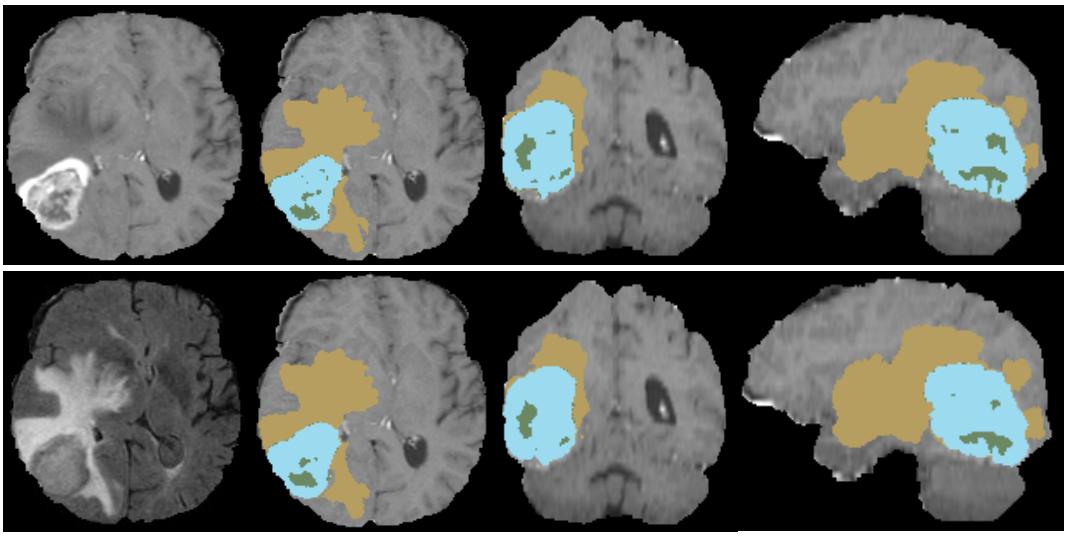

Figure 24. Comparison of tumor segmentation using the proposed method and ground truth. Top row from left to right: T1ce image, segmented tumor overlaid with T1ce in axial view, in coronal view, and in sagittal view. Bottom row from left to right: FLAIR image, ground truth overlaid with T1ce in axial view, in coronal view, and in sagittal view.

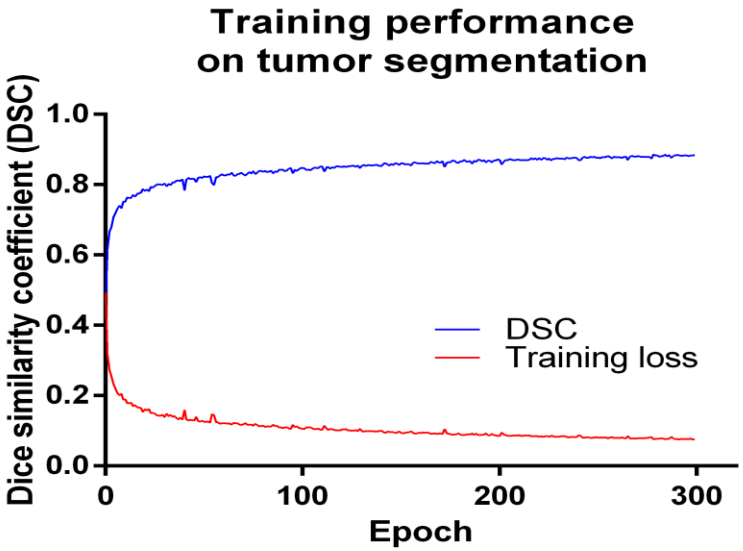

Figure 25. The DSC and loss changes in training stage.

Table 14. Dice coefficient results for tumor segmentation in the validation and testing datasets.

Phase	Post-process	Dice_ET	Dice_WT	Dice_TC	Hausdorff 95_ET	Hausdorff 95_WT	Hausdorff 95_TC
Validation	No	0.73856	0.90496	0.81496	4.09623	4.91633	6.80917
Validation	Yes	0.77273	0.90496	0.81496	3.22012	4.91633	6.80917
Testing	Yes	0.8133	0.8867	0.84031	2.22904	4.78833	4.14805

Experiment 2: tumor classification. We applied the proposed method to CPM-RadPath 2019 validation dataset, then wrapped the trained model using Docker [151], and shared with the CPM-RadPath Challenge organizer. In the testing phase, the organizer executed the wrapped algorithm to obtain tumor subtype classification result for the final competition. The online performance of validation (35 cases) and testing datasets (73 cases) is shown in Table 15. In the testing phase, our result is ranked at 2nd place [27].

Table 15. Online evaluation of tumor classification on CPM-RadPath 2019 validation and testing datasets.

Phase	Dice	Average	Kappa	Balance_acc	F1_micro
Validation	0.749	0.764	0.715	0.749	0.829
Testing	0.596	NA	0.39	0.596	0.603

Experiment 3: overall survival prediction. There are only 29 valid cases in BraTS 2019 validation dataset. Our accuracy is 0.586 using online evaluation, as shown in Table 16. In the testing phase (107 cases), the proposed method offers an accuracy of 0.439 with mean square error (MSE) of 449009.

Table 16. Survival prediction performance of the validation dataset obtained from online evaluation.

Phase	Accuracy	MSE	medianSE	stdSE	SpearmanR
Validation	0.586	79146	24362	113801	0.502
Testing	0.439	449009	44604	1234471	0.279

5.5.2 Contributions

To the best of our knowledge, brain tumor segmentation, tumor subtype classification, and overall survival prediction have been studied independently, ignoring the inherent relationship among them. In this work, we propose an integrated method for brain tumor segmentation, tumor subtype classification, and overall survival prediction using deep learning and machine learning methods. The specific contributions are as follows.

First, we propose a context-aware deep learning-based method for brain tumor segmentation. Second, we utilize a hybrid method for overall survival predication. Specifically, we extract high-dimensional features using the proposed context aware based convolutional neural network (CANet), and subsequently perform a traditional machine learning method to select features, and finally apply a linear regression method for overall survival prediction. Third, in the framework, all sub-tasks are intercorrelated via the proposed deep learning methods, rather than studied independently.

Finally, though new WHO tumor classification criteria indicate the use of both pathology images and proteomics information along with MRI, the proposed method is effective in tumor classification using structural MRI data only. The proposed tumor classification results in this work is ranked second place in the testing phase of the 2019 CPM-RadPath global challenge among 86 registered teams.

5.6 Discussion

Deep learning-based methods have been widely applied to many fields, and have achieved start-of-the-art performance. However, brain tumor segmentation poses several unique challenges. First, image quality has a critical impact on segmentation

performance. For example, blurred images result in poor outcomes. Second, image pre-processing steps also have an impact on the performance. For example, intensity normalization across cases is critical for tumor segmentation. Third, tumor tissue heterogeneity may pose a serious challenge to the developing an effective method. Finally, data imbalance is common and poses another intricate challenge for the use of deep learning. Figure 26 shows the data distribution in the training phase for tumor classification and overall survival prediction in our experiments. Cases of glioblastoma make up more than 50% of the training data. In survival prediction, range of survival days for mid-term survival is too narrow compared to the short- and long-term ranges, creating a data imbalance. This data imbalance can result in misclassification. In segmentation step, samples for edema is generally much more than other abnormal tissues. In order to address the potential data imbalance problem in tumor segmentation,

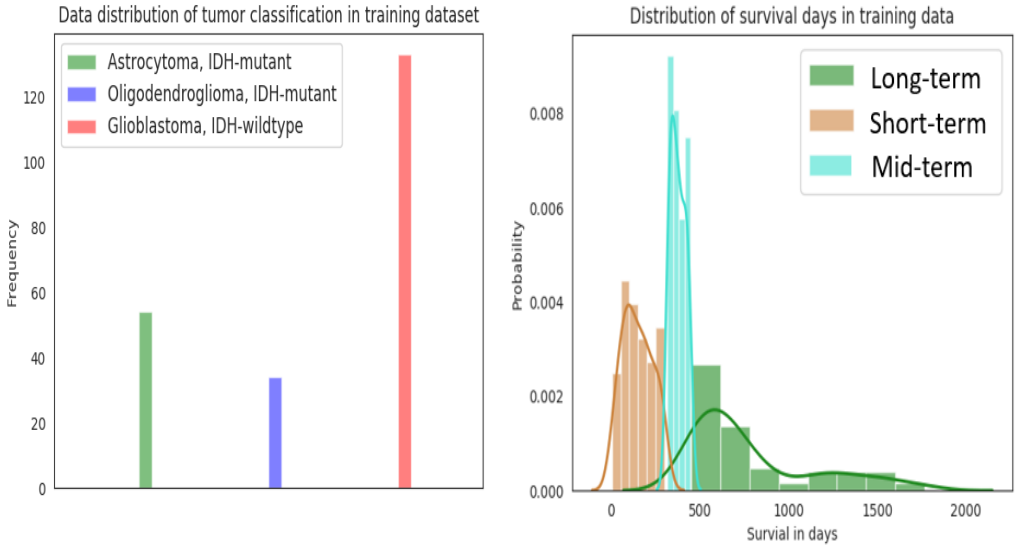

Figure 26. Data distribution of training data for tumor classification and overall survival prediction. (left) Frequency counts of cases for different classes of tumor. (right) Distribution of survival days for short-term (<10 months), mid-term (between 10-15 months), and long-term (>15 months) categories.

we implement tumor segmentation based on MRI sub-regions, rather than using each abnormal tissue individually.

For tumor classification, the main issue is lack of data. In this work, even though we increase training sample size using data augmentation techniques, 221 cases may still be insufficient number for deep learning. Similar data shortage issue also exists in overall survival prediction. There are only 210 cases available in training phase for the CPM-RadPath 2019 Challenge.

In addition to the deep learning-based approach, we also implement overall survival prediction using a conventional machine learning method by extracting features, such as, gray-level co-occurrence matrix (GLCM), intensity, etc., then applying LASSO to select features, and finally using linear regression for survival prediction. We compare the result with that of our proposed method. The comparison shows that the proposed method achieves better performance (as shown in Table 17).

Table 17. Performance comparison of overall survival prediction using different methods on BraTS 2019 validation dataset.

Method	Accuracy	MSE	medianSE	stdSE	SpearmanR
Machine learning	0.483	128594	20898	233919	0.044
The proposed method	0.586	79146	24362	113801	0.502

We also analyze the impact of gender and age on overall survival in this work. In the training data, patients with high-grade glioma (HGG) have 461.0314 average survival (AS) days, and 376 median survival (MS) days. Low-grade glioma (LGG) patients have 1199.8 AS with 814 MS. We investigate impact of average age (AA), median age (MA), and gender information to average survival (AS) and median survival (MS), then

compare the overall performance. The comparison results are shown in Table 18. For patients with HGG, both male and female have similar average and median age (mean age difference is less than 1 year), but males have much more AS days (520.6 versus 433), as well as MS days (426.5 versus 291). However, female patients with LGG (about 3 years younger) have longer AS period and MS period. Overall, regardless of tumor grade, male patients that are older have fewer survival days as shown in our experimental data.

Table 18. Age and survival days comparison based on gender.

	HGG					LGG					Overall				
	Case	AA	MA	AS	MS	Case	AA	MA	AS	MS	Case	AA	MA	AS	MS
Male	58	60.9	60.6	520.6	426.5	7	51.7	53.8	1188.6	788	65	59.9	59.3	592.6	448
Female	31	59.3	61.5	433.1	291	10	48.1	50.1	1207.7	983	41	56.6	57.6	622	370

We also conduct statistical analysis on the impact of gender and age to overall survival using analysis of variance (ANOVA). The p-value is shown in Table 19. The statistical analysis suggests that gender and age are not significant for overall survival for this dataset with only 106 patients.

Table 19. P-value using ANOVA.

	$p-value$
Gender	0.1636
Age	0.101

5.7 Summary

In this Chapter, we investigate multiple tasks in brain tumor analysis by applying deep learning-based methods to structural multimodal MRI (mMRI) images. These brain tumor analysis tasks consist of tumor segmentation, tumor classification, and overall survival prediction. We propose a context-aware deep learning method for tumor segmentation since the context encoding module captures global context encoding

features. The segmented tumor is then used for tumor classification by utilizing a 3D CNN. Moreover, we also propose a hybrid method for overall survival prediction. Specifically, we obtain high-dimensional feature extraction using front-end of the CANet, then apply the least absolute shrinkage and selection operator (LASSO) feature selection method to these extracted features, and finally implement an overall survival prediction method based on the selected features.

CHAPTER 6

CONCLUSIONS AND FUTURE WORKS

6.1 Conclusion

The overall goal of this dissertation is to obtain improved longitudinal brain tumor segmentation, tracking, tumor grading, and patient survival prediction. The first goal of the dissertation is to improve longitudinal brain tracking. We propose two novel methods: feature fusion-based and joint label fusion-based. The feature fusion-based method offers improved texture-based brain tumor segmentation in longitudinal mMRI by fusing the tumor cell density patterns obtained from biophysical tumor growth modeling with the stochastic texture features in a RF-based segmentation method. Statistical analysis shows significant performance improvement for the proposed feature fusion method for the areas of TC and ET. The JLF-based method fuses results obtained from RF with those from GB and helps to improve GB, a state-of-the-art method on longitudinal brain tumor segmentation.

Longitudinal brain tumor tracking not only offers tumor segmentation at current stage, but also shows how the tumor changes over time. This may facilitate clinical decision making, including treatment management and patient follow-up.

The second dissertation goal is to build a deep learning-based method for brain tumor type and subtype grading, using both pathology and proteomics data, following the new 2016 WHO tumor classification criteria. The classification method integrates a cellularity feature which is derived from the morphology of histologic images to improve classification performance. The experiments show that, while the type of DNN may not be critical in the discrimination of low-grade from high-grade glioma, DNN may have a

significant impact in discriminating Grade II versus Grade III. Moreover, we investigate the impact of proteomics and cellularity information on glioma grading. An interesting finding of this work is that the cellularity features show promise in prediction of a subtype of LGG grade III with *IDH* mutation. Specifically, for patients with LGG Grade III, cellularity of Wild-type *IDH* is higher than that of Mutant type, suggesting that the cellularity feature obtained from a pathology image may be used to classify the more aggressive Wild-type *IDH* subtype of LGG Grade III that has the proteomics histopathology of Grade IV.

An accurate tumor grade combining the phenotype and proteomics information, following the latest standard of WHO tumor classification, provides a reliable diagnosis and assessment of a brain tumor. This may help healthcare professionals to make good treatment planning decisions.

The final dissertation goal is to propose a universal deep learning model for brain tumor segmentation, tumor subtype classification, and overall patient survival prediction. We propose a context-aware deep learning method for tumor segmentation, since the context encoding module captures global context encoding features. The segmented tumor is then used for tumor classification by utilizing a 3D CNN. Moreover, we also propose a hybrid method for overall survival prediction. Specifically, we obtain high-dimensional feature extraction, using the front-end of the CANet, and then we apply the least absolute shrinkage and selection operator (LASSO) feature selection method to these extracted features, and finally we implement an overall survival prediction method based on the selected features.

Brain tumor segmentation, tumor subtype classification, and overall patient survival prediction are of importance for brain tumor analysis. With the capability of a deep neural network, these brain tumor analysis steps are becoming more robust, which may help the clinical outcomes for patients with a brain tumor.

The overall goals, novel contributions, and outcomes of this dissertation are summarized in Table 20.

Table 20. Summary of novel contributions

Chapter	Topic	Contributions	Results	Publications
3	A longitudinal brain tumor tracking using feature and label fusion	• Exploited tumor cell density as a feature to predict brain tumor segmentation prediction • Improved the performance of another successful tumor segmentation method GB, by fusing with RF-based segmentation labels.	The proposed pipeline shows improved longitudinal brain tumor tracking compared to the state-of-the-art.	Published **two conference** papers: [14, 15] and **one journal** paper [13]
4	A deep learning-based tumor grading method using pathology and proteomics data	• Integrated cellularity features from improving tumor grading • Discovered the potential correlation between cellularity and *IDH* types.	The proposed pipeline shows the deep learning-based method for tumor grading having the state-of-the-art performance	**One journal** paper (under review)

5	A context-aware deep learning for brain tumor segmentation, subtype classification and overall survival prediction	• Proposed a context-aware deep learning-based method for brain tumor segmentation • Utilized a hybrid method for overall survival prediction • Proposed a tumor classification using structural MRI data only	The proposed method shows a competitive performance on tumor segmentation, promising performance on overall survival prediction, and state-of-the-art on tumor subtype classification	**One journal** paper (under review) **One conference** paper published in SPIE-Medical Imaging **Won the 2nd** place in CPM-RadPath Challenge 2019

6.2 Future Works

Even though our proposed work either exceeds and/or reaches state-of-the-art performance in the proposed goals, there is a lot of space for improvement. For the first dissertation goal, we propose two methods for longitudinal brain tumor tracking, and the performance of the experiment shows the state-of-the-art. To make the proposed framework even more useful, we plan to extend the models for segmentation of other abnormal tissues, such as the cysts and necrosis associated with brain tumor. A more robust label fusion may help, for the second method to obtain improved longitudinal tumor segmentation prediction. We further plan to improve the underlying feature extraction, tumor growth, and segmentation models. A more comprehensive tumor growth model development that also considers the treatment modalities may be interesting.

For the second dissertation goal, we propose a deep learning-based method for tumor grading by following the new WHO criterion. The experimental results show the promising performance. However, this still has challenges. First, development of an

automated method may be needed, since region of interest (ROI) selection from the WSI is critical for the tasks. Second, we plan to repeat the proposed method and the experiments using larger patient data, in order to validate the findings in this study for improved tumor type and subtype classification.

For the final dissertation goal, we propose a deep learning-based method for multiple tumor analysis tasks. These tasks are studied together, considering the underlying relationship. Although the performances are good, especially for tumor segmentation and tumor subtype classification, the performance on overall survival prediction is unstable, due to the small number of cases in training. Therefore, we plan to increase the number of patient cases to improve the performance. Furthermore, we will integrate the whole slide image and the proteomics genetic features for tumor classification, following the new WHO criterion.

APPENDICES

APPENDIX A: ALL 30 FEATURES USED in OUR PROPOSED METHOD

1	2	3	4	5	6
Intensity of T1 (pre)	PTPSA of T1	mBm of T1	Intensity of T2 (pre)	PTPSA of T2	mBm of T2
7	8	9	10	11	12
Intensity of FL (pre)	PTPSA of FL	mBm of FL	Intensity of T1c (pre)	PTPSA of T1c	mBm of T1c
13	14	15	16	17	18
Texton of T2 (No. 37)	Texton of T2 (No. 38)	Texton of FL (No. 4)	Texton of FL (No. 37)	Texton of FL (No. 38)	Texton of T1c (No. 37)
19	20	21	22	23	24
Intensity of T1 (post)	Intensity of T2 (post)	Intensity of FL (post)	Intensity of T1c (post)	D21	D21C
25	26	27	28	29	30
D2f	Hist. T1	Hist. T2	Hist. FL	Hist. T1c	CSF mask

Note: Note: In the Table, “pre” means before normalization, “post” is after normalization. “FL” represents FLAIR modality, “D21” is the intensity difference between T2 and T1. “D21C” is intensity difference between T2 and T1C, and “D2f” is for intensity difference between T2 and FLAIR. "Hist." means histogram matched.

APPENDIX B: AVERAGE FALSE NEGATIVE RATE (FNR) AND FALSE POSITIVE RATE (FPR) COMPARISON BETWEEN RESULT OF THE PROPOSED METHOD AND BRATUMIA (BTIA)

Tumor type	WT		TC		EN	
	JLF	BTIA	JLF	BTIA	JLF	BTIA
FNR	0.227	0.3426	0.2489	0.3833	0.1159	0.2698
FPR	0.000889	0.000956	0.000344	0.0006	0.0009	0.000778

REFERENCES

[1] S. Bakas *et al.*, "Identifying the best machine learning algorithms for brain tumor segmentation, progression assessment, and overall survival prediction in the BRATS challenge," *arXiv preprint arXiv:1811.02629,* 2018.

[2] Q. T. Ostrom, H. Gittleman, G. Truitt, A. Boscia, C. Kruchko, and J. S. Barnholtz-Sloan, "CBTRUS Statistical Report: Primary Brain and Other Central Nervous System Tumors Diagnosed in the United States in 2011–2015," *Neuro-oncology,* vol. 20, no. suppl_4, pp. iv1-iv86, 2018.

[3] D. N. Louis *et al.*, "The 2007 WHO classification of tumours of the central nervous system," *Acta neuropathologica,* vol. 114, no. 2, pp. 97-109, 2007.

[4] D. N. Louis *et al.*, "The 2016 World Health Organization classification of tumors of the central nervous system: a summary," *Acta neuropathologica,* vol. 131, no. 6, pp. 803-820, 2016.

[5] J. Chen, R. M. McKay, and L. F. Parada, "Malignant glioma: lessons from genomics, mouse models, and stem cells," *Cell,* vol. 149, no. 1, pp. 36-47, 2012.

[6] P. Lissoni *et al.*, "Increased survival time in brain glioblastomas by a radioneuroendocrine strategy with radiotherapy plus melatonin compared to radiotherapy alone," (in Eng), *Oncology,* vol. 53, no. 1, pp. 43-6, Jan-Feb 1996.

[7] Y. Zhang, A. Li, C. Peng, and M. Wang, "Improve Glioblastoma Multiforme Prognosis Prediction by Using Feature Selection and Multiple Kernel Learning," *IEEE/ACM Transactions on Computational Biology and Bioinformatics,* vol. 13, no. 5, pp. 825-835, 2016.

[8] A. R. Kansal, S. Torquato, G. R. Harsh, E. A. Chiocca, and T. S. Deisboeck, "Simulated Brain Tumor Growth Dynamics Using a Three-Dimensional Cellular Automaton," *Journal of Theoretical Biology,* vol. 203, no. 4, pp. 367-382, 2000/04/21/ 2000.

[9] S. Banerjee, S. Mitra, F. Masulli, and S. Rovetta, "Deep Radiomics for Brain Tumor Detection and Classification from Multi-Sequence MRI," *arXiv preprint arXiv:1903.09240,* 2019.

[10] K. Popuri, D. Cobzas, A. Murtha, and M. Jägersand, "3D variational brain tumor segmentation using Dirichlet priors on a clustered feature set," *International Journal of Computer Assisted Radiology and Surgery,* journal article vol. 7, no. 4, pp. 493-506, 2012.

[11] J. R. Wood, S. B. Green, and W. R. Shapiro, "The prognostic importance of tumor size in malignant gliomas: a computed tomographic scan study by the Brain Tumor Cooperative Group," *Journal of clinical oncology,* vol. 6, no. 2, pp. 338-343, 1988.

[12] B. H. Menze *et al.*, "The multimodal brain tumor image segmentation benchmark (BRATS)," *IEEE transactions on medical imaging,* vol. 34, no. 10, pp. 1993-2024, 2014.

[13] L. Pei, S. Bakas, A. Vossough, S. M. Reza, C. Davatzikos, and K. M. Iftekharuddin, "Longitudinal brain tumor segmentation prediction in MRI using feature and label fusion," *Biomedical Signal Processing and Control,* vol. 55, p. 101648, 2020.

[14] L. Pei, S. M. Reza, W. Li, C. Davatzikos, and K. M. Iftekharuddin, "Improved brain tumor segmentation by utilizing tumor growth model in longitudinal brain MRI," in *Medical Imaging 2017: Computer-Aided Diagnosis*, 2017, vol. 10134, p. 101342L: International Society for Optics and Photonics.

[15] L. Pei, S. M. Reza, and K. M. Iftekharuddin, "Improved brain tumor growth prediction and segmentation in longitudinal brain MRI," in *2015 IEEE International Conference on Bioinformatics and Biomedicine (BIBM)*, 2015, pp. 421-424: IEEE.

[16] S. M. Reza and K. M. Iftekharuddin, "Glioma grading using cell nuclei morphologic features in digital pathology images," in *Medical Imaging 2016: Computer-Aided Diagnosis*, 2016, vol. 9785, p. 97852U: International Society for Optics and Photonics.

[17] S. M. S. Reza, A. Islam, and K. M. kiftekha@odu.edu, "Texture Estimation for Abnormal Tissue Segmentation in Brain MRI," in *The Fractal Geometry of the Brain*, A. Di Ieva, Ed. New York, NY: Springer New York, 2016, pp. 333-349.

[18] B. H. Menze *et al.*, "The Multimodal Brain Tumor Image Segmentation Benchmark (BRATS)," *IEEE Transactions on Medical Imaging,* vol. 34, no. 10, pp. 1993-2024, 2015.

[19] B. M. Ellingson *et al.*, "Consensus recommendations for a standardized Brain Tumor Imaging Protocol in clinical trials," *Neuro-oncology,* vol. 17, no. 9, pp. 1188-1198, 2015.

[20] N. E. A. Khalid, S. Ibrahim, and P. Haniff, "MRI Brain Abnormalities Segmentation using K-Nearest Neighbors(k-NN)," *International Journal on Computer Science and Engineering,* vol. 3, no. 2, pp. 980-990, 2011.

[21] K. M. Iftekharuddin, J. Zheng, M. A. Islam, R. J. Ogg, and F. Lanningham, "Brain Tumor Detection in MRI: Technique and Statistical Validation," in *2006 Fortieth Asilomar Conference on Signals, Systems and Computers*, 2006, pp. 1983-1987.

[22] P. Linmin, S. M. S. Reza, and K. M. Iftekharuddin, "Improved brain tumor growth prediction and segmentation in longitudinal brain MRI," in *Bioinformatics and Biomedicine (BIBM), 2015 IEEE International Conference on*, 2015, pp. 421-424.

[23] E. Konukoglu *et al.*, "Image Guided Personalization of Reaction-Diffusion Type Tumor Growth Models Using Modified Anisotropic Eikonal Equations," *IEEE Transactions on Medical Imaging,* vol. 29, no. 1, pp. 77-95, 2010.

[24] O. Clatz *et al.*, "Realistic simulation of the 3-D growth of brain tumors in MR images coupling diffusion with biomechanical deformation," *IEEE Transactions on Medical Imaging,* vol. 24, no. 10, pp. 1334-1346, 2005.

[25] S. Tanzeem, W. E. Reddick, and K. M. Iftekharuddin, "3D quantitative brain tumor growth model based on cell proliferation and diffusion," in *Electrical and Computer Engineering (ICECE), 2014 International Conference on*, 2014, pp. 9-12.

[26] CPM-RadPath. (2019, 2019-08-30). *Computational Precision Medicine 2019: Brain Tumor Classification*. Available: https://www.med.upenn.edu/cbica/cpm2019-data.html

[27] C.-R. Ranking. (2019, 2019-11-04). *NIH Computational Precision Medicine 2019 Challenge Ranking*. Available: https://www.med.upenn.edu/cbica/miccai-tactical-2019/rankings.html

[28] L. Tang *et al.*, "Computational Modeling of 3D Tumor Growth and Angiogenesis for Chemotherapy Evaluation," *PLOS ONE,* vol. 9, no. 1, p. e83962, 2014.

[29] S. Pereira, A. Pinto, V. Alves, and C. A. Silva, "Brain Tumor Segmentation Using Convolutional Neural Networks in MRI Images," *IEEE Transactions on Medical Imaging,* vol. 35, no. 5, pp. 1240-1251, 2016.

[30] J. Sachdeva, V. Kumar, I. Gupta, N. Khandelwal, and C. K. Ahuja, "Multiclass Brain Tumor Classification Using GA-SVM," in *2011 Developments in E-systems Engineering*, 2011, pp. 182-187.

[31] S. M. Reza, R. Mays, and K. M. Iftekharuddin, "Multi-fractal detrended texture feature for brain tumor classification," in *Medical Imaging 2015: Computer-Aided Diagnosis*, 2015, vol. 9414, p. 941410: International Society for Optics and Photonics.

[32] A. Islam, S. M. Reza, and K. M. Iftekharuddin, "Multifractal texture estimation for detection and segmentation of brain tumors," *IEEE transactions on biomedical engineering,* vol. 60, no. 11, pp. 3204-3215, 2013.

[33] A. Myronenko, "3D MRI brain tumor segmentation using autoencoder regularization," in *International MICCAI Brainlesion Workshop*, 2018, pp. 311-320: Springer.

[34] M. Havaei *et al.*, "Brain tumor segmentation with deep neural networks," *Medical image analysis,* vol. 35, pp. 18-31, 2017.

[35] M. Retsky, D. Swartzendruber, R. Wardwell, and P. Bame, "Is Gompertzian or exponential kinetics a valid description of individual human cancer growth?," *Medical hypotheses,* vol. 33, no. 2, pp. 95-106, 1990.

[36] J. A. Lazareff, R. Suwinski, R. De Rosa, and C. E. Olmstead, "Tumor volume and growth kinetics in hypothalamic-chiasmatic pediatric low grade gliomas," *Pediatric neurosurgery,* vol. 30, no. 6, pp. 312-319, 1999.

[37] Z. Bajzer, "Gompertzian growth as a self-similar and allometric process," *Growth, development, and aging: GDA,* vol. 63, no. 1-2, pp. 3-11, 1999.

[38] M. Marušić, "Mathematical models of tumor growth," *Mathematical Communications,* vol. 1, no. 2, pp. 175-188, 1996.

[39] C. Hogea, C. Davatzikos, and G. Biros, "Modeling glioma growth and mass effect in 3D MR images of the brain," (in Eng), *Med Image Comput Comput Assist Interv,* vol. 10, no. Pt 1, pp. 642-50, 2007.

[40] A. Gooya *et al.*, "GLISTR: Glioma Image Segmentation and Registration," *IEEE Transactions on Medical Imaging,* vol. 31, no. 10, pp. 1941-1954, 2012.

[41] L. M *et al.*, "MRI Based Bayesian Personalization of a Tumor Growth Model," *IEEE Transactions on Medical Imaging,* vol. 35, no. 10, pp. 2329-2339, 2016.

[42] H. RiCha and R. XiaoGang, "A logistic cellular automaton for simulating tumor growth," in *Intelligent Control and Automation, 2002. Proceedings of the 4th World Congress on*, 2002, vol. 1, pp. 693-696 vol.1.

[43] L. Sallemi, I. Njeh, and S. Lehericy, "Towards a computer aided prognosis for brain glioblastomas tumor growth estimation," *IEEE transactions on nanobioscience,* vol. 14, no. 7, pp. 727-733, 2015.

[44] K. C. Wong, R. M. Summers, E. Kebebew, and J. Yao, "Tumor growth prediction with reaction-diffusion and hyperelastic biomechanical model by physiological data fusion," (in Eng), *Med Image Anal,* vol. 25, no. 1, pp. 72-85, Oct 2015.
[45] O. Clatz *et al.*, "Brain tumor growth simulation," INRIA, 2004.
[46] J. Xu, G. Vilanova, and H. Gomez, "A mathematical model coupling tumor growth and angiogenesis," *PloS one,* vol. 11, no. 2, p. e0149422, 2016.
[47] S. Bauer, C. Seiler, T. Bardyn, P. Buechler, and M. Reyes, "Atlas-based segmentation of brain tumor images using a Markov Random Field-based tumor growth model and non-rigid registration," in *2010 Annual International Conference of the IEEE Engineering in Medicine and Biology*, 2010, pp. 4080-4083.
[48] S. Bakas *et al.*, "GLISTRboost: Combining Multimodal MRI Segmentation, Registration, and Biophysical Tumor Growth Modeling with Gradient Boosting Machines for Glioma Segmentation," in *Brainlesion: Glioma, Multiple Sclerosis, Stroke and Traumatic Brain Injuries: First International Workshop, Brainles 2015, Held in Conjunction with MICCAI 2015, Munich, Germany, October 5, 2015, Revised Selected Papers*, A. Crimi, B. Menze, O. Maier, M. Reyes, and H. Handels, Eds. Cham: Springer International Publishing, 2016, pp. 144-155.
[49] R. Meier *et al.*, "Clinical evaluation of a fully-automatic segmentation method for longitudinal brain tumor volumetry," *Scientific reports,* vol. 6, p. 23376, 2016.
[50] W. D. Heiss, P. Raab, and H. Lanfermann, "Multimodality assessment of brain tumors and tumor recurrence," (in Eng), *J Nucl Med,* vol. 52, no. 10, pp. 1585-600, Oct 2011.
[51] C. I. Hill, C. S. Nixon, J. L. Ruehmeier, and L. M. Wolf, "Brain Tumors," *Physical Therapy,* vol. 82, no. 5, pp. 496-502, 2002.
[52] S. F. Kralik, A. Taha, A. P. Kamer, J. S. Cardinal, T. A. Seltman, and C. Y. Ho, "Diffusion imaging for tumor grading of supratentorial brain tumors in the first year of life," (in Eng), *AJNR Am J Neuroradiol,* vol. 35, no. 4, pp. 815-23, Apr 2014.
[53] C. L. Appin and D. J. Brat, "Molecular genetics of gliomas," *The Cancer Journal,* vol. 20, no. 1, pp. 66-72, 2014.
[54] A. Olar and E. P. Sulman, "Molecular markers in low-grade glioma—toward tumor reclassification," in *Seminars in radiation oncology*, 2015, vol. 25, no. 3, pp. 155-163: Elsevier.
[55] K. Ichimura, "Molecular pathogenesis of IDH mutations in gliomas," *Brain tumor pathology,* vol. 29, no. 3, pp. 131-139, 2012.
[56] B. J. Theeler, W. A. Yung, G. N. Fuller, and J. F. De Groot, "Moving toward molecular classification of diffuse gliomas in adults," *Neurology,* vol. 79, no. 18, pp. 1917-1926, 2012.
[57] A. Mukasa *et al.*, "Significance of IDH mutations varies with tumor histology, grade, and genetics in Japanese glioma patients," *Cancer science,* vol. 103, no. 3, pp. 587-592, 2012.
[58] K. Masui, P. S. Mischel, and G. Reifenberger, "Chapter 6 - Molecular classification of gliomas," in *Handbook of Clinical Neurology*, vol. 134, M. S. Berger and M. Weller, Eds.: Elsevier, 2016, pp. 97-120.

[59] A. El-Shahat, *Advanced Applications for Artificial Neural Networks*. BoD–Books on Demand, 2018.
[60] M. A. Nielsen, *Neural networks and deep learning*. Determination press San Francisco, CA, USA:, 2015.
[61] D. E. Rumelhart, G. E. Hinton, and R. J. Williams, "Learning representations by back-propagating errors," *nature,* vol. 323, no. 6088, pp. 533-536, 1986.
[62] S. Srinivas, R. K. Sarvadevabhatla, K. R. Mopuri, N. Prabhu, S. S. Kruthiventi, and R. V. Babu, "An Introduction to Deep Convolutional Neural Nets for Computer Vision," in *Deep Learning for Medical Image Analysis*: Elsevier, 2017, pp. 25-52.
[63] Y. LeCun, L. Bottou, Y. Bengio, and P. Haffner, "Gradient-based learning applied to document recognition," *Proceedings of the IEEE,* vol. 86, no. 11, pp. 2278-2324, 1998.
[64] K. O'Shea and R. Nash, "An Introduction to Convolutional Neural Networks," *ArXiv e-prints,* 11/01 2015.
[65] N. Kumar *et al.*, "A multi-organ nucleus segmentation challenge," *IEEE transactions on medical imaging,* 2019.
[66] M. Ahmad *et al.*, "Deep belief network modeling for automatic liver segmentation," *IEEE Access,* vol. 7, pp. 20585-20595, 2019.
[67] X. Zhao, Y. Wu, G. Song, Z. Li, Y. Zhang, and Y. Fan, "A deep learning model integrating FCNNs and CRFs for brain tumor segmentation," *Medical image analysis,* vol. 43, pp. 98-111, 2018.
[68] S. Chakraborty, F. Priamo, and J. A. Boockvar, "Magnetic Resonance Imaging to Identify Glioblastoma Molecular Phenotypes," *Neurosurgery,* vol. 78, no. 2, pp. N20-N21, 2016.
[69] Z. A. Shboul, M. Alam, L. Vidyaratne, L. Pei, M. I. Elbakary, and K. M. Iftekharuddin, "Feature-Guided Deep Radiomics for Glioblastoma Patient Survival Prediction," (in English), *Frontiers in Neuroscience,* Original Research vol. 13, no. 966, 2019-September-20 2019.
[70] W. B. Pope, J. Sayre, A. Perlina, J. P. Villablanca, P. S. Mischel, and T. F. Cloughesy, "MR imaging correlates of survival in patients with high-grade gliomas," *American Journal of Neuroradiology,* vol. 26, no. 10, pp. 2466-2474, 2005.
[71] D. A. Gutman *et al.*, "MR imaging predictors of molecular profile and survival: multi-institutional study of the TCGA glioblastoma data set," *Radiology,* vol. 267, no. 2, pp. 560-569, 2013.
[72] J. Fu *et al.*, "An automatic deep learning-based workflow for glioblastoma survival prediction using pre-operative multimodal MR images," *arXiv preprint arXiv:2001.11155,* 2020.
[73] Y. Zhang, E. M. Lobo-Mueller, P. Karanicolas, S. Gallinger, M. A. Haider, and F. Khalvati, "CNN-based survival model for pancreatic ductal adenocarcinoma in medical imaging," *BMC Medical Imaging,* vol. 20, no. 1, pp. 1-8, 2020.
[74] A. Gooya, G. Biros, and C. Davatzikos, "Deformable Registration of Glioma Images Using EM Algorithm and Diffusion Reaction Modeling," *IEEE Transactions on Medical Imaging,* vol. 30, no. 2, pp. 375-390, 2011.

[75] M. B. Cuadra, C. Pollo, A. Bardera, O. Cuisenaire, J. G. Villemure, and J. P. Thiran, "Atlas-based segmentation of pathological MR brain images using a model of lesion growth," *IEEE Transactions on Medical Imaging,* vol. 23, no. 10, pp. 1301-1314, 2004.

[76] A. Islam, S. M. S. Reza, and K. M. Iftekharuddin, "Multifractal Texture Estimation for Detection and Segmentation of Brain Tumors," *IEEE Transactions on Biomedical Engineering,* vol. 60, no. 11, pp. 3204-3215, 2013.

[77] S. Reza and K. M. Iftekharuddin, "Multi-fractal texture features for brain tumor and edema segmentation," 2014, vol. 9035, pp. 903503-903503-10.

[78] H. Wang and P. A. Yushkevich, "Multi-atlas segmentation without registration: a supervoxel-based approach," (in Eng), *Med Image Comput Comput Assist Interv,* vol. 16, no. Pt 3, pp. 535-42, 2013.

[79] P. Su, J. Yang, H. Li, L. Chi, Z. Xue, and S. T. Wong, "Superpixel-Based Segmentation of Glioblastoma Multiforme from Multimodal MR Images," in *Multimodal Brain Image Analysis: Third International Workshop, MBIA 2013, Held in Conjunction with MICCAI 2013, Nagoya, Japan, September 22, 2013, Proceedings*, L. Shen, T. Liu, P.-T. Yap, H. Huang, D. Shen, and C.-F. Westin, Eds. Cham: Springer International Publishing, 2013, pp. 74-83.

[80] K. Kamnitsas *et al.*, "Efficient multi-scale 3D CNN with fully connected CRF for accurate brain lesion segmentation," *Medical Image Analysis,* vol. 36, pp. 61-78.

[81] L. Breiman, "Random forests," *Machine learning,* vol. 45, no. 1, pp. 5-32, 2001.

[82] H. Wang, J. W. Suh, S. R. Das, J. B. Pluta, C. Craige, and P. A. Yushkevich, "Multi-Atlas Segmentation with Joint Label Fusion," *IEEE Transactions on Pattern Analysis and Machine Intelligence,* vol. 35, no. 3, pp. 611-623, 2013.

[83] M. R. Sabuncu, B. T. T. Yeo, K. V. Leemput, B. Fischl, and P. Golland, "A Generative Model for Image Segmentation Based on Label Fusion," *IEEE Transactions on Medical Imaging,* vol. 29, no. 10, pp. 1714-1729, 2010.

[84] L. G. Nyúl, J. K. Udupa, and X. Zhang, "New variants of a method of MRI scale standardization," *IEEE transactions on medical imaging,* vol. 19, no. 2, pp. 143-150, 2000.

[85] K. Zeng *et al.*, "Segmentation of Gliomas in Pre-operative and Post-operative Multimodal Magnetic Resonance Imaging Volumes Based on a Hybrid Generative-Discriminative Framework," *Brainlesion : glioma, multiple sclerosis, stroke and traumatic brain injuries : second International Workshop, BrainLes 2016, with the challenges on BRATS, ISLES and mTOP 2016, held in conjunction with MICCAI 2016, Athens, Greece, Octob.,* vol. 10154, pp. 184-194, 04/12 2016.

[86] S. Bakas *et al.*, "Advancing The Cancer Genome Atlas glioma MRI collections with expert segmentation labels and radiomic features," (in eng), *Sci Data,* vol. 4, p. 170117, Sep 5 2017.

[87] T. Rohlfing, N. M. Zahr, E. V. Sullivan, and A. Pfefferbaum, "The SRI24 multichannel atlas of normal adult human brain structure," *Human brain mapping,* vol. 31, no. 5, pp. 798-819, 2010.

[88] W. Ngamsaad, W. Triampo, P. Kanthang, I. Tang, N. Nuttawut, and C. Modjung, "A one-dimensional Lattice Boltzmann method for modeling the dynamic pole-to-pole oscillations of Min proteins for determining the position of the midcell division plane," *arXiv preprint q-bio/0412018,* 2004.

[89] L. R. Dice, "Measures of the amount of ecologic association between species," *Ecology,* vol. 26, no. 3, pp. 297-302, 1945.
[90] M. Peikari, S. Salama, S. Nofech‐Mozes, and A. L. Martel, "Automatic cellularity assessment from post‐treated breast surgical specimens," *Cytometry Part A,* vol. 91, no. 11, pp. 1078-1087, 2017.
[91] M. J. van den Bent, "Interobserver variation of the histopathological diagnosis in clinical trials on glioma: a clinician's perspective," *Acta neuropathologica,* vol. 120, no. 3, pp. 297-304, 2010.
[92] H. S. Mousavi, V. Monga, G. Rao, and A. U. K. Rao, "Automated discrimination of lower and higher grade gliomas based on histopathological image analysis," *Journal of pathology informatics,* vol. 6, pp. 15-15, 2015.
[93] J. Barker, A. Hoogi, A. Depeursinge, and D. L. Rubin, "Automated classification of brain tumor type in whole-slide digital pathology images using local representative tiles," *Medical Image Analysis,* vol. 30, pp. 60-71, 2016/05/01/ 2016.
[94] S. M. Reza, M. D. Samad, Z. A. Shboul, K. A. Jones, and K. M. Iftekharuddin, "Glioma grading using structural magnetic resonance imaging and molecular data," *Journal of Medical Imaging,* vol. 6, no. 2, p. 024501, 2019.
[95] F. Citak-Er, Z. Firat, I. Kovanlikaya, U. Ture, and E. Ozturk-Isik, "Machine-learning in grading of gliomas based on multi-parametric magnetic resonance imaging at 3T," *Computers in biology and medicine,* vol. 99, pp. 154-160, 2018.
[96] C.-F. Lu *et al.*, "Machine learning–based radiomics for molecular subtyping of gliomas," *Clinical Cancer Research,* vol. 24, no. 18, pp. 4429-4436, 2018.
[97] K. M. Priya, S. Kavitha, and B. Bharathi, "Brain tumor types and grades classification based on statistical feature set using support vector machine," in *Intelligent Systems and Control (ISCO), 2016 10th International Conference on*, 2016, pp. 1-8: IEEE.
[98] M. G. Ertosun and D. L. Rubin, "Automated grading of gliomas using deep learning in digital pathology images: A modular approach with ensemble of convolutional neural networks," in *AMIA Annual Symposium Proceedings*, 2015, vol. 2015, p. 1899: American Medical Informatics Association.
[99] Y. Pan *et al.*, "Brain tumor grading based on neural networks and convolutional neural networks," in *2015 37th Annual International Conference of the IEEE Engineering in Medicine and Biology Society (EMBC)*, 2015, pp. 699-702: IEEE.
[100] E. I. Zacharaki *et al.*, "Classification of brain tumor type and grade using MRI texture and shape in a machine learning scheme," *Magnetic Resonance in Medicine: An Official Journal of the International Society for Magnetic Resonance in Medicine,* vol. 62, no. 6, pp. 1609-1618, 2009.
[101] K. L.-C. Hsieh, C.-M. Lo, and C.-J. Hsiao, "Computer-aided grading of gliomas based on local and global MRI features," *Computer methods and programs in biomedicine,* vol. 139, pp. 31-38, 2017.
[102] K. Skogen, A. Schulz, J. B. Dormagen, B. Ganeshan, E. Helseth, and A. Server, "Diagnostic performance of texture analysis on MRI in grading cerebral gliomas," *European journal of radiology,* vol. 85, no. 4, pp. 824-829, 2016.
[103] A. Kharrat, K. Gasmi, M. B. Messaoud, N. Benamrane, and M. Abid, "A hybrid approach for automatic classification of brain MRI using genetic algorithm and

support vector machine," *Leonardo journal of sciences,* vol. 17, no. 1, pp. 71-82, 2010.

[104] A. Yonekura, H. Kawanaka, V. S. Prasath, B. J. Aronow, and H. Takase, "Improving the generalization of disease stage classification with deep CNN for glioma histopathological images," in *Bioinformatics and Biomedicine (BIBM), 2017 IEEE International Conference on*, 2017, pp. 1222-1226: IEEE.

[105] S. W. Coons, P. C. Johnson, B. W. Scheithauer, A. J. Yates, and D. K. Pearl, "Improving diagnostic accuracy and interobserver concordance in the classification and grading of primary gliomas," *Cancer: Interdisciplinary International Journal of the American Cancer Society,* vol. 79, no. 7, pp. 1381-1393, 1997.

[106] M. Weller *et al.*, "Personalized care in neuro-oncology coming of age: why we need MGMT and 1p/19q testing for malignant glioma patients in clinical practice," *Neuro-oncology,* vol. 14, no. suppl_4, pp. iv100-iv108, 2012.

[107] J. E. Eckel-Passow *et al.*, "Glioma groups based on 1p/19q, IDH, and TERT promoter mutations in tumors," *New England Journal of Medicine,* vol. 372, no. 26, pp. 2499-2508, 2015.

[108] M. D. Wood, A. M. Halfpenny, and S. R. Moore, "Applications of molecular neuro-oncology-a review of diffuse glioma integrated diagnosis and emerging molecular entities," *Diagnostic pathology,* vol. 14, no. 1, p. 29, 2019.

[109] A. L. Cohen, S. L. Holmen, and H. Colman, "IDH1 and IDH2 mutations in gliomas," *Current neurology and neuroscience reports,* vol. 13, no. 5, pp. 345-345, 2013.

[110] J. Kong, O. Sertel, H. Shimada, K. L. Boyer, J. H. Saltz, and M. N. Gurcan, "Computer-aided evaluation of neuroblastoma on whole-slide histology images: Classifying grade of neuroblastic differentiation," *Pattern Recognition,* vol. 42, no. 6, pp. 1080-1092, 2009/06/01/ 2009.

[111] K. Chang *et al.*, "Residual convolutional neural network for the determination of IDH status in low-and high-grade gliomas from MR imaging," *Clinical Cancer Research,* vol. 24, no. 5, pp. 1073-1081, 2018.

[112] P. Nandakumar, A. Mansouri, and S. Das, "The Role of ATRX in Glioma Biology," *Frontiers in oncology,* vol. 7, pp. 236-236, 2017.

[113] H. E. Leeper, A. A. Caron, P. A. Decker, R. B. Jenkins, D. H. Lachance, and C. Giannini, "IDH mutation, 1p19q codeletion and ATRX loss in WHO grade II gliomas," *Oncotarget,* vol. 6, no. 30, p. 30295, 2015.

[114] M. E. Hegi *et al.*, "MGMT gene silencing and benefit from temozolomide in glioblastoma," *New England Journal of Medicine,* vol. 352, no. 10, pp. 997-1003, 2005.

[115] M. N. Gurcan, L. E. Boucheron, A. Can, A. Madabhushi, N. M. Rajpoot, and B. Yener, "Histopathological image analysis: a review," *IEEE reviews in biomedical engineering,* vol. 2, pp. 147-171, 2009.

[116] A. Vahadane *et al.*, "Structure-Preserving Color Normalization and Sparse Stain Separation for Histological Images," (in eng), *IEEE Trans Med Imaging,* vol. 35, no. 8, pp. 1962-71, Aug 2016.

[117] A. Rakhlin, A. A. Shvets, A. A. Kalinin, A. Tiulpin, V. I. Iglovikov, and S. Nikolenko, "Breast Tumor Cellularity Assessment using Deep Neural Networks," *arXiv preprint arXiv:1905.01743,* 2019.

[118] S. Akbar, M. Peikari, S. Salama, A. Y. Panah, S. Nofech-Mozes, and A. L. Martel, "Automated and manual quantification of tumour cellularity in digital slides for tumour burden assessment," *Scientific reports,* vol. 9, no. 1, pp. 1-9, 2019.

[119] O. Ronneberger, P. Fischer, and T. Brox, "U-net: Convolutional networks for biomedical image segmentation," in *International Conference on Medical image computing and computer-assisted intervention*, 2015, pp. 234-241: Springer.

[120] K. He, X. Zhang, S. Ren, and J. Sun, "Deep residual learning for image recognition," in *Proceedings of the IEEE conference on computer vision and pattern recognition*, 2016, pp. 770-778.

[121] N. Kumar, R. Verma, S. Sharma, S. Bhargava, A. Vahadane, and A. Sethi, "A dataset and a technique for generalized nuclear segmentation for computational pathology," *IEEE transactions on medical imaging,* vol. 36, no. 7, pp. 1550-1560, 2017.

[122] G. E. Nasr, E. Badr, and C. Joun, "Cross entropy error function in neural networks: Forecasting gasoline demand," in *FLAIRS conference*, 2002, pp. 381-384.

[123] D. P. Kingma and J. Ba, "Adam: A method for stochastic optimization," *arXiv preprint arXiv:1412.6980,* 2014.

[124] A. Basavanhally *et al.*, "Multi-field-of-view framework for distinguishing tumor grade in ER+ breast cancer from entire histopathology slides," *IEEE transactions on biomedical engineering,* vol. 60, no. 8, pp. 2089-2099, 2013.

[125] A. Bagari, A. Kumar, A. Kori, M. Khened, and G. Krishnamurthi, "A Combined Radio-Histological Approach for Classification of Low Grade Gliomas," in *International MICCAI Brainlesion Workshop*, 2018, pp. 416-427: Springer.

[126] L. Hou, D. Samaras, T. M. Kurc, Y. Gao, J. E. Davis, and J. H. Saltz, "Patch-based convolutional neural network for whole slide tissue image classification," in *Proceedings of the IEEE Conference on Computer Vision and Pattern Recognition*, 2016, pp. 2424-2433.

[127] A. W. Simonetti, W. J. Melssen, F. S. d. Edelenyi, J. J. van Asten, A. Heerschap, and L. M. Buydens, "Combination of feature‐reduced MR spectroscopic and MR imaging data for improved brain tumor classification," *NMR in Biomedicine: An International Journal Devoted to the Development and Application of Magnetic Resonance In vivo,* vol. 18, no. 1, pp. 34-43, 2005.

[128] N. B. Bahadure, A. K. Ray, and H. P. Thethi, "Image analysis for MRI based brain tumor detection and feature extraction using biologically inspired BWT and SVM," *International journal of biomedical imaging,* vol. 2017, 2017.

[129] Q. Shen, W.-M. Shi, W. Kong, and B.-X. Ye, "A combination of modified particle swarm optimization algorithm and support vector machine for gene selection and tumor classification," *Talanta,* vol. 71, no. 4, pp. 1679-1683, 2007.

[130] T. Kaur, B. S. Saini, and S. Gupta, "An adaptive fuzzy K-nearest neighbor approach for MR brain tumor image classification using parameter free bat optimization algorithm," *Multimedia Tools and Applications,* pp. 1-38, 2019.

[131] S. Bauer, L.-P. Nolte, and M. Reyes, "Fully automatic segmentation of brain tumor images using support vector machine classification in combination with hierarchical conditional random field regularization," in *international conference on medical image computing and computer-assisted intervention*, 2011, pp. 354-361: Springer.
[132] Y. LeCun, Y. Bengio, and G. Hinton, "Deep learning," *Nature,* vol. 521, p. 436, 05/27/online 2015.
[133] I. Goodfellow, Y. Bengio, and A. Courville, *Deep learning*. MIT press, 2016.
[134] I. Goodfellow *et al.*, "Generative adversarial nets," in *Advances in neural information processing systems*, 2014, pp. 2672-2680.
[135] Z. Akkus, A. Galimzianova, A. Hoogi, D. L. Rubin, and B. J. Erickson, "Deep learning for brain MRI segmentation: state of the art and future directions," *Journal of digital imaging,* vol. 30, no. 4, pp. 449-459, 2017.
[136] D. Amodei *et al.*, "Deep speech 2: End-to-end speech recognition in english and mandarin," in *International conference on machine learning*, 2016, pp. 173-182.
[137] J. Y. Kim, H. E. Lee, Y. H. Choi, S. J. Lee, and J. S. Jeon, "CNN-based diagnosis models for canine ulcerative keratitis," *Scientific Reports,* vol. 9, no. 1, pp. 1-7, 2019.
[138] N. Beig *et al.*, "Radiogenomic analysis of hypoxia pathway is predictive of overall survival in Glioblastoma," *Scientific reports,* vol. 8, no. 1, p. 7, 2018.
[139] S. Saman and S. J. Narayanan, "Survey on brain tumor segmentation and feature extraction of MR images," *International Journal of Multimedia Information Retrieval,* vol. 8, no. 2, pp. 79-99, 2019.
[140] M. F. Othman and M. A. M. Basri, "Probabilistic neural network for brain tumor classification," in *2011 Second International Conference on Intelligent Systems, Modelling and Simulation*, 2011, pp. 136-138: IEEE.
[141] N. Zulpe and V. Pawar, "GLCM textural features for brain tumor classification," *International Journal of Computer Science Issues (IJCSI),* vol. 9, no. 3, p. 354, 2012.
[142] Z. A. Shboul, L. Vidyaratne, M. Alam, and K. M. Iftekharuddin, "Glioblastoma and survival prediction," in *International MICCAI Brainlesion Workshop*, 2017, pp. 358-368: Springer.
[143] H. Zhang *et al.*, "Context encoding for semantic segmentation," in *Proceedings of the IEEE Conference on Computer Vision and Pattern Recognition*, 2018, pp. 7151-7160.
[144] R. Tibshirani, "Regression shrinkage and selection via the lasso," *Journal of the Royal Statistical Society: Series B (Methodological),* vol. 58, no. 1, pp. 267-288, 1996.
[145] S. Bakas *et al.*, "Advancing the cancer genome atlas glioma MRI collections with expert segmentation labels and radiomic features," *Scientific data,* vol. 4, p. 170117, 2017.
[146] S. Bakas *et al.*, "Segmentation labels and radiomic features for the pre-operative scans of the TCGA-LGG collection," *The Cancer Imaging Archive,* vol. 286, 2017.

[147] S. Bakas *et al.*, "Segmentation labels and radiomic features for the pre-operative scans of the TCGA-GBM collection. The Cancer Imaging Archive (2017)," ed, 2017.
[148] T. K. Benjamin Bearce, Spyridon Bakas, Keyvan Farahani, MacLean Nasrallah, Jayashree Kalpathy-Cramer, "Computational Precision Medicine: Radiology-Pathology Challenge on Brain Tumor Classification 2019 (CPM-RadPath)," 2019.
[149] K. Clark *et al.*, "The Cancer Imaging Archive (TCIA): maintaining and operating a public information repository," *Journal of digital imaging,* vol. 26, no. 6, pp. 1045-1057, 2013.
[150] M. BRATS. (2019, 2019-07-12). *CBICA's Image Processing Portal (IPP)*. Available: https://ipp.cbica.upenn.edu/
[151] Docker. (2019, 2019-08). *Docker: Empowering App Development for Developers*. Available: https://www.docker.com/
[152] D. P. Huttenlocher, G. A. Klanderman, and W. J. Rucklidge, "Comparing images using the Hausdorff distance," *IEEE Transactions on pattern analysis and machine intelligence,* vol. 15, no. 9, pp. 850-863, 1993.

VITA

Linmin Pei

Department of Electrical and Computer Engineering

Old Dominion University

Norfolk, VA 23529

EDUCATION

- Old Dominion University, Norfolk, VA, USA

  Ph.D. Candidate, Electrical and Computer Engineering, Aug. 2012 - Present

- Norfolk State University, Norfolk, VA, USA

  M.S., Electrical Engineering, Aug. 2009 - Dec. 2011

ACADEMIC EXPERIENCE

- Old Dominion University, Norfolk, VA, USA
  - Graduate Research Assistant, Aug. 2012 – Present
  - Teaching Assistant, Jan. 2018 - Present
- Norfolk State University, Norfolk, VA, USA
  - Graduate Research Assistant, Aug. 2009 – Dec. 2011

HONORS AND AWARDS

- 2nd Place in NIH Computational Precision Medicine: Radiology-Pathology Challenge on Brain Tumor Classification 2019 (October 2019)
- 5th place in MICCAI BraTS 2018 Challenge; Survival Prediction (October 2018)
- 27th Place in Multi-Organ Nuclei Segmentation 2018 (September 2018)

PROFESSIONAL SERVICES

- Served as reviewer for IEEE Symposium Series on Computational Intelligence (IEEE SSCI) 2019

LIST OF PUBLICATIONS

JOURNAL

- **L. Pei**, S. Bakas, A. Vossough, S. M. Reza, C. Davatzikos, and K. M. Iftekharuddin, "Longitudinal brain tumor segmentation prediction in MRI using feature and label fusion," *Biomedical Signal Processing and Control,* vol. 55, p. 101648, 2020.
- **L. Pei**, K. Jones, Z. Shboul, J. Chen, and K. M. Iftekharuddin, "Glioma type and subtype grading using pathology and molecular data," *Medical Image Analysis*, 2019 (under review)
- **L. Pei**, L. Vidyaratne, M. M. Rahman, and K. M. Iftekharuddin, "Context Aware Deep Learning for Brain Tumor Segmentation, Subtype Classification, and Survival Prediction Using Radiology Images," *Scientific Reports*, 2020 (under review)
- Shboul, Z.A., Alam, M., Vidyaratne, **L., Pei**, L., Elbakary, M.I. and Iftekharuddin, K.M., 2019. Feature-Guided Deep Radiomics for Glioblastoma Patient Survival Prediction. *Frontiers in Neuroscience*, *13*.
- Kumar N, Verma R, Anand D, Zhou Y, Onder OF, **L. Pei,** Tsougenis E, et al. A multi-organ nucleus segmentation challenge. IEEE transactions on medical imaging. 2019 Oct 23.
- Maier O, Menze BH, von der Gablentz J, Häni L, Heinrich MP, **L. Pei,** Liebrand M, Winzeck S, Basit A, Bentley P, Chen L, Christiaens D. ISLES 2015-A public

evaluation benchmark for ischemic stroke lesion segmentation from multispectral MRI. Medical image analysis. 2017 Jan 1;35:250-69.

- Bakas S, Reyes M, Jakab A, Bauer S, Rempfler M, Crimi A, Shinohara RT, Berger C, Ha SM, Rozycki M, **L. Pei,** Prastawa M. Identifying the best machine learning algorithms for brain tumor segmentation, progression assessment, and overall survival prediction in the BRATS challenge. arXiv preprint arXiv:1811.02629. 2018 Nov 5.

CONFERENCES

- L. Pei, L. Vidyaratne, M. M. Rahman, and K. M. Iftekharuddin, “Deep Learning with Context Encoding for Semantic Brain Tumor Segmentation and Patient Survival Prediction,” SPIE 2020 (Accepted)
- **L. Pei**, S. M. Reza, W. Li, C. Davatzikos, and K. M. Iftekharuddin, "Improved brain tumor segmentation by utilizing tumor growth model in longitudinal brain MRI," in *Medical Imaging 2017: Computer-Aided Diagnosis*, 2017, vol. 10134, p. 101342L: International Society for Optics and Photonics.
- **L. Pei**, S. M. Reza, and K. M. Iftekharuddin, "Improved brain tumor growth prediction and segmentation in longitudinal brain MRI," in *2015 IEEE International Conference on Bioinformatics and Biomedicine (BIBM)*, 2015, pp. 421-424: IEEE.
- Reza, S. M., Linmin Pei, and K. Iftekharuddin. "Ischemic stroke lesion segmentation using local gradient and texture features." *Ischemic Stroke Lesion Segmentation* (2015): 23.